Evaluating Renewable Energy Applications in Libya

Ali S A Garada

A thesis submitted to the Cardiff University in candidature for the degree of Doctor of Philosophy

School of Engineering, Cardiff University, Department of Electrical Engineering

Wales, United Kingdom

(September,2023)

ACNOWLEDGEMENTS

This study was conducted at the School of Engineering, Electrical and Electronic Engineering, Cardiff School of Engineering, Cardiff University, with the aim of exploring distributed generation technologies for power systems. First and foremost, I thank ALLAH for helping me to complete this thesis. The author acknowledges the support and resources provided by Cardiff University, without which this have not been possible. The author would like to express their sincere appreciation to their academic supervisors, Prof. Liana Cipcigan and Prof. Jun Liang, for their excellent guidance and support throughout the research process. I would like to express my most sincere gratitude to my family, especially my mother and father, for their unconditional love, support, and encouragement throughout my life.

ABSTRACT

Modern power systems have been turning to distributed generation (DG) due to the increasing demand for electricity, fuel cost uncertainties, and environmental constraints. Particularly in developing countries, where DG technologies are being adopted for power system expansion planning, renewable energy sources, especially solar energy, have received significant attention. It may be possible to reconsider the traditional power grid paradigm by adopting small networks in islanded configurations in remote villages. This study presents a methodology for calculating and analysing the load demand of Al Marj City in Libya, utilizing a single calculation approach tool. To estimate the electricity load demand for future energy scenarios, it takes into account projected population growth and missing data for electricity distribution networks. Using renewable energy technologies, the study proposes solutions to Libya's random blackouts. Models and simulations are presented for two scenarios utilizing different renewable energy technologies (photovoltaic and wind) and considering standalone and grid-connected scenarios for Al-Marj city. For the photovoltaic and wind systems, the stand-alone cost of energy (COE) is 0.19 US$/kWh and 0.23 US$/kWh, respectively. In the grid-connected case, the COE is 0.15 US$/kWh for photovoltaics and 0.16 US$/kWh for wind systems. In addition, an LSTM neural network is developed and trained using historical data to forecast three crucial indicators, Consumption per capita, Primary energy consumption, and Population. The model's strong fitting accuracy indicates its potential for load demand forecasting in 2030. These forecasting outcomes significantly contribute to the modelling of a stand-alone system scenario through the utilization of Homer Pro software. This allows for the exploration and identification of the optimal system configuration required to meet the increasing load demand by the year 2030. The study employs MATLAB software, utilizing Sensitivity and Particle Swarm Optimization algorithms, to assess the placement and dimensions of distributed generation technologies. The primary objective is to minimize power losses. By comparing scenarios with and without distributed generators, a noteworthy decline in losses is observed, dropping from 0.74786 MW to 0.271021 MW. Furthermore, the investigation delves into the microgrid's behaviour during abrupt load fluctuations while operating in island mode. The simulation results affirm the adeptness of the controller in preserving voltage and frequency within acceptable thresholds, guaranteeing seamless system functioning. Moreover, the research employs HOMER Pro simulation to assess the financial viability of a Storage System aimed at achieving complete decarbonization. Notably, second-

life electric vehicle (SL-EV) batteries emerge as the most fitting storage technology. The estimated cost of energy (COE) for systems utilizing SL-EV batteries is approximately 0.46 US$/kWh, notably lower than the calculated 0.67 US$/kWh for systems employing lead-acid batteries. Additionally, in terms of net present cost (NPC), the system integrated with SL-EV batteries necessitates an investment of 6.81 billion dollars, outperforming the lead-acid battery system, which requires an allocation of 7.5 billion dollars. This underlines the superior economic performance of SL-EV batteries in comparison to the conventionally utilized lead-acid batteries.

LIST OF ABBREVIATIONS AND NOMENCLATURES

ABC	Artificial Bee Colonies
AC	Alternating Current
AI	Artificial Intelligence
ANFIS	Adaptive Neural Fuzzy Inference Systems
ARIMA	Autoregressive Integrated Moving Average
B	Billion
BA	Bat Algorithms
CO_2	Carbon Dioxide
COE	Cost Of Energy
CPF	Continuation Power Flow
DC	Direct Current
DEA	Differential Evolution Algorithms
DG	Distributed Generation
DP	Dynamic Programming
ELMs	Learning Machines
ES	Exhaustive Search
GA	Genetic Algorithms
GDP	Gross Domestic Product
GECOL	General Electrical Company of Libya
GNA	Government of National Accord
GNC	General National Congress
GS	Gradient Search
HOR	House Of Representatives
HRES	Hybrid Renewable Energy System
HSA	Harmony Search Algorithms
HVDC	High Voltage Direct Current
IA	Improved Analytical

IEA	International Energy Agency
IEEE	Institute of Electrical and Electronics Engineers
IMDE	Intersect Mutation Differential Evolution
IMF	International Monetary Fund
LMPs	Locational Marginal Prices
LNA	Libyan National Army
LPA	Libyan Political Agreement
LSTM	Long Short-Term Memory
MENA	Middle East and North Africa
MPGSA	Modified Plant Growth Simulation Algorithm
NASA	National Aeronautics and Space Administration
NOC	National Oil Corporation
NPC	Net Present Cost
NREL	National Renewable Energy Laboratory
NSRDB	National Solar Radiation Database
OO	Orthogonal Optimization
OPFs	Optimal Power Flows
O&M	Operation And Maintenance
OST	Optimal System Type
PABC	Particle Artificial Bee Colony
PSO	Particle Swarm Optimization
PV	Photovoltaic
RBF	Radial Basis Functions
RDG	Renewable Distributed Generation
REAOL	Renewable Energy Authority Of Libya
REMG	Renewable Energy Microgrid
RES	Renewable Energy Sources
RET	Renewable Energy Technology
RGA	Refined Genetic Algorithm
RNNs	Recurrent Neural Networks

RT	Renewable Technologies
SARIMA	Seasonal Autoregressive Integrated Moving Averages
SFLA	Shuffled Frog Leaping Algorithms
SIRES	Smart Integrated Renewable Energy Systems
SL-EV	Second Life Electrical Vehicle
SVR	Support Vector Regression
TS	Tabu Searches
UN	United Nation

LIST OF PUPOLICATIONS

Conference Papers

[1] A. Garada, A. Shaher, S. Alqahtani and L. Cipcigan, "Optimal configuration using renewable technologies for overcome blackouts in Libya power system: Al-Marj city case study," *2022 57th International Universities Power Engineering Conference (UPEC)*, Istanbul, Turkey, 2022, pp. 1-8, doi: 10.1109/UPEC55022.2022.9917984.

[2] S. Alqahtani, A. Shaher, A. Garada and L. Cipcigan, "Frequency Stability in Renewable-Rich Modern Power Systems, Saudi Grid Case Study," *2022 57th International Universities Power Engineering Conference (UPEC)*, Istanbul, Turkey, 2022, pp. 1-6, doi: 10.1109/UPEC55022.2022.9917788.

[3] A. Shaher, S. Alqahtani, A. Garada and L. Cipcigan, "Technical potential for rooftop solar photovoltaic in Commercial and Residential Areas in Saudi Arabia," *2022 57th International Universities Power Engineering Conference (UPEC)*, Istanbul, Turkey, 2022, pp. 1-6, doi: 10.1109/UPEC55022.2022.9917795.

Journal Papers

[1] S. Alqahtani, A. Shaher, A. Garada, and L. Cipcigan, “Impact of the high penetration of renewable energy sources on the frequency stability of the Saudi grid,” Electronics, vol. 12, no. 6, p. 1470, 2023. doi:10.3390/electronics12061470

[2] A. Shaher, S. Alqahtani, A. Garada, and L. Cipcigan, “Rooftop solar photovoltaic in Saudi Arabia to supply electricity demand in localised urban areas: A study of the city of abha,” Energies, vol. 16, no. 11, p. 4310, 2023. doi:10.3390/en16114310

Journal Papers prepared for submission

[1] Design and Analysis of Optimal Sizing for Hybrid Renewable Energy System to Overcome Blackouts in Libya Power System: A Case Study of Al-Marj City, Including Life Cycle and Energy Cost Analysis.

[2] An analysis of the optimal location and size of DG using a practical swarm methodology and sensitivity analysis for a real radial distribution system in Libya: case study Al Marj.

CONTENTS

LIST OF FIGURES

Chapter 1

Chapter 2

Chapter 3

Chapter 4

Chapter 5

Chapter 6

LIST OF TABLES

Chapter 1

Chapter 2

Chapter 3

Chapter 4

Chapter 5

Chapter 6

CHAPTER 1

Introduction and Objectives of Thesis

1.1. Background

Libya is in North Africa and borders the Mediterranean Sea to the north, Chad and Niger to the south, Egypt and Sudan to the east, and Tunisia and Algeria to the west. In terms of area, Libya covers 1,759,540 square kilometres (km^2) and is the fourth largest African country. Its Mediterranean coast extends 1,770 km [1]. As in other countries, Libya's power supply system is designed to meet the needs of society. In most parts of the country, electricity is currently available to 99% of households [2]. Moreover, the electricity network is available to all cities and villages throughout the country, even in desert regions or far away from power plants. The majority of power plants are located along coastal areas where the majority of the population resides [3]. Libya's energy sector is managed by the General Electrical Company of Libya (GECOL), which was established in 1984. This company is responsible for supplying electricity to the entire population of Libya. In addition, it maintains power grids, power plants, transmission lines, and distribution stations. Libya heavily relies on fossil fuels for electricity generation. Renewable Energy Sources (RES) are not promoted by the government or the private sector. Compared to other countries, Libya emits a large amount of carbon dioxide (CO_2). According to the CO_2 emissions rankings for countries, Libya ranked 134th in 2021 with its CO_2 emissions of 63.278 megatons, a growth of 29.42% over 2020 [4].

Over long distances, High-Voltage Direct-Current (HVDC) technology is used to transfer electricity to regions that are located far from power plants, which decreased electricity losses in national electricity networks. In addition to converting Direct Current (DC) to Alternating Current (AC), and centralizing the distribution system, there are even greater losses in electricity when it comes to conversion DC with AC. According to the national electricity network, Libya's losses in 2017 were 12% of the total output [5],[6]. This is considered as one of several problems facing the national electric network of Libya at the present time. Additionally, since February 17, 2011, the electricity sector's operations have worsened, which is reflected in the performance of the country's core business units and its electricity infrastructure. The deterioration of security and political instability has resulted in the suspension of most projects, repeated attacks on GECOL assets and staff, an increase in thefts, especially of conductors and electrical equipment, and a decline in the ability of GECOL to carry out maintenance. In some parts of the country, especially during peak load periods during the summer and winter, there have been long power cuts due to the loss of infrastructure assets and a decrease in power network performance. Also, a major problem is a growing population, and increasing construction projects in the housing, commercial, industrial, and agricultural sectors make increasing energy production a priority [6][7].

Generally, Libya's electricity production and supply systems are experiencing several problems at both national and global levels. A national problem is an inability to meet society's energy demand, harm to the environment caused by conventional electricity generation, and no sharing of Renewable Energy Sources despite electricity shortages and outages impeding economic progress. At the global level, Libya needs to be a part of the fight against global warming and climate change. It also needs to be a part of the development of its energy sector for a sustainable future. Therefore, the focus of this thesis is to utilize RES to benefit the Libyan energy supply system. This is to overcome the problems that the energy sector faces both in the country and globally. A case study method is being used to design a hybrid renewable energy system (HRES) in Al Marj city. The results of this case study will also be applied to other regions of Libya in order to achieve this goal. The solutions gained from this study can enable Libya to overcome its electricity capacity shortage and to optimize the energy supply system through the sustainable use of RES.

1.1.1. Libyan Electricity Network Overview

Natural gas and oil are the main sources of energy in Libya. By 2005, Libya had 35 billion barrels of oil reserves and by 2012 it had 47 billion barrels and 54 trillion cubic feet of natural gas. Generally, oil was regarded as the largest primary energy source in the year 2000, with a share of 66%, although that has decreased to 62% in recent years. Figure 1.1 shows that natural gas, which accounts for 38% of electricity generation, has replaced heavy fuel oil with light fuel oil with a share of 20% [8].

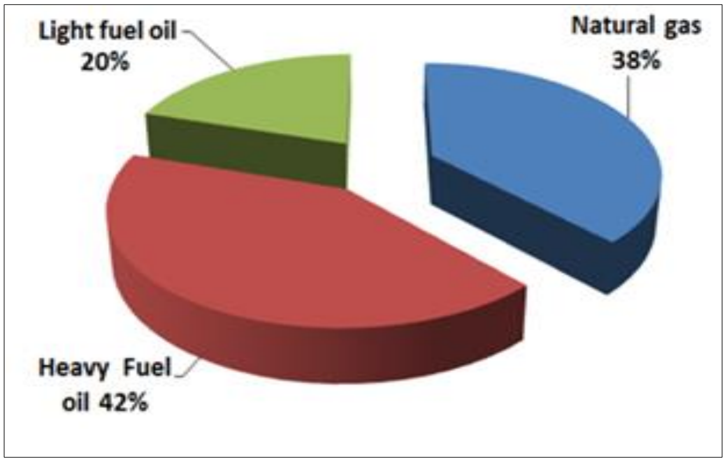

Figure 1. 1 Electricity generation by fuel type in Libya [8].

Since Libya relies heavily on oil and natural gas for its energy needs, it becomes one of the countries that rely on non-sustainable sources of energy. Since most of these energy sources are non-renewable, they cannot be sustained. A 50-year life expectancy is expected for discovered oil reserves at the current rate of production, which stands at 40 billion barrels [9]. Figure 1.2 illustrates the location of most fossil-fuelled power plants along the coast [10][11][12].

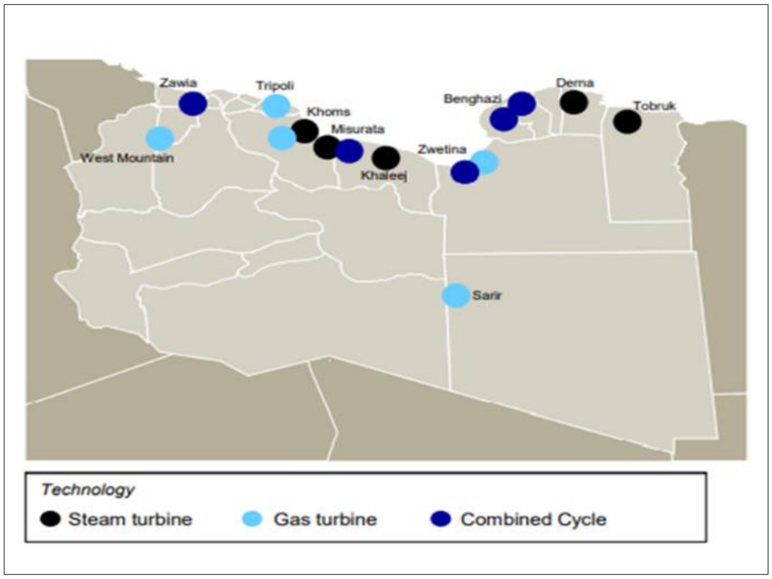

Figure 1. 2 Installed power plants in Libya [13].

The last registered data about the Libyan national electric grid is shown in Table 1.1. It includes the number of power plants, as well as their installed and available capacity [13].

Table 1. 1 Type of production units and capacity.

Production Technology	Number of Units	Planned Capacity (MW)	Available Capacity (MW)
Steam Turbine	14	1240	590
Gas Turbine	32	4611	3487
Combined Cycle	17	2937	2280
Total	63	8788	6357

1.1.2. Power Transmission and Distribution System in Libya

The voltage levels of transmission networks are divided into 400 kV, 220 kV, 66 kV and 30 kV. In contrast, the medium distribution voltages are 30kV. In addition to voltage levels, the total lengths, and types of the lines, as well as the number of substations are listed in Table 1.2 [13].

Table 1. 2 Transmission networks lines and substations.

Voltage Level (kV)	Overhead line (km)	Cables (km)	Number of Substations
400	2290	-	13
220	13,706	154	87
66	14,311	165	195
30	11,142	5084	461

1.1.3. Environmental Effects

CO_2 is emitted primarily by fossil fuel-burning power plants in Libya, at 40%. It is also emitted by transportation at 22% and by all other sources combined at 38%. Petroleum products account for 58% of carbon emissions, and natural gas for 42%. Carbon emissions will decrease as natural gas dependence increases. As the energy sector has grown, Libya's contribution to CO_2 emissions have increased. Since fossil fuels generate more than 70% of the world's electricity, continued combustion of them results in serious environmental pollution and global warming issues. Increasing energy demand is also causing the depletion of traditional fuels with limited resources. In some developing countries, including Libya, renewable energy is viewed as a green solution for mitigating emissions and meeting upcoming energy demands. Globally, renewable energy currently accounts for 15–20% of global energy demand [14]. In Libya, major actions are being taken to address climate change. These include the approval of the Kyoto Protocol and the goal of producing 10% of its electricity from renewable sources by 2020. The use of smart integrated renewable energy systems (SIRES) may be one solution to Libya's energy challenges. By utilizing a hybrid system, electricity can be generated for less than the cost of conventional stand-alone units. The environment would also benefit from reducing the amount of emissions generated per unit of electricity produced. Carbon emissions will decrease as natural gas dependence increases.

1.1.4. Load Shedding In Developing Countries

In an electrical system that lacks sufficient generation, load shedding is used to balance the load with the supply. This is done by temporarily switching off some loads in different parts of the system. There are many countries that utilize load shedding, including India, Sri Lanka, Lebanon, Iraq, Zambia, and Libya, when their electrical supplies can't meet demand during peak times [16] [17]. In Libya, GECOL is currently dealing with the issue of managing power outages through a strategy of rotational load shedding, also referred to as rolling blackouts. The objective is to establish a fair load-shedding plan that applies to all customers [18].

1.1.5. Al Marj City

Al Marj is a city located in the north-eastern region of Libya, situated near the Akhdar mountain range and north of the Mediterranean Sea, as depicted in Figure 1.3. Its historical roots trace back to around 600 BC when it was a part of the ancient Greek empire known as Barca, before coming under Arab control in 642 AD. The city of Al Marj as it exists today was built around a Turkish fort constructed in 1842. During the period of Italian rule from 1913 to 1941, the city was transformed into an administrative centre, market, and mountain resort destination. The population of Al Marj is approximately 84,406. Due to the modern construction, the redevelopment of the city and plans for future developments after it was destroyed by an earthquake in 1963, it was selected as a case study for this thesis. [19][20][21].

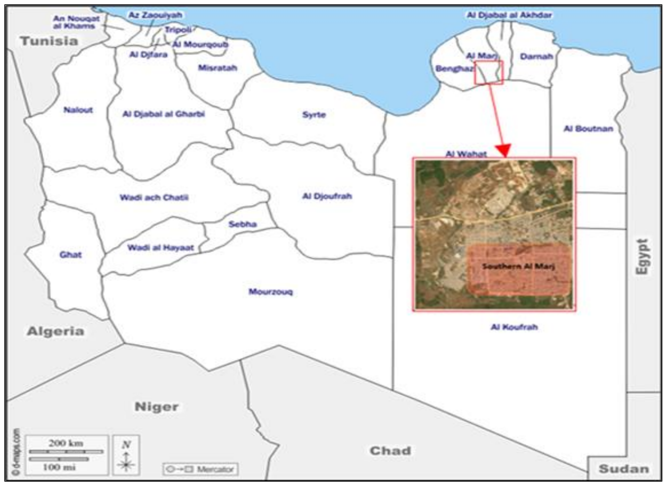

Figure 1. 3 Location of Al Marj city in Libyan map.

Based on research carried out by other researchers, Libya has significant potential for producing renewable energy that would be sufficient for domestic use and could be exported to countries in Europe. Most renewable energy sources are not being used currently. 42% of the country's energy comes from heavy fuels, 20% from light fuels, 38% from natural gas, and 0% from sustainable sources [22].

1.2. Research Challenges

Following the Arab Spring protests in 2011, Libya experienced a complete uprising against its ruling political regime. However, the country subsequently plunged into a civil war marked by frequent use of heavy weapons in inter-factional fighting. This ongoing crisis presents significant obstacles to maintaining the power grid infrastructure to this day. There are several significant challenges facing Libya's electrical energy situation:

- Gathering data regarding the country's electrical energy since GECOL hasn't published any annual reports since 2012.
- Continuously population growing, with a consequence in the increase of the electricity demand. This increase in the demand is requiring new power plants in the near future to meet the needs of new projects and industries.
- During the war, there was damage and destruction to some of its power plants and transmission network assets as well as sabotage and vandalism, particularly in the east and

west of the country. Therefore, it was very difficult for Libya to generate electricity to meet the demand with consequences in severe shortages and power cuts in recent years.

- The loss of electricity occurs over long distances in Libya because of its large area.
- Electricity losses within Libya's network accounted for 12% of the total output, deviating from global levels. This constitutes a significant challenge among several confronting Libya's national electric grid.
- Foreign companies are facing difficulties in completing maintenance and suspended projects in Libya, primarily due to a lack of funds. This led to grid operators having to resort to rolling blackouts when the actual electricity generation falls below the demand to prevent a system-wide collapse. Despite some businesses, homes, and health centres using mobile diesel generators, many Libyans still lack access to grid electricity, emphasizing the need for solutions to bridge this gap. To overcome some of these challenges it is important to install renewable generation contributing to mitigate the negative effects of fossil fuel use and ensure sustainable growth.

1.3. Objectives of the Thesis

This thesis aims to Formulate a comprehensive and sustainable energy management strategy for Al Marj City, Libya, by synergistically addressing the challenges of load demand analysis, renewable energy integration, predictive modelling using LSTM, and optimal configuration of distributed generators within a microgrid system. This integrated approach aims to develop a resilient and cost-effective energy infrastructure, considering the projected population growth, historical energy indicators, and dynamic responses to varying loads, ultimately contributing to a reliable and sustainable energy future for Al Marj City. These objectives have been addressed as follows:

Objectives of Chapter 3

Develop a methodological solution for analysing load demand in Al Marj City, Libya, using a single calculation approach tool design. The proposed solution is addressing missing data for electricity distribution networks and incorporates projected population growth to calculate electricity load demand for future energy scenarios.

Objectives of Chapter 4

- Choose a real case study of Al Marj City.
- Propose a Hybrid Renewable Energy System (HRES) in Al Marj City to overcome electricity generation challenges to meet the demand.
- Develop different HRES configurations using solar and wind generation for both grid-connected and islanded modes.
- Determine the optimal configuration of renewable technologies to overcome blackouts Al-Marj city.

Objectives of Chapter 5

- Gathering historical data for the key energy indicators: Consumption per capita, Primary energy consumption, and Population.
- Create and training a Long Short-Term Memory (LSTM) neural network using the historical data to predict the future values of the energy indicators for year 2030.
- Evaluate the effectiveness of the LSTM model in predicting future values of energy indicators and its potential for practical use in supporting informed decision-making for energy management.
- Apply the load data of 2030 to determine the optimal configuration of a stand-alone HRES with PV system.
- Identify the best cost-effective solution for the stand-alone system, taking into account factors such as net present cost and cost of energy for customers.

Objectives of Chapter 6

- Identify the optimum location and size for Distributed Generators in a 22-bus radial distribution network within Al Marj City to reduce the energy loss.
- Develop a dynamic model of the power system in Al Marj City and analyse the response of the microgrid system in the islanded mode to sudden changes in load.
- Evaluate the most economical configuration for the islanded system with batteries.

1.4. Thesis structure

This thesis comprises seven chapters.

Chapter 1 is introducing the background of the challenges encountered by power systems in Libya in meeting the escalating demand for electricity. Furthermore, it outlines the objectives of the research endeavor.

Chapter 2 comprises a literature review that examines previous research related to the identification of the optimal configuration of renewable energy sources (REs), the optimization of distributed generator placement, and load forecasting. The review is focusing on evaluating the optimal methods and techniques employed in these domains, highlighting the challenges encountered, and assessing the current state of knowledge to enhance understanding and identify research gaps for future investigations.

Chapter 3 is presenting a methodological solution to calculate and analyze missing load demand data in Al Marj City. This chapter outlines the approach taken to address the absence of demand data, allowing for accurate estimation and analysis of load demand in the city.

Chapter 4 investigates the utilization of distributed generation technologies that harness local renewable resources to mitigate blackouts in the Libyan power system. The case study specifically focuses on Al-Marj City and aims to identify the optimal configuration of renewable energy sources (RES) to enhance power generation and delivery efficiency.

In **Chapter 5** a proposal is made to employ an LSTM neural network for load demand forecasting in Al Marj City. The model utilizes normalized historical data on population, primary energy consumption, and consumption per capita for training purposes. Once trained, the model predicts load demand for future years and assess its performance using the R-square value. The research outcomes make a valuable contribution to the modeling of a stand-alone system scenario. This facilitates the exploration and identification of the optimal system configuration required to meet the increasing load demand by the year 2030.

Chapter 6 focuses on the application of distributed generation technologies that leverage local renewable resources to electrify remote distribution networks. This chapter explores methods to minimize power losses and the number of required generators and examines the microgrid's response to sudden load changes. Additionally, the optimal energy storage system was determined. This analysis provides valuable insights into the economic implications associated with the selected storage system.

Chapter 7 presents the conclusions drawn from the research and provides recommendations for future work based on the study's findings. These conclusions summarize the key insights and outcomes obtained throughout the research process. Additionally, the chapter offers suggestions for further investigations and areas that can be explored to expand on the current study, paving the way for future research endeavors in the field.

1.5. Structural Flowchart of the Thesis

This structure is divided into seven distinct chapters, each serving a specific purpose. It also highlights the key objectives of the thesis and demonstrates the interconnections between these chapters.

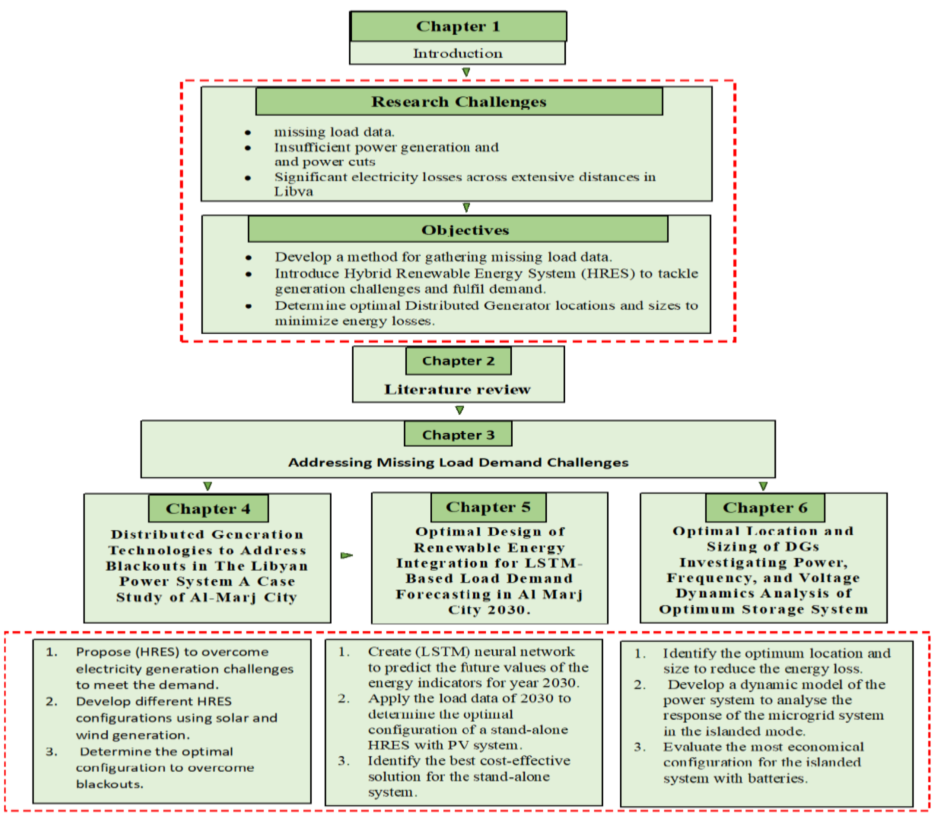

Figure 1. 4 Thesis structure

1.6. Contributions

This study addresses a pertinent issue in the power system of Libya, where blackouts have posed significant challenges for the power supplier. By providing practical and effective solutions, this study offers valuable insights for planners and researchers to improve the current and future state of the power system, thereby bridging the research gap between this study and previous research. The study examines several critical factors that must be taken into account, thereby contributing to a better understanding of the problem. Overall, the study's contribution lies in providing clear and concise recommendations to improve the power system in Libya as:

- **The implementation of a tool to deal with the absence of load profiles in the distribution networks.**

This contribution presents a methodological solution to determine and analyse the load demand for Al Marj City in Libya using a unified calculation approach tool. The study specifically addresses the issue of missing data for electricity distribution networks and incorporates projections of population growth to calculate electricity load demand in accordance with future energy scenarios. The proposed approach enables the assessment of electricity demand and its potential variations under different conditions, thereby facilitating the identification of optimal strategies for energy planning and management. The methodology presented in this study contributes to the body of knowledge on load demand analysis and provides a valuable tool for energy planners and decision-makers.

- **Identify Optimal configuration using REs for overcoming blackouts in the distribution networks.**

This contribution presents several solutions that utilize renewable energy technologies to mitigate the issue of random blackouts in Libya. The study conducted a case analysis in Al-Marj city simulating two different scenarios, each involving a particular type of renewable energy technology (PV and wind) with varying components. The research findings reveal that establishing a PV hybrid energy system, whether as a stand-alone or grid-connected system, is highly feasible in the region. The study also recommends renewable energy technology as the most sustainable approach to develop the Libyan energy sector and address its current energy shortage crisis. The study's results contribute to the existing knowledge base on RESs and provide valuable insights for policymakers and energy planners in Libya.

- **Using LSTM Neural Networks to Predict Energy Indicators: A Case Study Analysis**

This study presents a novel contribution where a neural network, utilizing LSTM layers, is trained on historical data to forecast three significant indicators: Consumption per capita, Primary energy consumption, and Population. The research findings demonstrate that the LSTM neural network exhibits a high level of effectiveness in predicting future values of the selected indicators. The model showcases excellent performance metrics, highlighting its potential for practical applications in forecasting future trends and facilitating informed decision-making. The model can be further improved by incorporating additional data sources, which may enhance its accuracy. The outcomes of this research contribute to the modelling of a stand-alone system scenario, enabling the investigation and determination of the optimal system configuration to meet the growing load demand by the year 2030.

- **Sizing and Positioning Distributed Generation Technologies for Electrifying Remote Distribution Networks: A Sensitivity and Particle Swarm Optimization Approach**

The study analyses the response of the island mode microgrid to sudden changes in load through simulation. The simulation results indicate that the designed controller was successful in operating the system seamlessly, without any disruptions or exceeding the voltage and frequency limits. The findings of this research provide valuable insights into the application of distributed generation technologies in remote areas and can inform energy planners and policymakers in their efforts to develop sustainable energy solutions. Additionally, this study aims to explore the potential of distributed generation technologies that utilize local renewable resources to electrify remote distribution networks. The study employed Sensitivity and Particle Swarm Optimization (PSO) algorithms to analyse the optimal location and size of distributed generation (DG) units. The primary objective of the study was to minimize the total real power losses and the number of DGs required.

CHAPTER 2

Literature Review

This literature review critically analyses the existing body of knowledge related to three key topics: the identification of the most suitable configuration for renewable energy systems (RE), the optimization of distributed generator locations, and load forecasting. The primary objective of conducting a literature review is to pinpoint existing research voids and propel investigation to push the boundaries of the current state of knowledge.

2.1. Power Energy Sector of Libya

In Libya, the energy sector and state governance are overseen by the Council of Ministers of the Libyan Government. The energy sector operates through two distinct bodies: the National Oil Corporation (NOC) and the Ministry of Electricity and Renewable Energy. The National Oil Corporation (NOC) is primarily responsible for the production of gas and oil and manages all development activities related to the oil sector, including the development of ports, airports, buildings, and other essential infrastructure [28]. The Ministry of Electricity and Renewable Energy comprises two key entities: the General Electricity Company of Libya (GECOL) and the Renewable Energy Authority of Libya (REAOL). Established in 1984, the GECOL plays a crucial role in the country's power sector, supplying electricity to the entire population of Libya. It is also responsible for operating and maintaining power systems, power plants, distribution and transmission stations, electrical cables, and other related infrastructure [29]. On the other hand, the Renewable Energy Authority of Libya (REAOL) was established in 2007 with the aim of promoting the use of renewable energy and coordinating its integration into the national energy supply system. While there is limited available data showcasing the achievements of this institution in terms of renewable energy technologies, studies have outlined future strategies for RE implementation in Libya. However, currently, no concrete projects are in place related to renewable energy initiatives [29]. The development of renewable energy in Libya remains a potential avenue for future progress, but practical implementation is yet to be fully realized.

2.2. Current Situation of Energy System

2.2.1. Electricity Supply System

In Libya, an established power system is responsible for generating, distributing, and transmitting electricity to cater to the demands of residential areas. This power system effectively fulfils nearly 99% of the country's electricity needs, covering both urban and rural regions, including some inhabitants living in desert areas [30]. To reach remote regions located far from the main grid system, High Voltage Direct Current (HVDC) transmission is utilized. However, it should be noted that HVDC transmission is associated with higher losses in the conversion of AC to DC power. These losses were recorded at approximately 12% of the total power generation in the country in 2014 [31]. This phenomenon indicates that efforts to transmit electricity over longer distances through HVDC come at the cost of increased energy losses, affecting overall power efficiency.

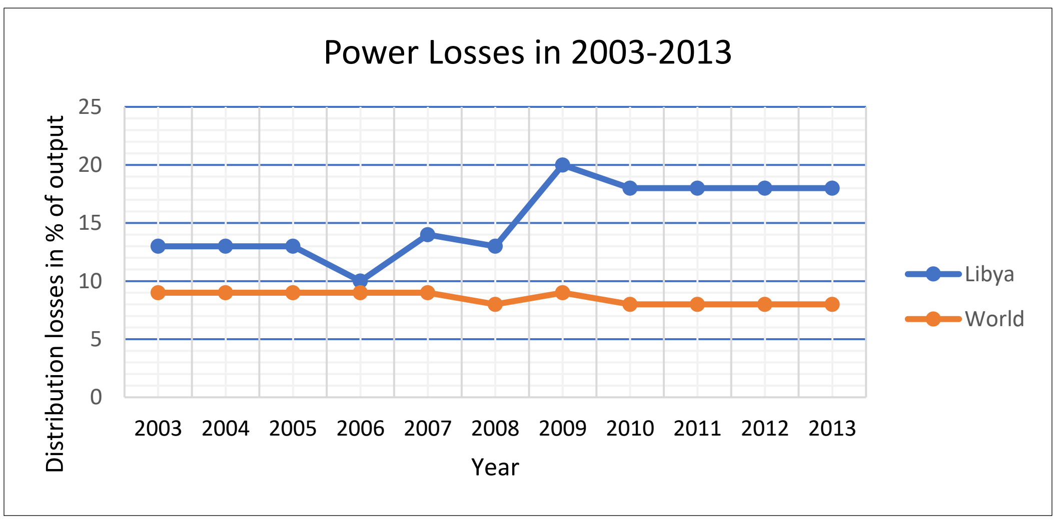

Figure 2. 1 Comparison of the power losses in Libya from 2003 to 2013 with global power loss [31].

The major challenge faced by Libya's power sector revolves around managing power losses within the centralized grid. Figure 2.2 illustrates a comparison of power losses in Libya between 2003 and 2013 with global power loss percentages. It indicates that the controlling authorities effectively managed losses in 2006. However, the losses increased again in 2007 and reached their peak in 2009. Subsequently, efforts were made to control and stabilize the losses at a lower level. Nevertheless, Libya's power system continues to experience higher losses compared to other regions worldwide, according to a study published by the World Bank [31]. On a global scale, Libya's power system is interconnected with neighbouring countries like Egypt and Tunisia. This interconnection facilitates power sharing to meet peak load demands in border regions and to exchange excess loads. However, despite these efforts, the power supply remained insufficient to meet the needs of these regions and prevent power outages.

In response to this issue, Libya entered into agreements to participate in an international power supply system known as DESERTEC. This initiative aimed to establish a global power network for sharing energy between the Middle East and North Africa (MENA) countries and European nations, with a particular focus on promoting the use of renewable energy (RE). Unfortunately, due to the prevailing instability of Libya's political situation and the civil war, the implementation of this project has not materialized. As of now, there are no activities related to DESERTEC in Libya, and the project appears to have been effectively cancelled. The study [31] concludes that Libya's electric system experiences significant power losses, primarily due to the challenges of distributing power to regions located far from power plants. Despite this, a substantial portion of the population still has access to electricity.

2.2.2. Energy Sources and Production Technology

As of 2017, Libya's electric power system comprises 26 power plants, equipped with a total of 85 generating units of various power ratings, collectively amounting to 10.24 GW. These power plants are primarily situated along the coast of the Mediterranean and are responsible for distributing electricity throughout the country, under the management of the General Electricity Company of Libya (GECOL).

However, it is important to note that nearly 48% of the total power generation capacity, approximately 5.35 GW, is currently unavailable due to maintenance or operational constraints in power transmission or generation. This substantial portion of the power generation, which accounts for 52% of the total power generation in Libya, is impacted by shutdown conditions or readiness for decommissioning. In particular, 19 out of the 85 generating units are currently non-operational and ready for decommissioning, with a combined generating capacity of 483MW. As a result, only 54.8% of the total installed capacity is currently operational and capable of meeting the electricity demand in Libya. This situation highlights the significant challenges faced by the country's power sector in ensuring a reliable and efficient supply of electricity to meet the nation's energy needs.

An analysis of GECOL's power generation infrastructure indicates that the age limit is heavily skewed towards basic cycle and combined cycle gas turbine units, which represent 86% of the installed capacity and 94% of the available capacity. Notably, GECOL has not built a new steam power station since 1985, until the new Gulf power station's first unit came online in 2014. The Southern region of Libya has no power generation, resulting in voltage insecurities and prolonged power blackouts compared to other parts of the country. The new Ubari power plant is expected to be a significant initial step in addressing this issue. Power generation in the eastern region is limited to two aging steam power plants, while the Benghazi Region has one large power generating complex at Benghazi North. The Eastern power network suffered frequent power outages between 2015 and 2016, during which the Eastern and Western power systems were separated due to damage to overhead lines. This was mainly due to its reliance on Benghazi North as the sole primary source of power supply. Recently, a contract was signed for four new gas turbine units in Tobruk, which will help alleviate this dependence. From 2010 to 2016, there have been significant changes in Libya's electric power sector. During this period, the weighted average generating unit availability experienced a decrease from 78.3% to 66.0%, while the available capacity dropped from 64.6% to 53.7% of the total installed capacity. Despite these challenges, the demand for electricity has continued to grow steadily at an approximate rate of 4% per year. However, there have been positive developments in terms the warm effectiveness of GECOL's power generation witnessed an increase of 7.3%. This improvement can be attributed primarily to the introduction of steam units associated with the combined cycle gas turbine units at Benghazi North and Misurata, as well as the increased utilization of natural gas instead of liquid fuel. The proportion of energy generated from gas rose significantly from 41% in 2010 to 80% in 2016. Notably, despite the challenging operating environment in Libya since 2011, GECOL managed to commission 14 new generating units between 2012 and August 2017. These additions contributed a total of 2.295 GW to the country's installed capacity, representing positive strides in expanding the power generation capabilities of the nation.

One of the major concerns impeding the optimal functioning of GECOL's power generation assets and leading to the current power shortages in Libya is the delay in maintenance. The reduced power outputs of several units have resulted from limitations on GECOL's ability to perform significant maintenance works and upgrades of the power generating units, with estimated potential increases of 2GW or more to GECOL's available capacity if these works were to be completed. Factors contributing to the increasing backlog of overdue maintenance works include:

Firstly, upgrades of power generating units are considered a capital investment, and therefore funded by the Libyan Development Budget, which is financed by the State. As a result, GECOL does not have control over the supply of resources.

Secondly, most of GECOL's generating units are gas turbines, which have much higher maintenance requirements than steam turbines. These units may require significant upgrades as often as once every three to four years, with up to 10 to 15 major upgrades required each year to maintain the condition of its units. This would require the government to allocate more than 250 USD million annually for upgrades.

Thirdly, although GECOL has developed technical expertise to carry out much of the work in major upgrades, the nature of significant upgrades often requires the involvement of the generating units' providers to carry out upgrades and specialized works. However, the security and stability situation in Libya along with advice from foreign governments have led many providers to prohibit their personnel from traveling to Libya, thus impacting GECOL's ability to carry out upgrades. Figure 2.3. illustrates the growing backlog of significant upgrades that GECOL is facing [31].

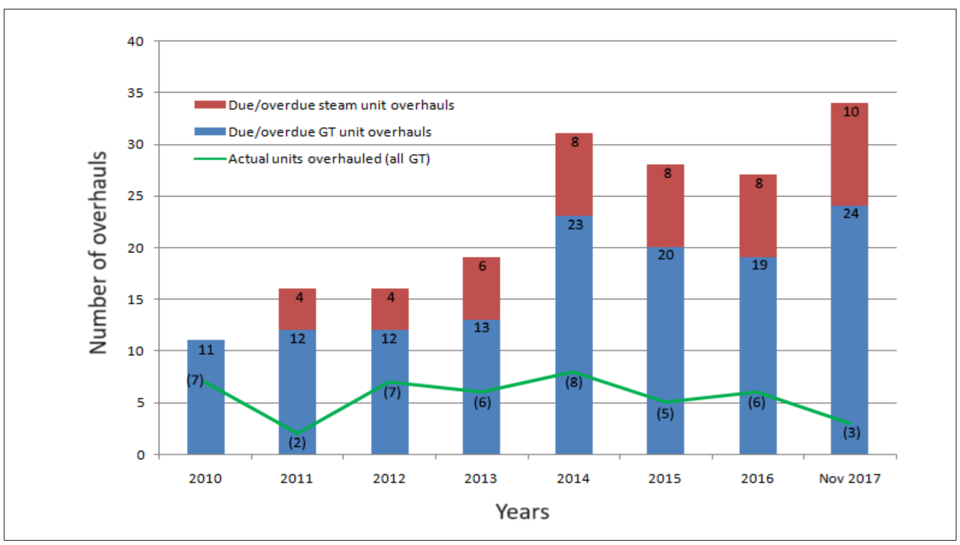

Figure 2. 2 Overhauls data for generating units in Libya [31].

The World Bank's study on CO_2 emissions in Libya categorized the sources of emissions into four main categories: power and heat production, manufacturing industries and construction, residential and commercial buildings, and transportation. Among these categories, the energy sector, particularly electrical and heat production, emerged as the largest contributor to CO_2 emissions. This sector accounted for a significant 62.1% of the total pollution, as shown in Figure 2.4 [32]. The findings highlight the importance of addressing emissions from the energy sector to effectively mitigate the country's overall carbon footprint.

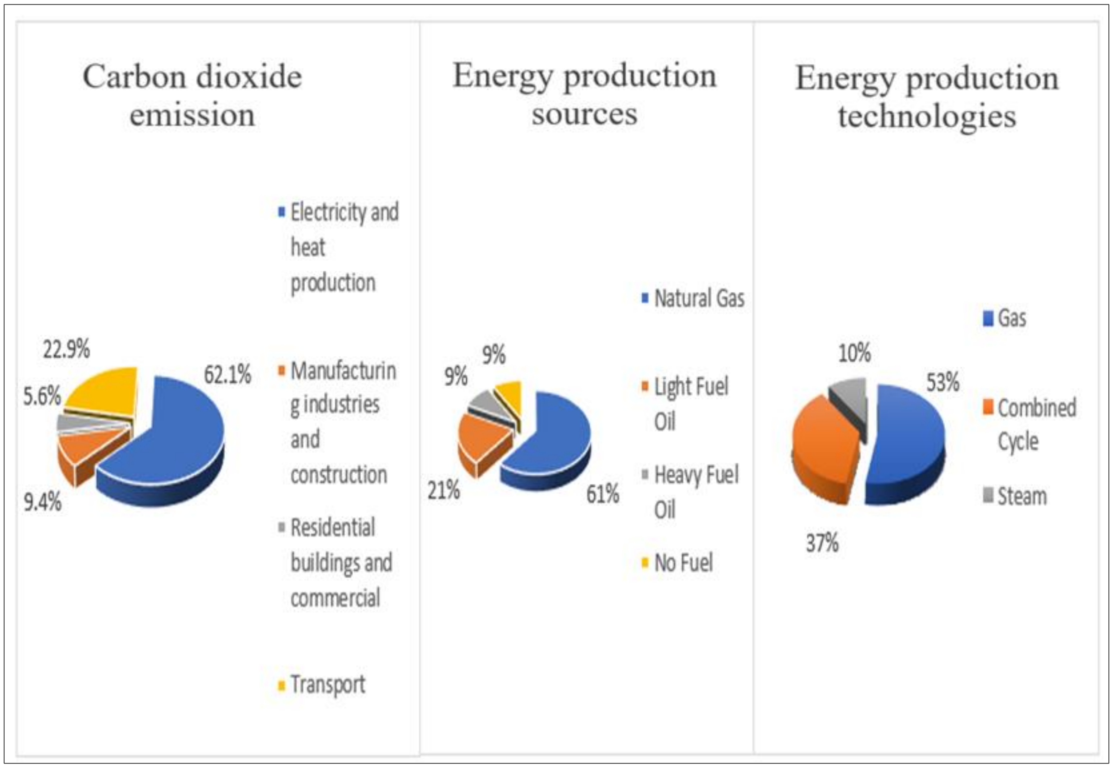

Figure 2. 3 Energy production sources in Libya [32].

2.2.3. Energy Demand and Generation

The rising population and development projects in Libya have led to a gradual increase in energy demand. Furthermore, the country's power consumption is relatively high, with Libya being the largest continental consumer of electricity [32]. This trend can be attributed to various factors, such as social norms and public behaviour, but the most significant reason is the subsidized power tariff. An International Monetary Fund (IMF) study revealed that "*subsidies have resulted in high energy consumption compared to Libya's GDP*." The energy tariffs and rates in Libya are divided into 0.015 $/kWh for domestic use, 0.052 $/kWh for administrative and corporate use, while the production cost to the government is 0.2 $/kWh. Therefore, the significant difference between the production cost and tariff cost constitutes a high subsidy. Conversely, the proposed HRES development aims to reduce generation costs.

In conclusion, the rising energy demand in Libya has resulted in higher peak loads and frequent power outages in certain cities, lasting for extended periods, sometimes spanning hours or even days. Managing this challenge stands as one of the key issues confronting the country's energy sector. However, the Libyan government is proactively engaged in finding solutions to tackle this problem and ensure a reliable energy supply that aligns with the present and future needs of society. The efforts to address the energy shortfall demonstrate the government's commitment to meet the growing energy demands of the nation while maintaining a stable and sustainable power system.

2.3. Current State of The Renewable Energy Sector

In 1980, Libya took a step towards renewable energy by implementing a photovoltaic system for microwave repeater stations near Zella City. This initiative was necessary due to the distance from traditional power generation stations. However, since then, the adoption of solar PV systems in Libya has remained limited to small-scale applications for remote areas where transmission is impractical. Despite the immense potential of solar energy, there has been a lack of significant efforts to develop large-scale solar power plants capable of meeting the country's substantial power demands. Similarly, in the wind energy sector, a 25MW plant was installed in Derna City, but it remains incomplete and non-functional for electricity supply. Other renewable energy technologies, such as biomass, geothermal, and hydropower, are also largely absent from both small- and large-scale production in Libya.

Presently, only small-scale solar power installations contribute to the grid, which is insufficient to meet the national power generation requirements. The examination assignment underscores the necessity of exploring the utilization of these renewable energy technologies on a larger scale, as exemplified in the case study presented in subsequent sections. Table 2.1 provides an overview of the existing applications of renewable energy technologies in Libya, along with their current installed capacity [33]. This data highlights the limited progress in harnessing the potential of renewable energy and emphasizes the need for more ambitious and comprehensive initiatives to tap into its vast renewable energy resources.

Table 2. 1 Existing uses of RE technologies and their installed capacity in Libya [33].

RE technology	Existing applications	Installed capacity
Biomass energy	No applications	Not installed
Geothermal Energy	No applications	Not installed
Hydropower energy	No applications	Not installed
Solar energy	PV system stand-alone application in the field of communication, water pumping, ruler electrification	1525 kW peak
Wind energy	Horizontal Axis Wind Turbines (HAWTs) technology	Projects to provide 25 MW, but is not yet operational

2.4. Identify The Optimal Configuration Using Renewable Energy Systems

A multitude of research investigations have delved into the economic feasibility of renewable energy systems (RES), encompassing scenarios of both autonomous off-grid configurations and interconnected grid setups. In 1998, a pioneering effort laid down a framework for optimizing the dimensions of hybrid systems. Evolving from this seminal work, subsequent scholarly inquiries have been dedicated to the mathematical delineation of sizing hybrid systems, as evidenced in the works of [34], [35], and [36]. These methods utilize iterative approaches to minimize energy costs effectively. Apart from the mathematically oriented techniques, several efforts have been made to develop software tools aimed at simplifying the techno-economic calculations involved in RES analysis. These software solutions offer practical ways to tackle the complexities of evaluating and optimizing renewable energy projects. By combining mathematical models and software tools, researchers have sought to enhance the understanding and decision-making process related to renewable energy integration and its economic feasibility [37] [38]. Several software packages have been reported for optimizing renewable energy systems, including HOMER Pro, Hybrid2, RETScreen, iHOGA, and INSEL. Among these tools, HOMER Pro (Hybrid Optimization Model for Electric Renewable Energy) stands out as one of the most popular choices in recent years for

RES applications. HOMER Pro was developed by the National Renewable Energy Laboratory (NREL), an American public agency, as part of its research and development program [39]. This powerful software enables users to evaluate all feasible configurations of renewable energy systems, allowing them to identify the optimal setup that results in the minimum Net Present Cost (NPC) and Levelized Cost of Energy (COE) [40]. In 2010, a renewable energy microgrid (REMG) system was implemented in a rural area of Ethiopia as a hybrid REMG system. The project utilized HOMER to estimate critical information about the hybrid system, incorporating models and satellite data. The study's outcome revealed cost-effective options for various sizes of REMG systems, enabling a comprehensive analysis of the system's economics [41]. Reference [42] highlights a project in a remote rural location in Kerman, Iran, where HOMER Pro was employed to assess the feasibility of a standalone REMG with battery storage, tailored to meet the area's load requirements. A comparison between PV-battery, wind/battery, and hybrid PV/wind/battery systems showed that PV-battery systems offered the lowest Net Present Cost (NPC) and excess electricity fractions. Another significant project in Binalood, Iran, utilized HOMER Pro to evaluate a hybrid REMG. The study considered options such as wind/diesel batteries and PV/wind/diesel/battery systems, demonstrating their economic and environmental benefits for transmission lines.

In a study documented in reference [43], an island-scale university campus microgrid at Cyprus Eastern Mediterranean University was analysed as a hybrid PV/Wind/battery system. The objective was to determine the optimal configuration, considering low Levelized Cost of Energy (COE) and Net Present Cost (NPC) values. To achieve this, an hourly time-stepping approach was utilized to specify the sizes of energy generators and storage units for the small community. The results of the analysis indicated that the PV/Wind hybrid configuration emerged as the most favourable option for the microgrid, offering promising economic benefits.

Diverging from previous scholarly endeavours, which had not undertaken a thorough examination, a notable gap existed in the comprehensive economic assessment of hybrid systems within microgrids, specifically within the confines of Al Marj City, Libya. To address this research void, the present study selected the Homer Pro software as a pivotal tool. Through the strategic utilization of this software, this research embarked on a mission to meticulously scrutinize and ascertain the optimal configuration of hybrid systems, harnessing the potential of renewable energy sources. This endeavour encompassed a multifaceted evaluation, integrating crucial parameters such as Net Present Cost (NPC), and Cost of Energy (COE) in units of $/kWh. In essence, this study constitutes a robust and pioneering contribution to the extant knowledge base.

2.5. Optimal location of Distributed Generators

In the electric energy industry, there has been a notable resurgence of interest in distributed generation sources over the past few decades. Researchers are now keen on thoroughly examining various crucial aspects and challenges associated with the implementation of renewable distributed generation (RDG), particularly within distribution systems. RDGs offer diverse possibilities for enhancing the overall efficiency of an electrical grid and minimizing power losses, depending on their location and capacity. This advancement towards a sustainable and intelligent grid represents a key focus for researchers [44].

Furthermore, Renewable Distributed Generation (RDG) systems present a propitious avenue for energizing microgrids, a stride that profoundly augments grid robustness by enabling autonomous operations when exigencies arise. The implementation of RDG units engenders a myriad of environmental, economic, and technical dividends [45]. Viewed through the lens of economics and the environment, this technology begets substantial merits. It precipitates curtailed fuel consumption, mitigates distribution and transmission expenditures, and engenders a curbing of greenhouse gas emissions. These constructive consequences vividly underscore the economic and ecological viability of RDGs as a judicious alternative. Moreover, the technical virtues and assets of this approach are nothing short of remarkable. Integration of RDGs defers the immediate imperative for electrical system upgrades. Concurrently, it augments the voltage profile, fortifies voltage stability, diminishes power losses, guarantees the reliability of the protection system, and heightens overall power quality. These technical enhancements collectively conduce to a more streamlined and dependable electrical grid system. While RDGs offer considerable advantages, it's imperative to also acknowledge their potential disadvantages.

Nonetheless, it's worth acknowledging the potential disadvantages of RDGs. For instance, the intermittent nature of some renewable energy sources, such as solar and wind, can lead to fluctuations in power output, potentially requiring additional energy storage solutions or backup systems to ensure a consistent energy supply. Additionally, the initial investment and maintenance costs of RDG units could pose financial challenges for some installations. Careful consideration of these factors is essential to holistically assess the applicability of RDGs within specific microgrid contexts [46].

The term "*distribution generation*" pertains to power generation units with capacities ranging from 50 MW to 100 MW, commonly interlinked with the distribution network. Furthermore, according to the Electric Power Research Institute (EPRI), "distributed resources" encompass modest power plants (ranging from 1 kW to 50 MW) and/or energy storage apparatuses positioned in close proximity to customers, distribution, or sub-transmission substations [47].

The Institute of Electrical and Electronics Engineers (IEEE) further clarifies "distributed generation" as electric generation facilities linked to an area electric power system (EPS) via a point of common coupling, which forms a subset of distributed resources. The International Energy Agency (IEA) designates "distributed power generation" as power generated on-grid for consumption or distribution, integrated into the grid at distributed voltage levels. This approach to power generation is significant on a global scale, and its utilization is projected to expand in the future [48].

The depletion of fossil fuel resources and growing environmental concerns have driven the emergence of various alternative energy solutions, among which are wind, solar power and biomass. Distributed generation technologies offer versatile applications that cater to different load requirements. DG systems can serve as stand-up sources during grid outages, providing reliable backup power when the main grid is unavailable. They also act as standby sources in isolated areas, serving rural and remote communities with a dependable electricity supply. Additionally, DG technologies are employed to address peak loads during high-demand periods, effectively reducing power costs, supporting the grid, and alleviating the load on the main power supply. These applications lead to improvements in voltage profiles, power quality, and a reduction in power losses, all contributing to a more efficient and stable electrical grid [49].

In recent times, there has been a significant focus on finding the best locations and sizes for distributed generators within distribution networks to effectively minimize power and energy losses. Utilizing DG units in inappropriate locations can lead to adverse effects on network performance, such as increase in steady state voltage beyond the permissible limits. This issue is particularly critical in developing countries with high power losses and inadequate voltage profiles. As a result, a considerable amount of research has been dedicated to developing methodologies aimed at minimizing power losses by strategically allocating DGs in optimal locations. The primary goal is to maximize the overall efficiency of the distribution network [50]. By carefully considering the placement and sizing of DG units, these studies aim to enhance the performance and reliability of power systems while reducing losses and improving voltage stability. In Chapter 6 of the thesis, a methodology is introduced for identifying suitable locations and optimal sizes of DGs within the Libyan distribution network of Al Marj City.

2.6. Distributed Generation Allocation

In this section, various techniques for optimally sizing and locating Distributed Generation (DG) units to minimize real power losses are explored. Three main categories of optimization techniques are investigated: analytical, non-heuristic, and meta-heuristic methods, all striving to achieve the same goal of minimizing real power loss [51]. Analytical methods perform effectively for small and simple systems but become inefficient when applied to large and complex systems. Four types of analytical methods are identified, namely the 2/3 rule or Golden rule, Kalman filter, Sensitive factor analysis, and iterative analysis [52].

As an alternative, non-heuristic methods have demonstrated better performance in finding near-optimal solutions with higher accuracy compared to analytical methods. Several approaches fall under this method, including Gradient Search (GS), Dynamic Programming (DP), Orthogonal Optimization (OO), Continuation Power Flow (CPF), and Exhaustive Search (ES) [53]. Lastly, the Meta-Heuristic method relies on swarm-based optimization techniques and evolutionary optimization techniques. Key approaches within this method include Genetic Algorithms (GA), Tabu Searches (TS), Bat Algorithms (BA), Shuffled Frog Leaping Algorithms (SFLA), Artificial Bee Colonies (ABC), and Particle Swarm Optimizations (PSO) [54].

Recent studies have shown that heuristic methods, such as hybrid harmony search algorithms (HSA), particle artificial bee colony (PABC), intersect mutation differential evolution (IMDE), and hybrid harmony search algorithms (HSA), have been successfully applied to optimize DGs and shunt capacitors in terms of their capacity and placement. While these studies often involve computationally intensive processes, their common objective remains the minimization of real power loss [55]. The method proposed in [56] employs analytical expressions to achieve a less computationally intensive approach. The objective is to strategically place DG units within the primary distribution system to minimize losses resulting from their placement. However, as multiple DGs are considered, the previous method becomes unsuitable for efficiently distributing power.

To address this, researchers have explored various approaches to reduce the search space and computational burden of the optimization algorithm. For instance, references [57] and [58] present methods of location optimization based on changes in real power loss in the line connecting a bus, as well as changes in active or reactive power at the same bus in a radial network. Nevertheless, when dealing with multiple DGs, this method proves inadequate for accurately distributing power. In order to optimize the placement of DG units in a network, several alternative approaches have been developed. One such approach involves using sensitivity indices derived from voltage stability improvements concerning changes in injected active and reactive power at a bus, leading to the development of an evolutionary programming optimization method to determine the optimal size of DGs using evolutionary programming algorithms [59]. Additionally, reference [60] adopts sensitivity analysis to determine the optimal size and operating point for DGs in distribution systems, effectively minimizing power losses. Separate analytical techniques have been developed based on constant impedance and constant current load models.

In [61], a Hybrid Harmony Search Algorithm (HSA) is utilized to identify the optimal locations for installing DG units in distribution networks. The HSA approach, combined with sensitivity analysis, yields the most suitable installation locations. The method is tested on 33-bus and 69-bus systems at various load levels, demonstrating reduced power losses and improved voltage profiles through simultaneous network reconfiguration and DG installation. It is worth noting that as the number of DGs increases at a given load level, the rate of improvement decreases. Furthermore, the HSA's performance is compared with Genetic Algorithm (GA) and Refined Genetic Algorithm (RGA), with the HSA yielding better computational results. In [62], the size and placement of DGs were determined using a classical grid search algorithm. However, this approach proved to be excessively time-consuming due to long computation times, depending on the system's size. As evident from these studies, various methods have been explored to optimize the placement and sizing of DG units in distribution networks, each with its own advantages and limitations in terms of computational efficiency and accuracy. In [63], a loss sensitivity factor for distribution systems is formulated using an analytical method based on equivalent current injection. This method closely aligns with the classical grid search algorithm, which relies on successive load flows in the grid. However, the proposed method proves to be much faster in terms of computation time than the classical grid search algorithm.

In [64], the authors present two new methodologies for optimizing the placement of DGs in wholesale electricity markets using optimal power flows (OPFs). The optimization problem aims to either optimize the social welfare of the population or maximize the profit for the organization. Candidate locations for DG placement are identified based on Locational Marginal Prices (LMPs), which reflect local market prices.

In reference to [65], a methodology is presented for the strategic siting of Distributed Generators (DGs) grounded on the reactive power flow as a foundational criterion for allocation. This particular approach was executed within the distribution test system situated in the Kumamoto region of Japan. Through a meticulous scrutiny of the influence of DGs on the voltage profile and stability of the system, the study expounded on the sensitivity of renewable energy placements. This intricate analysis led to the identification of optimal positions for the incorporation of wind and solar installations, culminating in a fortification of the system's stability parameters. The envisaged system configuration yielded tangible benefits including a reduction in power losses and a diminution in the requisite size of compensatory devices. In [66], an optimal DG placement solution is proposed using practical swarm optimization (PSO) and Differential Evolution Algorithms (DEA). This technique is applied to two IEEE 33-bus and 69-bus systems. According to the authors, combining PSO and DEA resulted in a more successful reduction of system losses in DG placement problems. Additionally, [67] presents a method for optimizing the siting and sizing of multiple DGs using PSO and compares the results with Improved Analytical (IA) techniques. The research finds that PSO is the most effective optimization technique for small DG sizes, leading to enhanced voltage profiles and reduced loss percentages. Overall, these studies demonstrate various approaches, including analytical methods, swarm-based optimization techniques like PSO, and optimal power flows, to determine the optimal placement and sizing of DGs in distribution systems, resulting in improved system stability, reduced power loss, and enhanced overall grid performance.

In [68], the authors propose using different types of DGs to supply real and reactive power to standard IEEE-33 bus radial distribution system. They compare the results of the Particle Swarm Optimization (PSO) approach with analytical methods. The PSO approach not only reduces line losses but also minimizes the size of DGs and satisfies permissible voltage limits, outperforming analytical methods.

In [69], GA, PSO, Differential Evolution (DE), and hybrid genetic algorithms are utilized to determine the optimum size and placement of DG sources in order to minimize active power losses and improve voltage stability. The GA/PSO algorithm is found to be highly efficient in achieving optimal distributed generation placement and size compared to GA, PSO, and DE algorithms applied individually. Reference [70] proposes a PSO method to study the Optimal Power Flow (OPF) of a power system integrated with renewable generators, such as wind or solar power, in an IEEE 30-bus system. The goal is to minimize transmission losses. Meanwhile, [71] presents an effective PSO-based method for reducing real and reactive power losses and enhancing bus voltage profiles in a 33-bus system with four DG units. PSO outperforms GA in terms of computation time, iterations, and power loss reductions. In [72], the PSO algorithm is used to minimize real power losses and enhance voltage profiles in radial distribution networks. Comparisons with Hybrid Harmony Search (HAS), modified plant growth simulation algorithm (MPGSA), and GA indicate the proposed PSO approach as more effective. Reference [73] introduces a strategy using Sensitivity Analysis to determine DG locations and PSO to calculate DG sizes, aiming to minimize power losses in distribution networks. This approach is tested on an IEEE 33-bus system, showing improved voltage profiles and reduced real power loss. The results demonstrate the effectiveness of the proposed strategy for optimal DG placement. In [74], the paper concludes that evolution algorithms, particularly PSO and its variants, are frequently used to place DGs. Artificial Intelligence (AI) methods are popular for solving both simple and complex optimization problems due to their efficiency and good convergence characteristics. A comprehensive review of DG placement methods reveals that optimizing the size and location of distributed generators can fulfil incremental demand, reduce real power losses, and enhance network performance.

The methodology encompassing Sensitivity Analysis and the Particle Swarm Optimization (PSO) technique has been employed for the purpose of identifying the optimal location and size of components within a real radial distribution network situated in Libya. This approach entails a comprehensive exploration of the network's response to variations in various parameters, thereby assessing its sensitivity to these changes. Subsequently, the PSO algorithm, a nature-inspired optimization technique, is leveraged to fine-tune the placement and dimensions of components to achieve the desired goals.

By integrating Sensitivity Analysis, the study gains insights into the network's behaviour, enabling informed decisions on where and how to introduce Distributed Generators (DGs) or other components. The PSO algorithm then optimizes the DGs' locations and sizes in a manner that minimizes losses, enhances voltage stability, and fulfils operational constraints. This holistic approach synergizes the analytical power of Sensitivity Analysis with the computational prowess of the PSO algorithm, ultimately resulting in an effective and efficient solution for optimal DG placement and sizing in the Libyan radial distribution network.

2.7. Load Forecasting

In the operation of electric power systems, load forecasting holds significant importance in the planning of the electricity industry. Accurate load forecasts are essential not only for economic growth but also for daily functioning of the power system. They play a vital role in the development of future power generation, transmission, and distribution systems. However, the accuracy of electric load forecasting is influenced by various uncertain and uncontrollable factors, such as economic growth, human activities, country policies, and climate change [75].

Electric load forecasts can be classified into different categories based on the prediction durations. Some researchers divide them into short-term, medium-term, and long-term forecasts [76], while others categorize them into long-term, mid-term, short-term, and very short-term forecasts.

- Long-term load forecasting covers periods of over one year to more than 20 years into the future and is essential for strategic planning, construction of new generation units, and developing power supply and distribution systems.
- Medium-term load forecasting typically spans from a week to a year and is used for maintenance scheduling, fuel purchases, energy trading, and revenue estimation.
- Short-term load forecasting is critical for managing utilities' day-to-day operations and spans from one hour to a week.
- Very short-term load forecasts range from a few minutes to an hour ahead and are used for real-time control [77].

There are two main types of electric load forecasting models: multi-factor forecasting methods and time series data-based forecasting methods. Multi-factor forecasting models are based on causal relationships between influencing factors and cross-sectional data. In contrast, time series forecasting relies on historical data. Time series forecasting is preferred over multi-factor methods as it avoids complexities and non-objective factors that may affect forecast accuracy, making it faster and easier. Time series forecasting models can be further divided into statistical models, machine learning models, and hybrid models [78][79].

Traditional statistical methods were initially used for electrical load forecasting, but advancements in modern science have led to significant improvements in load forecasting technologies. Machine learning models have gained popularity as they offer attractive alternatives to conventional methods, especially for dealing with non-linear data patterns and large computational possibilities [80]. For short-term load forecasting, various methods have been utilized, including Autoregressive Integrated Moving Average (ARIMA), Radial Basis Functions (RBF), Adaptive Neural Fuzzy Inference Systems (ANFIS), back-propagation algorithms with neural networks built on RBF, and extreme learning machines (ELMs). However, these methods may suffer from performance degradation when used for long-term predictions [81]. Artificial intelligence-based data analysis has undergone significant advancements through the adoption of machine learning, particularly deep learning techniques. These approaches have revolutionized data analytics by building models based on real data rather than relying solely on predictions.

To ensure the most effective learning model, it is crucial to determine the specific domain of the application. For time series data modelling, Recurrent Neural Networks (RNNs) have proven to be more suitable [82]. RNN-based models can be categorized into different types based on their ability to remember input data. Unlike vanilla RNNs, which lack the capacity to retain past information [83], the Long Short-Term Memory (LSTM) network, a specialized type of RNN, excels in modelling relationships between lengthy input and output data. These RNN-based models, known as feedback-based models, can effectively learn from historical data by incorporating various gates within their network architecture. This allows them to preserve past data and create predictive models by integrating past and present information in a sequential manner, moving from left to right through the input data [84]. This capability to handle sequential information makes them well-suited for tasks like time series data analysis.

In [85], researchers implemented an LSTM deep recurrent neural network to predict the electrical load time series for the Province of Ontario, Canada. The study concluded that their proposed method is reliable. Similarly, in [86], an LSTM-based RNN framework was utilized to forecast electricity consumption in individual residential households. The LSTM networks demonstrated efficient learning of long-term dependencies between sequential data with the proposed model. In the context of load forecasting, [87] presented an LSTM-RNN-based technique and compared its accuracy with Support Vector Regression (SVR)-based load forecasting. The study found that the LSTM-RNN approach achieved better accuracy, especially when using only historical load data. Furthermore, authors in [88] found that the LSTM-based forecasting method outperformed other techniques, including seasonal autoregressive integrated moving averages (SARIMA), nonlinear autoregressive neural networks with exogenous inputs, support vector regression (SVR), and traditional neural networks. Another study, [89], also emphasized the potential of Long-Short Term Memory (LSTM) neural networks as one of the most promising methodologies for time series forecasting.

In summary, the cited references collectively highlight the success and reliability of LSTM-based models for various time series forecasting tasks, particularly in the domain of electrical load prediction. The study unveiled that the identification of historical load data plays a crucial role as the most influential factor in determining the appropriate methods for long-term predictions. The type and granularity of the collected historical data also significantly impact the choice of methods. In the case study conducted in AL Marj city, Libya, this research applied the LSTM neural network model using MATLAB as their analysis tool.

2.8. Summary

This chapter provides an extensive review of diverse research inquiries pertaining to the economic viability of renewable energy systems (RES), encompassing both stand-alone off-grid configurations and interconnected grid setups. The selection process, following a thorough review, determined that the Homer Pro software emerged as a pivotal instrument for discerning the optimal configuration of hybrid systems, specifically within the contextual boundaries of Al Marj City, Libya. This strategic utilization aimed at harnessing the potential of renewable energy sources. The study undertook a multifaceted assessment, encompassing critical parameters such as the Net Present Cost (NPC) and the Cost of Energy (COE), measured in units of $/kWh. This investigation contributes substantively and innovatively to the existing reservoir of knowledge. Furthermore, the chapter offers an extensive survey of optimization methodologies, particularly focused on the latest research surrounding the optimal positioning and sizing of Distributed Generators (DGs) within distribution networks. Various optimization techniques were surveyed in the context of diverse systems to enhance the performance of power grids. Previous studies unequivocally demonstrate that well-placed DGs can offer grid benefits by endowing localized flexibility and aiding in mitigating blackout incidents.

The proposed methodology incorporates Sensitivity Analysis coupled with the Particle Swarm Optimization (PSO) technique to ascertain the optimal locations and dimensions of components within a real radial distribution network located in Al Marj city, Libya. This combined approach encompasses an exhaustive exploration of the network's response to parameter variations, thereby gauging its sensitivity to these alterations. Subsequently, the PSO algorithm, an optimization technique inspired by natural phenomena, is employed to finely calibrate the placements and sizes of components to achieve predefined objectives. By merging Sensitivity Analysis with the computational efficacy of the PSO algorithm, the study facilitates an in-depth understanding of the network's behaviour. This understanding informs judicious decisions about the integration of Distributed Generators (DGs) or other components. The PSO algorithm then optimizes the positioning and capacities of DGs to minimize losses, improve voltage stability, and adhere to operational constraints. This holistic approach, uniting analytical rigor with computational robustness, culminates in a potent solution for the optimal placement and sizing of DGs within the radial distribution network of Al Marj city, Libya. Lastly, the significance of Load Forecasting in power system operations is underscored, elucidating its role in aiding operators' consequential decisions encompassing generation dispatch and unit commitment. The cumulative body of references accentuates the efficacy and dependability of LSTM-based models in diverse time series forecasting tasks, specifically within the domain of electrical load prediction. The literature indicates that the historical load data's identification assumes a pivotal role as the most influential factor in selecting suitable methodologies for long-term predictions. Moreover, the nature and granularity of amassed historical data significantly influence the methodological choices made. The presented case study conducted in AL Marj city, Libya, stands as a practical exemplar, employing an LSTM neural network model implemented using MATLAB for analysis.

CHAPTER 3

Addressing Missing Load Demand Challenges in Al Marj City

3.1. Introduction

For distribution networks, analysis of load profiles is a common practice when measurements can be accessed. However, load profiles access is often challenging. This is because of a variety of reasons, including failures in metering, missing/lost data, partial or total, security issues or failure to maintain responsibilities for prompt data collection. In situations where data gaps arise, it becomes imperative to estimate "corrected" values. In the case of Libya, due to the prevailing war and conflict conditions, a substantial amount of daily and monthly load data spanning several years is entirely missing. Specifically, the absence of monthly load data dates back to 2012, while the hourly load data remains missing since 2008, as indicated in the latest reports furnished by the General Electricity Company of Libya (GECOL). This chapter presents a methodological solution that aims to address the aforementioned data gaps and facilitate the calculation and analysis of load demand for Al Marj City in 2018. A singular calculation approach tool design is employed for this purpose. The study primarily focuses on devising strategies to cope with missing data in the context of electricity distribution networks. Additionally, the investigation takes into account projected population growth and leverages the load ratio derived from available real data. By incorporating these elements, the proposed methodology endeavours to provide a comprehensive understanding of the load demand scenario in the absence of complete and up-to-date data.

3.1.1. Load Shedding In Developing Countries

In an electrical system that lacks sufficient generation to meet the demand, load shedding is used to balance the load with the supply. This is done by temporarily switching off some loads in different parts of the system. There are many countries that utilize load shedding, including India, Sri Lanka, Lebanon, Iraq, Zambia, Nigeria and Libya, when their electrical supplies can't meet demand during peak times. In Libya, GECOL is currently dealing with the issue of managing power outages through a strategy of rotational load shedding, also referred to as rolling blackouts. The objective is to establish a fair load-shedding plan that applies to all customers [90].

3.2. Case Study Area

The city of Al-Marj in Libya is faced with a critical issue of frequent power outages due to its reliance on power plants located in the nearby city of Benghazi. The lack of a local power plant in the region has perpetuated the city's dependency on electricity from the main stations located in the north of Benghazi. This has been exacerbated by the current shortage in Libya's electricity capacity, which has resulted in prolonged blackouts lasting for days. The current electricity system in Al-Marj is primarily dependent on imported electricity from the north station of Benghazi through high-voltage electricity lines. In addition, diesel generators are used to generate locally electricity to meet the load demands of residences during power outages. Thus, Al-Marj relies on electricity produced from a centralized station located far away from the city, which poses significant challenges to the city's energy security.

However, one of the significant issues facing the current electricity system in the area is the lack of accurate load demand data required to planning a reliable renewable energy system. This missing data presents a significant barrier to the effective integration of renewable energy sources into the region’s energy mix [90].

3.3. Methodology for Designing Demand Load

Various Libyan cities have experienced power outages that lasted for hours to days due to increasing energy demand. Currently, this issue is a key challenge for the Libyan electricity sector, and the lack of capacity in the system has led the government to take action to address the inadequate energy supply [91]. Figure 3.1 illustrates the methodological approach for calculating the missing electrical demand load. As the data load for upgrading the electricity supply systems is lacking, the growth rate of the population of Al Marj and load ratio for realistic past data are assessed to determine the required load capacity.

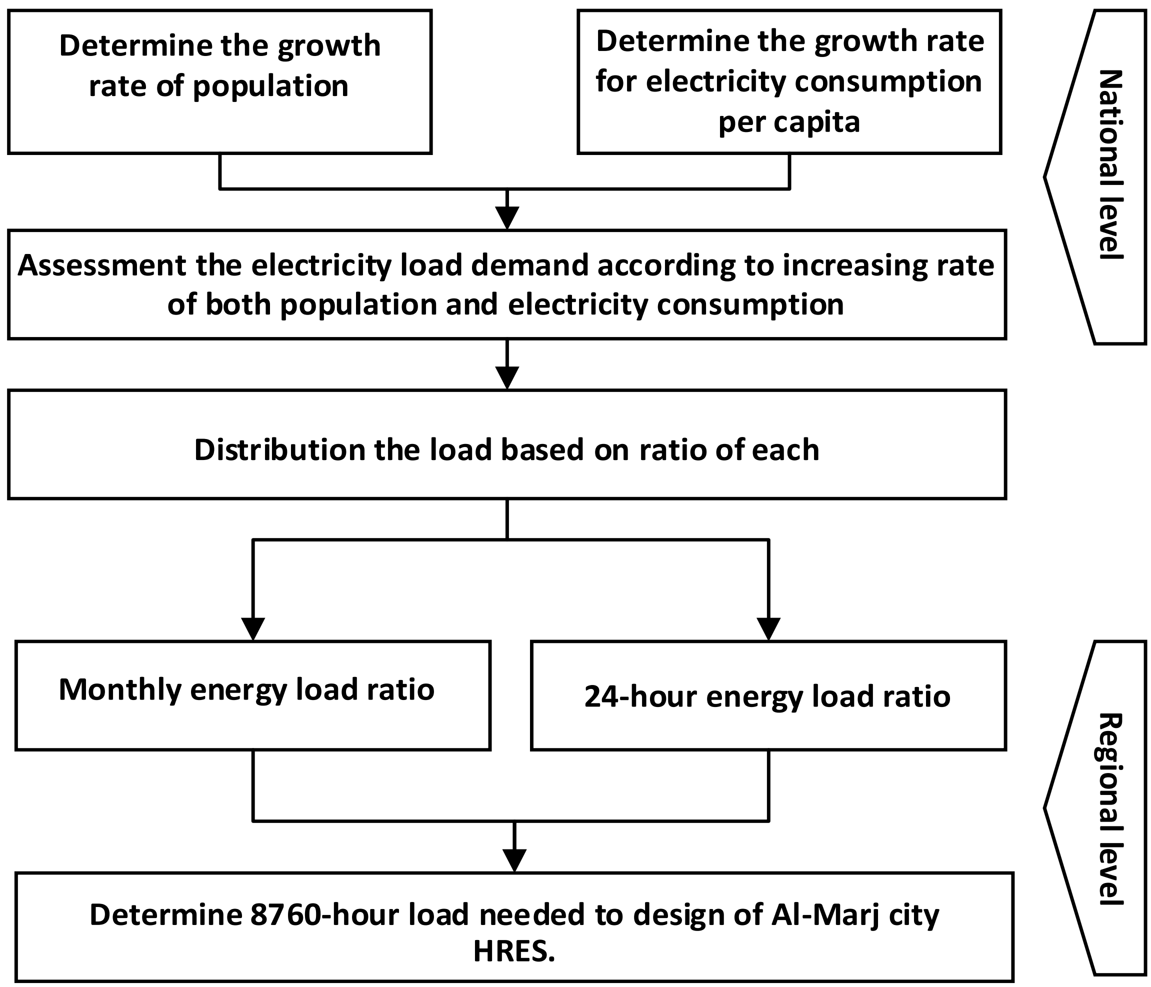

Figure 3. 1 Methodological approach in the calculation of electricity demand load.

3.3.1. Libya's Real Population Growth Rate

The population growth rate was computed for the area under study for calculating the missing electrical load data. Figure 3.2 and Table 3.1 are illustrating the average growth rate of the Libyan population from 2010 to 2018 [91]. The data shows that the population has expanded over the past nine years. The growth rate increase and decrease with varying years, where the average growth rate is 0.94 %. This represents the average growth rate over these nine years and was used to calculate the forthcoming electricity demand loads proportionate to the rise in population.

Table 3. 1 Average of growth rate of population 2010-2018

Year	Growth rate of population %
2010	1
2011	0.8
2012	0.6
2013	0.5
2014	0.7
2015	0.9
2016	1.1
2017	1.4
2018	1.5
Average	**0.94**

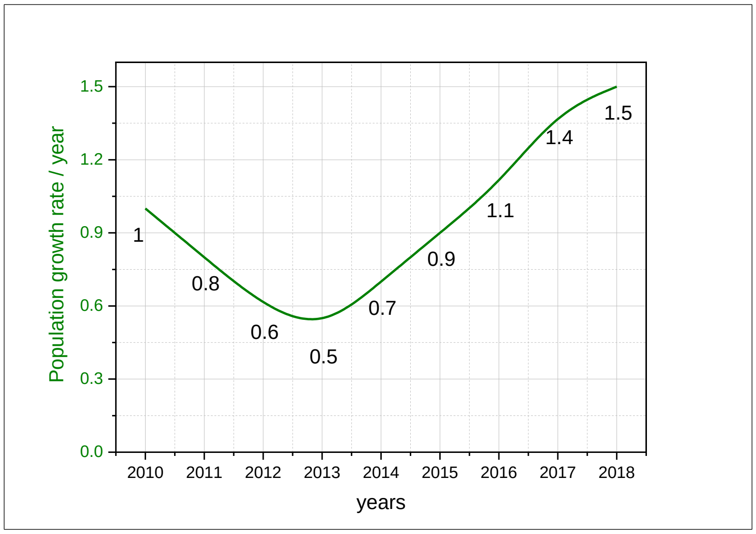

Figure 3. 2 Average growth rate population in Libya.

3.3.2. Electricity Consumption Per Capita In Libya

The actual data of the growing rate of electricity consumption per capita in Libya was measured as the increase per annum in the consumption of energy from 2003 until 2010, as shown in Figure 3.3 and Table 3.2 [91]. Based on these data, the electricity consumption per capita is predicted in the year of study 2018 in Al Marj city.

Table 3. 2 Real data of electricity consumption in Libya 2003-2010

Year	Electricity Consumption /Capita (kWh)	Growth rate %
2003	2947.7	-
2004	3106.2	5.4
2005	3427.8	10.3
2006	3792.6	10.6
2007	3792.7	0.02
2008	3165.4	-16.5
2009	3142.33	-0.73
2010	3361.75	6.9
Average	**-**	**2.28**

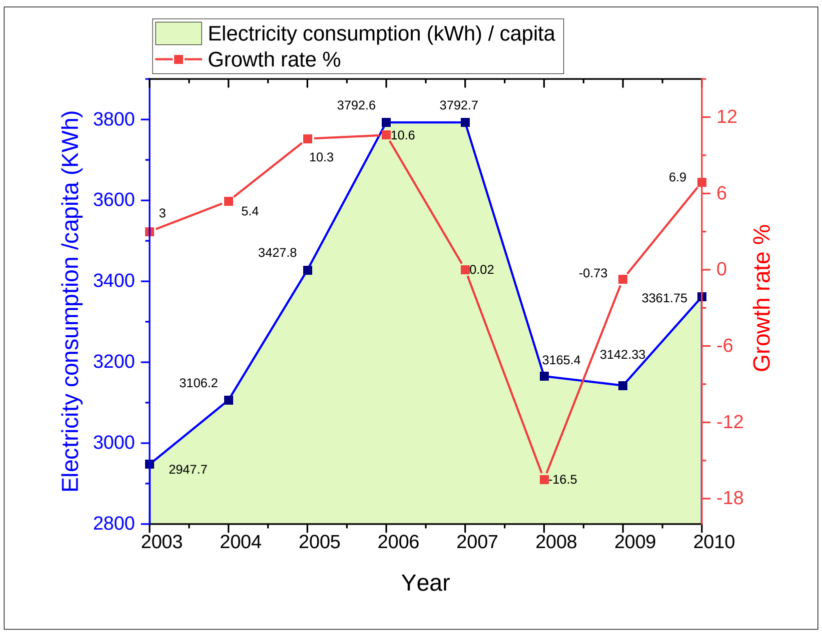

Figure 3. 3 Real data of electricity consumption in Libya.

3.4. Electricity Load Calculation for Al Marj City

The population of the south of Al Marj city is estimated to be 84406 people. A growth of 2.28% per year is applied using data from the World Bank [92]. Table 3.3 illustrates the necessary electrical loads for Al Marj city in 2018, which are calculated using the average increase in population and per capita electricity usage. The figures 3.4, 3.5 and 3.6 are ilustrating the population growth rate, electricity consumption per capita and lectricity demand per year respectivelly.

Table 3. 3 Calculation details for expected required electricity loads in of Al Marj city.

Year of the project	Population growth rate (=0.94 % ann.)	Electricity consumption growth rate (kWh per capita) (= 2.28% ann.)	Energy demand (MWh/year)
2012	79,800	3,516	280,576.8
2013	80,550	3,596	289,657.8
2014	81,307	3,678	299,047.1
2015	82,071	3,762	308,751.1
2016	82,842	3,848	318,776
2017	83,620	3,936	329,128.3
2018	84,406	4,025	339,734.1

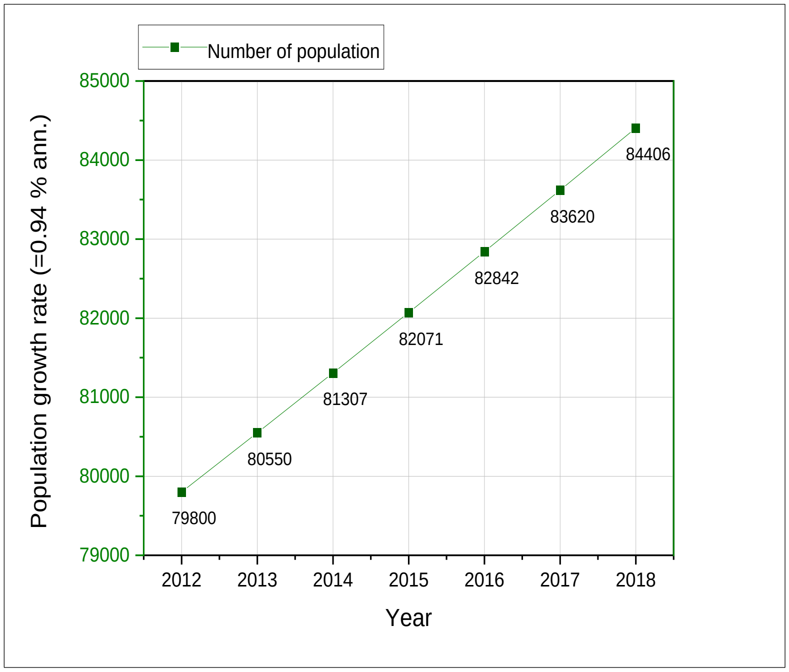

Figure 3. 4 Population growth rate in Al Marj city.

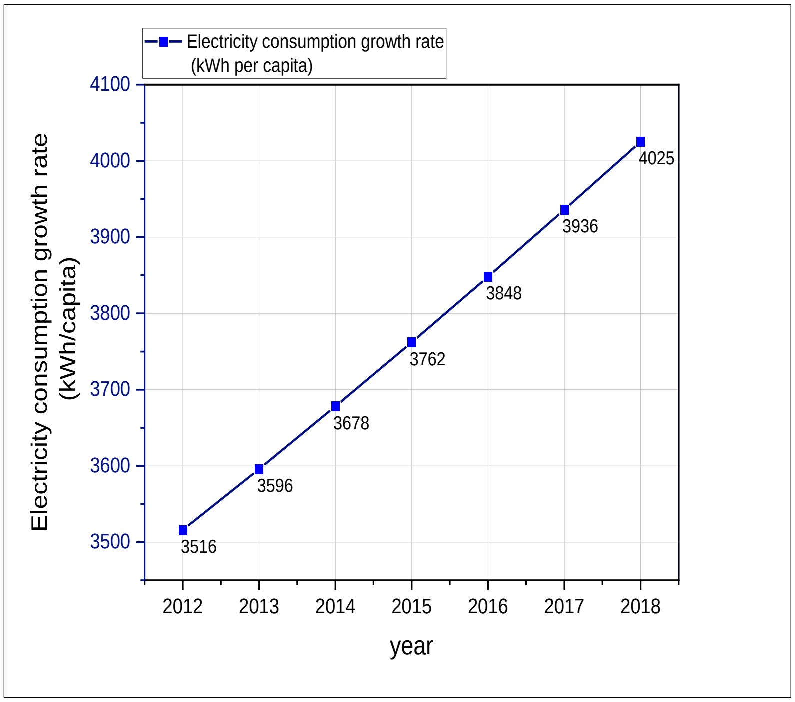

Figure 3. 5 Electricity consumption kWh per capita in Al Marj city.

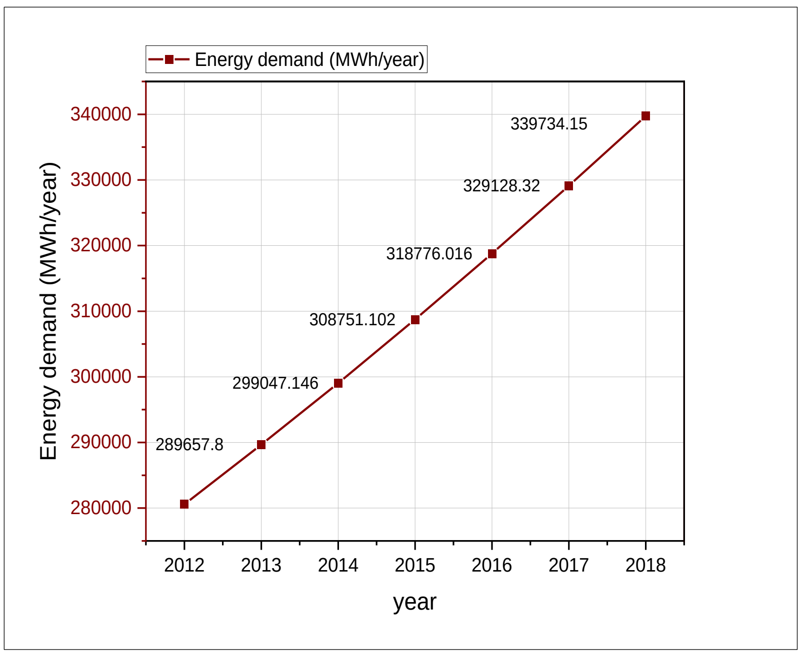

Figure 3. 6 Electricity demand MWh per year in of Al Marj city.

The load is calculated by considering both increasing rates of population and rates of electrical power consumption per capita. Table 3.4 presents the factors used to assess electricity system loads, with load estimates for Al Marj in 2018, which is used as input for building the HRES in

Homer Pro software. This case study will be used as a reference case for several regions in Libya that are facing the same issue.

Table 3. 4 Load estimates for Al Marj city in 2018.

Description	Values
Population estimate, Al Marj city for 2018.	84,406 people
The expected annual average of electricity consumption per capita at the start of the project in 2018	4,025 kWh/ann./capita
Energy demand required by the system in 2018 to meet Al Marj electricity demands	339,734.1 MWh/year
The average monthly energy demand for Al Marj city.	28311.17 MWh/month
Daily average energy demand for Al Marj city	930.77 MWh/day
Hourly average energy demand for Al Marj city	38.782 MWh

3.5. Determining Electricity Load Ratio at The National Level

3.5.1. Determining Monthly Load Ratio With Real Data

In Libya, various statistics have been gathered related to monthly energy load through the work of the GECOL in investigating peak usage. The data collected by GECOL can be found in a report covering the period 2007-2012, providing several years of comparable statistical information. The base case study for Al Maraj city relies on the data of last year of GECOL's monthly load curves which was 2012 for a monthly load, considering the growth of both numbers of inhabitants and demand for electricity. The 2012 load curves are provided in Table 3.5. This data covers total consumption of electrical power across Libya's electricity network, including all sector of consumption. Therefore, this load data gives both the highest and lowest electricity use across Libya and over consumption sectors including residential neighbourhoods, consumption by industry, agricultural production, commercial premises, and public utility facilities and infrastructure. Loads have been averaged across each month to produce monthly load curves [93].

Table 3. 5 Monthly load demand in Libya for 2012 year.

Month	Max. Load (kW)	Min. Load (kW)	Ave. Load (kW)	Monthly load (%)
Jan	5,560,000	3,200,000	4,380,000	9.13
Feb	5,627,000	2,388,000	4,007,500	8.35
Mar	4,925,000	2,205,000	3,565,000	7.43
Apr	3,850,000	2,080,000	2,965,000	6.18
May	4,355,000	2,307,000	3,331,000	6.94
Jun	5,300,000	2,638,000	3,969,000	8.27
Jul	5,740,000	3,851,000	4,795,500	9.99
Aug	5,981,000	3,807,000	4,894,000	10.2
Sep	5,595,000	3,135,000	4,365,000	9.1
Oct	5,250,000	3,408,000	4,329,000	9.02
Nov	4,220,000	2,201,000	3,210,500	6.69
Dec	5,810,000	2,547,000	4,178,500	8.7
Total			47,990,000	100

Due to security circumstances in the country, the monthly load data from 2012 to 2018 is unavailable, making it impossible to directly utilize the historical data for this period [94]. However, it is crucial to account for the rising energy demands annually, which is not reflected in the outdated 2012 data. To address this issue, Figure 3.7 illustrates an alternative approach for determining the monthly energy ratio, incorporating the actual data from 2012. This approach takes into consideration the population growth rate to estimate the expected demand in 2018. By adopting this method, the study aims to align with the changing energy demands over time while accounting for the unavailability of specific monthly load data.

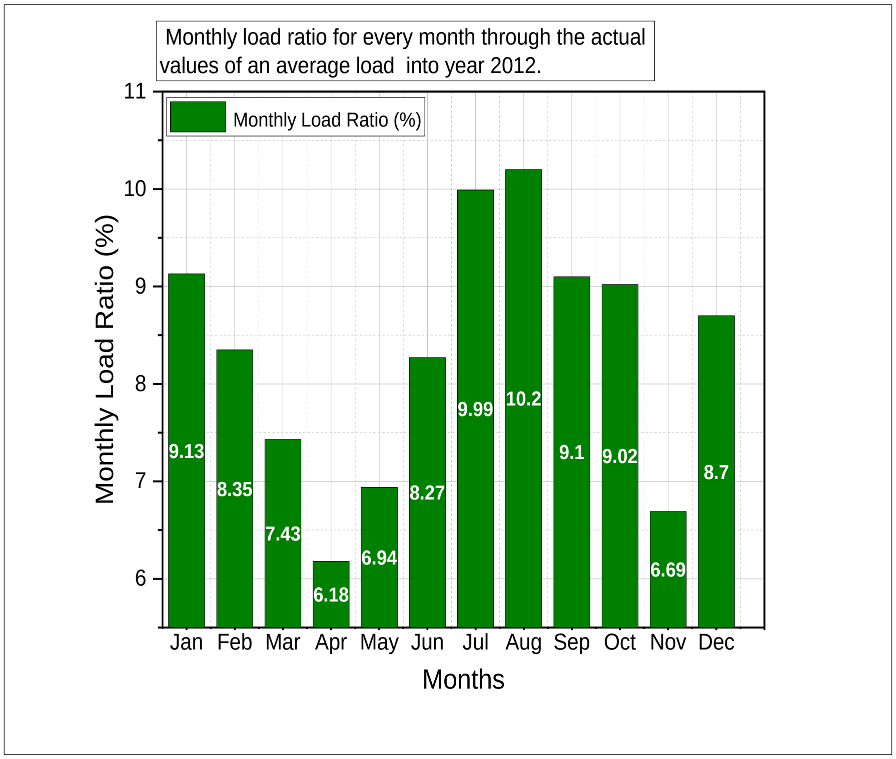

Figure 3. 7 Actual load ratio for every month based on monthly load in the year 2012.

3.5.2. Use of Actual Data To Determine Daily Load Ratio

According to the most recent report by GECOL, the availability of hourly load data has been absent since 2008. Subsequent updates or measurements of hourly load data have not been provided by GECOL in recent times. Consequently, in order to estimate the hourly load curve for a base case study in 2018, we must rely on two key factors: the population growth rate and the load ratio derived from the last documented hourly data. These factors will serve as the basis for approximating the hourly load curve in the absence of updated data.

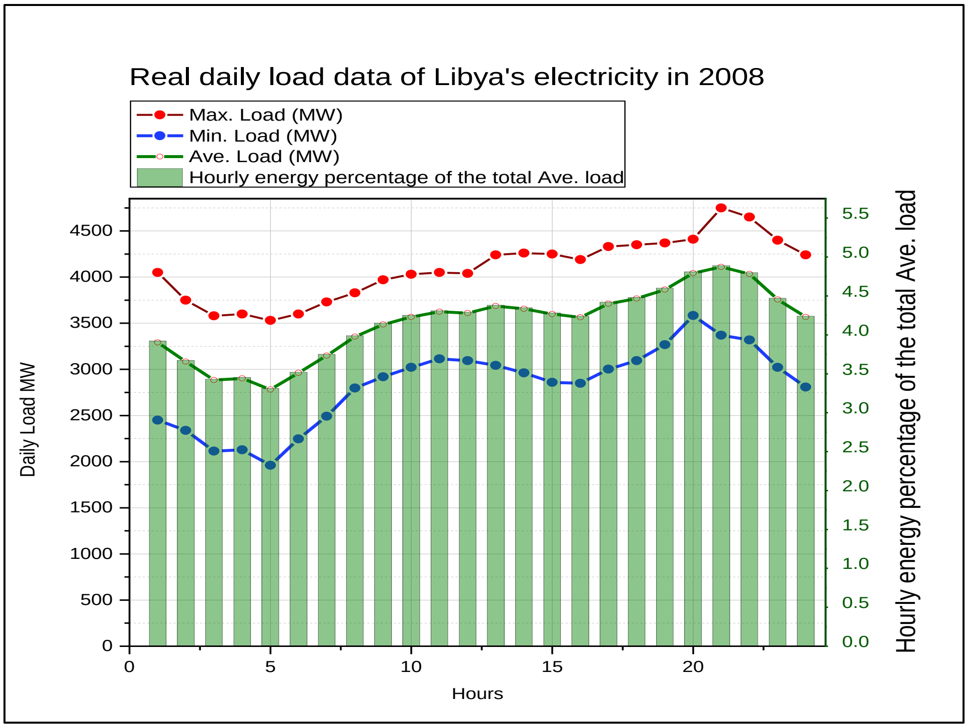

Figure 3. 8 Last real daily load data and hourly energy ratio in Libya for year 2008.

Table 3.6 and Figure 3.8 illustrate in detail the daily load values of Libya's electricity network in 2008, which has been used to determine hourly average percentages based on the average daily load values.

Table 3. 6 Realistic daily load data in Libya-2008.

Hour	**Max. Load (kW)**	**Min. Load (kW)**	**Ave. Load (kW)**	**Hourly energy (%)**
1	4,050,000	2,400,000	3,225,000	3.92
2	3,750,000	2,290,000	3,020,000	3.67
3	3,580,000	2,070,000	2,825,000	3.43
4	3,600,000	2,085,000	2,842,500	3.45
5	3,530,000	1,920,000	2,725,000	3.31
6	3,600,000	2,200,000	2,900,000	3.52
7	3,730,000	2,440,000	3,085,000	3.75
8	3,830,000	2,740,000	3,285,000	3.99
9	3,970,000	2,860,000	3,415,000	4.15
10	4,030,000	2,960,000	3,495,000	4.25
11	4,050,000	3,050,000	3,550,000	4.31
12	4,040,000	3,030,000	3,535,000	4.29

13	4,240,000	2,980,000	3,610,000	4.38
14	4,260,000	2,900,000	3,580,000	4.35
15	4,250,000	2,800,000	3,525,000	4.28
16	4,190,000	2,790,000	3,490,000	4.24
17	4,330,000	2,940,000	3,635,000	4.42
18	4,350,000	3,030,000	3,690,000	4.48
19	4,370,000	3,200,000	3,785,000	4.6
20	4,410,000	3,510,000	3,960,000	4.81
21	4,750,000	3,300,000	4,025,000	4.89
22	4,650,000	3,250,000	3,950,000	4.8
23	4,400,000	2,960,000	3,680,000	4.47
24	4,240,000	2,750,000	3,495,000	4.24

3.6. Defining Electricity Load Demand at The Regional Level

3.6.1. Design Load Per Month For Al Marj, 2018 At Regional Level

In 2012, the monthly average energy load ratio was calculated and shown in Figure 3.7. Using this data and the information on electricity consumption kWh per capita in Al Marj city, which is shown in Figure 3.5, the monthly load for the case study in 2018 was determined. A "top down" approach is used to calculate regional figures through scaled down from national level to the regional level. The results of this calculation can be found in Table 3.7.

Table 3. 7 Monthly loads in Al Marj city in a year 2018 based on actual monthly ratio.

Month	Monthly distribution load (%)	Yearly load of system (kWh/year)	Monthly load of system (kWh/mon.)	Daily load of system (kWh/day)
January	9.13	339734150	31017727.9	1000571.8
February	8.35	339734150	28367801.5	1013135.7
March	7.43	339734150	25242247.35	814266.04
April	6.18	339734150	20995570.47	699852.3
May	6.94	339734150	23577550.01	760566.12
June	8.27	339734150	28096014.21	936533.8
July	9.99	339734150	33939441.5	1094820.6

August	10.2	339734150	34652883.3	1117834.9
September	9.1	339734150	30915807.65	1030526.9
October	9.02	339734150	30644020.33	988516.78
November	6.69	339734150	22728214.64	757607.15
December	8.7	339734150	29556871.05	953447.45
Average	**-**	**-**	**28311179.2**	**930639.962**

3.6.2. Daily Load Design For Al-Marj For Year 2018 At Regional Level

This section discusses the process of calculating daily energy ratio estimates for designing the hourly load of Al-Marj city in 2018, using averaged daily load curves from 2008. Load ratios are determined for each hour of the 24-hour period, as shown in Figure 3.9. The daily energy ratios are then calculated by summing the average loading values for the day, and a similar approach is used to determine monthly load ratios. These energy ratios are then used to determine the daily load for Al-Marj in 2018 and beyond, based on the case study.

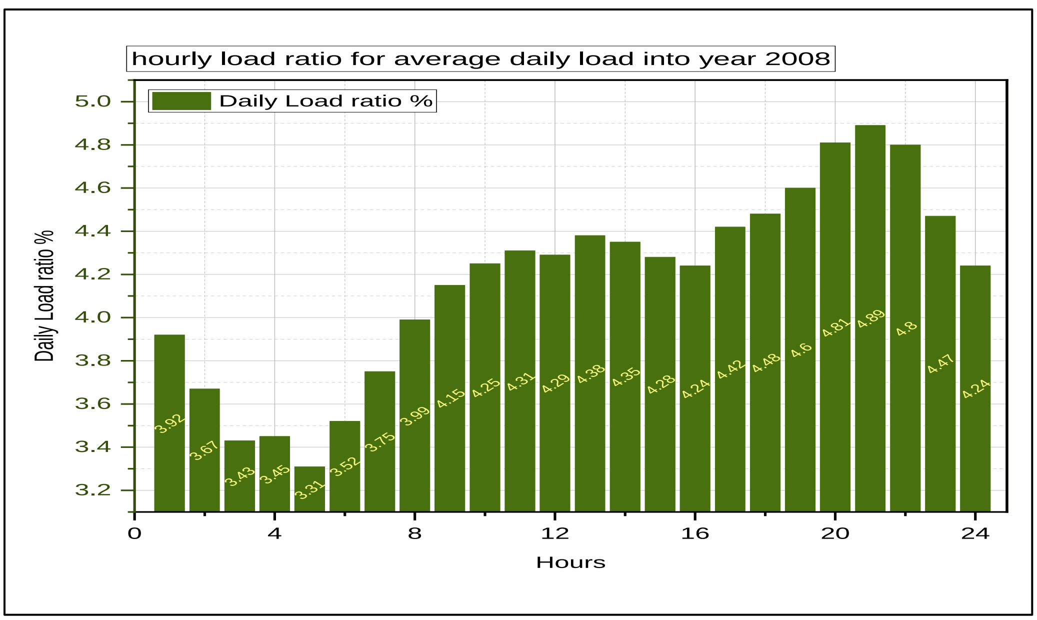

Figure 3. 9 Load ratio for 24-hour according to the values of average daily load curve for Libya's 2008.

It is assumed that the daily loads in Al-Marj are similar across all days within a month but vary across different months. This means that the load values for January 1st and January 31st are assumed to be similar, but the load for January is different from that of March. This assumption is made because no data on day-to-day variance is available for profiling these periods. Figure 3.10 displays the estimates for the load demand by average hourly load in 2018. Additionally, it shows the daily loading curves for each month in the form of an energy ratio per hour.

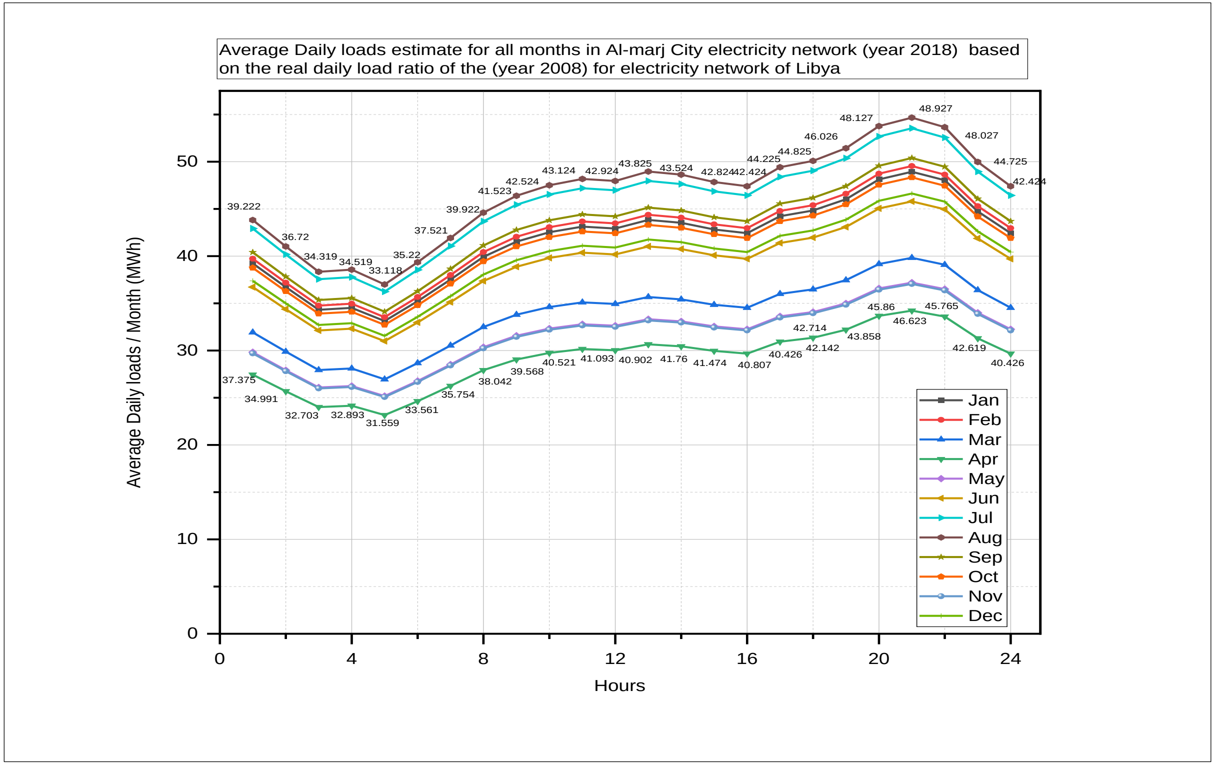

Figure 3. 10 Daily loads estimation as hourly average load in each month for electricity network of Al Marj City in 2018.

3.7. Summary

This chapter introduces a methodological approach aimed at addressing the calculation of electricity load demand for the design of a Hybrid Renewable Energy System (HRES) in the city of Al Marj, Libya. The design process is faced with a significant challenge due to the unavailability of both monthly and daily load data. Specifically, the monthly load data has been missing since 2012, while the hourly load data has not been updated since 2008, as indicated in the latest reports provided by the General Electricity Company of Libya. The proposed methodology calculates monthly and daily load demand for 2018 considering the last real data collected by the GECOL applying real population growth rate and the load ratio derived from the last documented data scaled down at the regional level. The methodological approach used in this study can be applied to other Libyan regions for estimating daily and monthly demand where significant amounts of data are missing. These results will be used in Chapter 4 to determine the alternative means of energy production instead of the fossil energy resources currently used.

CHAPTER 4

Distributed Generation Technologies to Address Blackouts in The Libyan Power System A Case Study of Al-Marj City

4.1. Introduction

This chapter introduced different solutions using renewable energy technologies to overcome the random blackouts that happen in Libya. Al-Marj city in Libya was considered for the case study. The modelling study was performed using HOMER Pro software tool. Two scenarios were considered one with PV and the other with wind generation. For both scenarios a Hybrid Renewable Energy System (HRES) was designed based on the available resources at the project site and considering both standalone and grid-connected cases. While these scenarios are different in terms of the type of renewable energy used, as well as the configuration of the hybrid system, they do however share similarities in the design methodology. For this reason, the same equipment was utilized in all scenarios related to systems configuration and their components, such as a diesel generator, battery, inverter, and grid utilities. Furthermore, the equipment considered was consistent in size and cost to make the study's findings as accurate as possible and compare the benefits of each proposed solution.

4.2. Methodology

Libya experienced a complete uprising against its ruling political regime, leading to a protracted civil war characterized by intense inter-factional fighting and the use of heavy weapons. This ongoing crisis has posed significant challenges for the maintenance and operation of the country's power grid infrastructure, which has recently resulted in regular unscheduled and scheduled power outages. These outages are most common in the peak demand periods in the summer and winter seasons and have only become frequent and critical after the Libyan uprising in 2011. Consequently, the primary objective of this study was to develop a robust methodology for designing a hybrid renewable energy system in Al-Marj City, with the ultimate aim of achieving self-sustainability in energy production. Designing a HRES for Al Marj city is focused on meeting electricity needs in the region and satisfying the shortages of electricity supply that are causing outages in the existing electricity supply system. Currently, there is no use of renewable energy technologies for generating electricity in Libya, and there is no contribution from renewables in the electricity production. Therefore, this study is focused on Al Marj City exploring the potential of renewable energy technologies in this area. To meet the electricity demand in the region, the system design criteria is focusing on the minimum cost of energy (COE), most cost-effective system, and optimal system type (OST). The selection of Al-Marj City as the focal point of this research was influenced by its unique characteristics, notably being built according to modern infrastructure standards established by the United Nations after a significant earthquake struck the region in 1963. This post-disaster reconstruction presented an opportunity to create a city with a well-designed infrastructure, making it an ideal candidate for exploring innovative energy solutions.

4.2.1. Software Tool Selection

Many software models and tools were developed to assess RE and energy efficiency technologies. Al Marj City HRES was designed using the Hybrid Optimization of Multiple Energy Resources (HOMER) developed by NREL. In both off-grid and grid-connected systems, HOMER offers a wide range of configuration options that allow for the design of a hybrid energy system (HES). Additionally, the software utilizes several technologies and parameters that allow it to model energy systems more accurately than other modelling tools. Moreover, its National Aeronautics and Space Administration (NASA) resource database provides measurements such as solar radiation, wind speed, air temperature, and site coordinates, which are important parameters for the design. Additionally, HOMER Pro simulates energy consumption and production for each hour of the year and matches the available renewable sources with the RE production that can be achieved. The software process is classified into three parts: simulation, optimization, and sensitivity analysis. As part of HOMER's evaluation of technical feasibility, it simulates and calculates sensitivities for selected system configurations throughout the year. The Net Present Cost (NPC) encompasses the combined expenses associated with the investment, operation, maintenance, and replacement of a HRES. To identify the most suitable system that adheres to the technical constraints of the NPC, HOMER Pro conducts comprehensive simulations of the energy system design, considering various configurations. Through sensitivity analyses, HOMER Pro assesses the effects of input variables on system configurations and measures the resultant changes in these configurations [96]. HOMER Pro's optimization algorithm flow chart shown in Figure 4.1, the process starts with defining the system configuration and input data, including the location information, load demand, weather data, economic data, and constraints. Then, the simulation is run to analyse the system behaviour. Next, the optimization process takes place, aiming to minimize the cost of energy (COE) and the net present cost (NPC) while ensuring the fulfilment of the load demand. The optimization process may involve adjusting various parameters, such as the size and location of distributed generators or renewable energy sources. After the optimization, feasible solutions are sorted based on their performance. This could involve categorizing winners according to specific criteria, such as the lowest COE or the highest NPC. Finally, the process reaches the end.

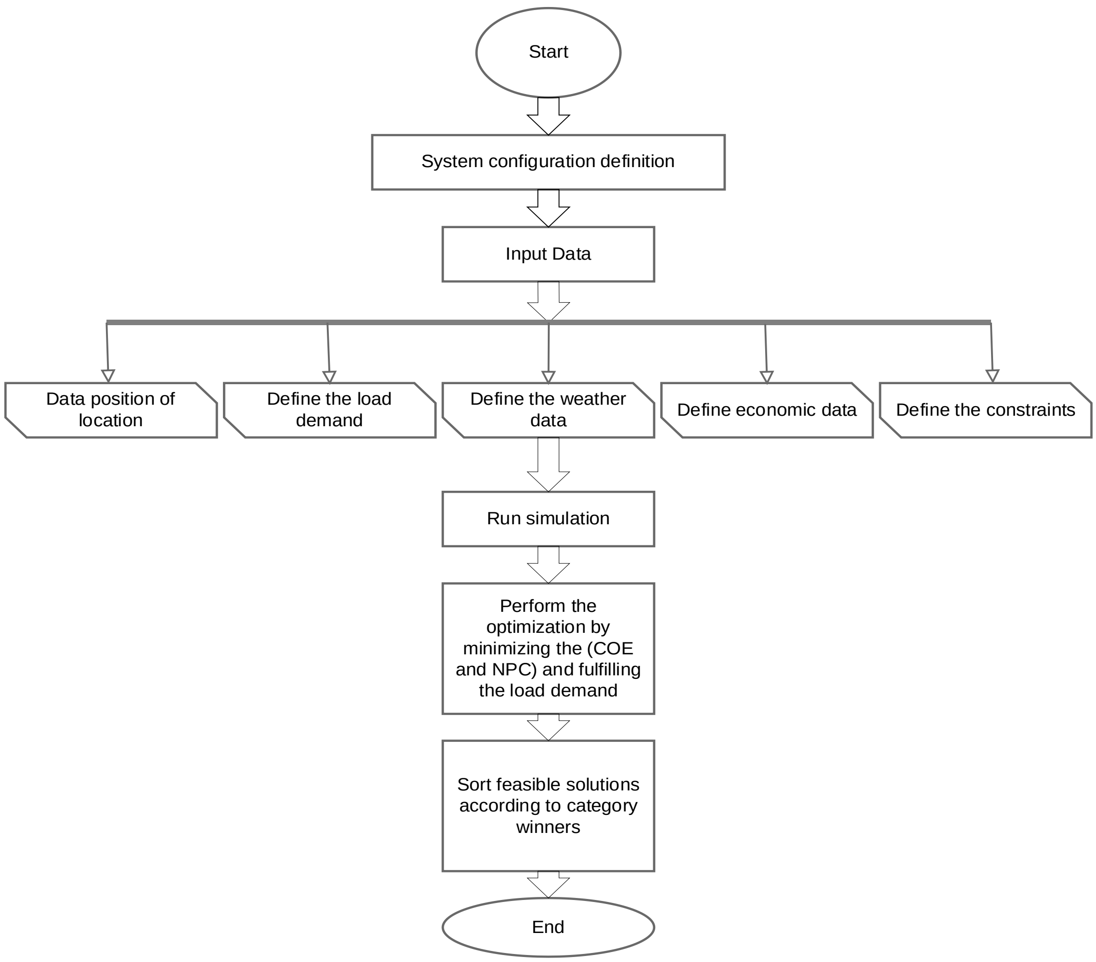

Figure 4. 1 HOMER Pro optimization algorithm flowchart simplified.

Figure 4.2 provides a visual representation of a window within the HOMER Pro software, illustrating the process of inputting the electrical load data that the system must satisfy to prevent any unmet load. The load demands for Al Marj City, which have been pre-configured in Chapter 3, are utilized as the input for the system. In this case, the load type is specified as an AC load supply. By selecting AC load, the software accommodates the specific requirements of the electrical load in Al Marj City, ensuring accurate modelling and analysis within the system design.

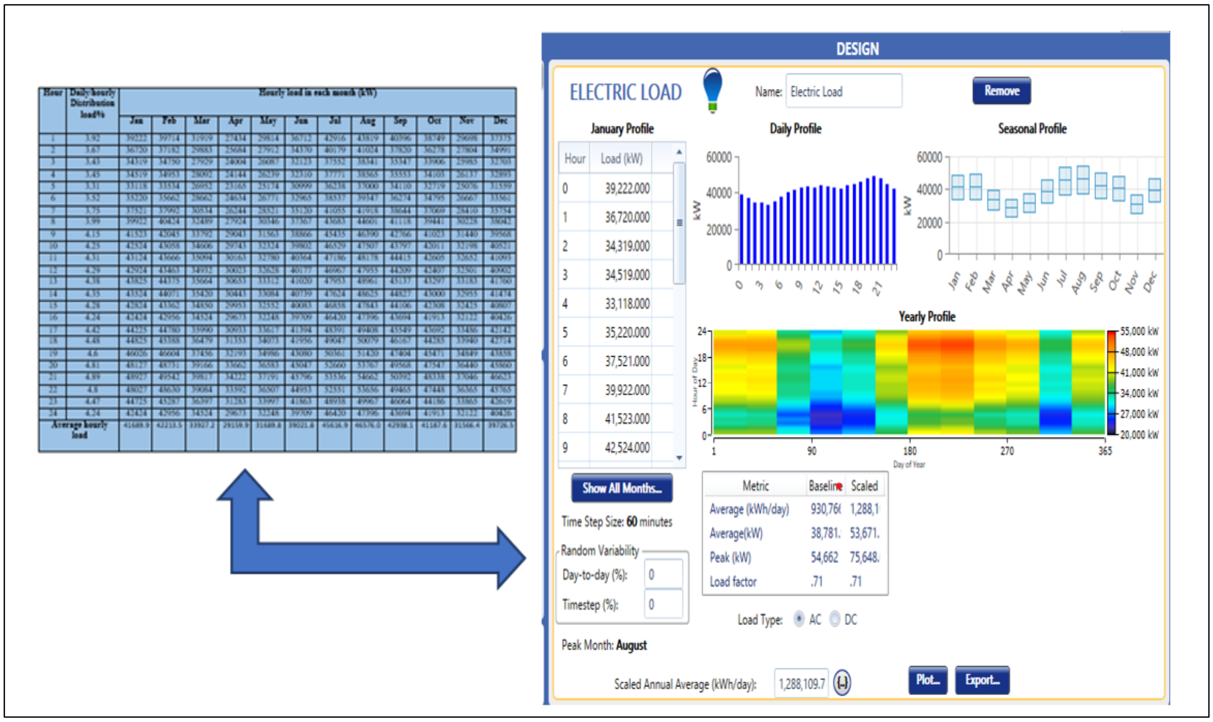

Figure 4. 2 Input data load window of HOMER Pro software.

4.2.2. System Characterization

The case study centres around Al Marj City, situated on Libya's Mediterranean coast [97], as depicted in Figure 4.3 and described in Table 4.1. The study underscores the significance of accurately determining the energy demand to design an efficient HRES for the region. Properly sizing the HRES requires a thorough estimation of the annual energy consumption, as outlined in detail in Chapter 3. The process involves the meticulous collection and evaluation of data relating to the load profile, available solar radiation, and wind speed in the region. These data act as essential prerequisites, providing critical insights into the energy demand and resource availability, which in turn inform the optimal sizing and configuration of the HRES. By emphasizing the importance of gathering and analysing these key data points, the study establishes a solid foundation for designing a sustainable and effective HRES that meets the specific energy needs of Al Marj City.

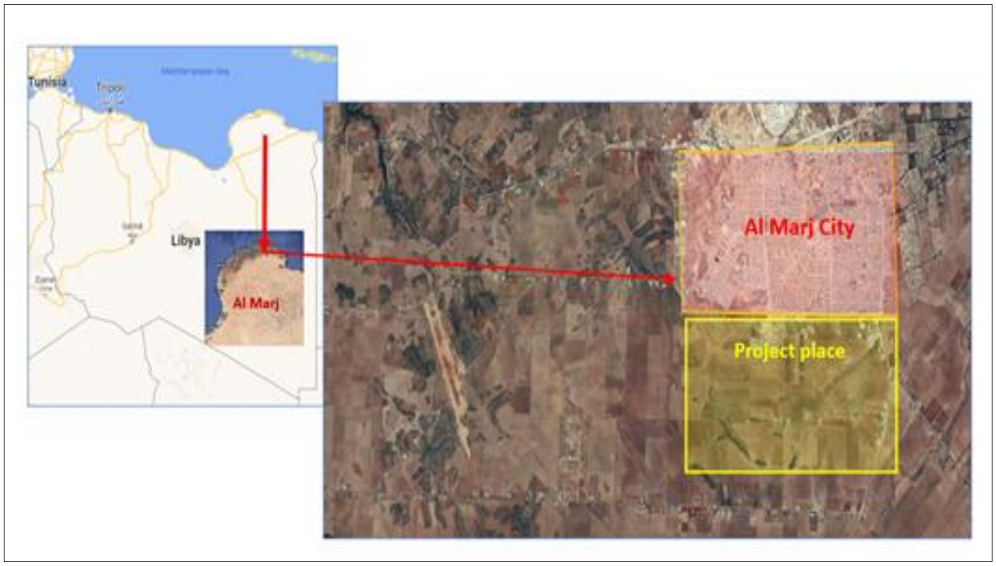

Figure 4. 3 Al-Marj City's location [97].

Table 4. 1 Description location of project.

Item	Description
Place of project	Al Marj City
Latitude	32° 29' 16.73" N
Longitude	20° 49' 54.26" E
Landform	Land almost flat
Annual average daily radiation	5.4 kWh/m^2/d
Annual average daily wind speed	4.3 m/s

To design the HRES for Al Marj City, several components are considered, such as solar photovoltaic (PV) panels, wind turbines, a converter, a diesel generator, and a battery bank. However, before proceeding with the system sizing, the first step in the study involves collecting and evaluating relevant data. The primary focus is on the load profile, available solar radiation data, and wind speed data for Al Marj City. These factors play a crucial role in determining the energy requirements and optimizing the configuration of the HRES specifically for Al Marj City. The collected data is providing valuable insights for designing an efficient and effective energy system.

- **Load profile**

In this case study, the load demand is an important aspect of the power-generating system. The study focuses on Al-Marj City and provides detailed information on the average monthly and daily energy load for the year 2018. These load profiles are illustrated in Figure 4.4 and Figure 4.5, and they are described in detail in Chapter 3. The minutely described load profiles offer valuable insights into the energy consumption patterns of Al-Marj City, which are important for accurately designing and optimizing the power-generating system.

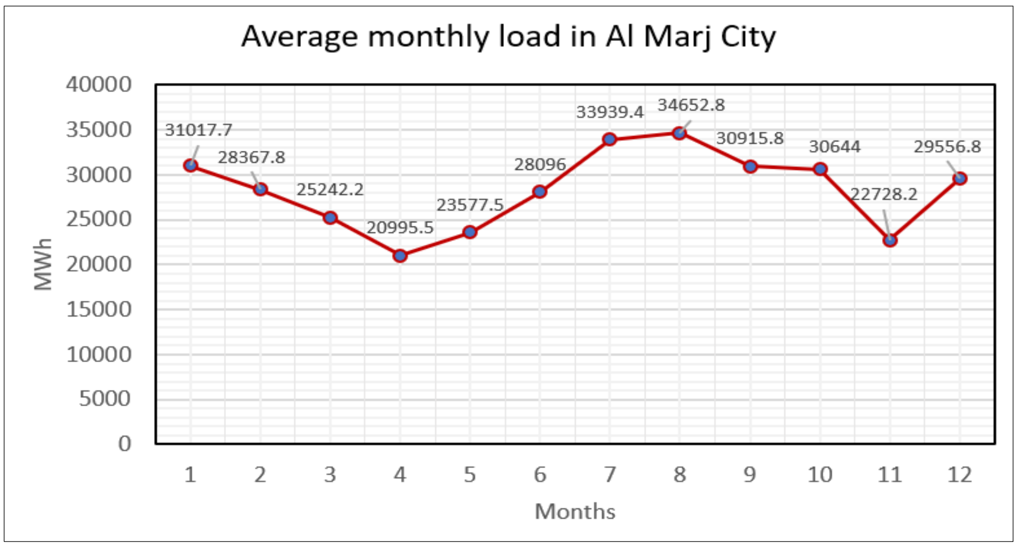

Figure 4. 4 Monthly energy load profile in 2018 in Al-Marj City.

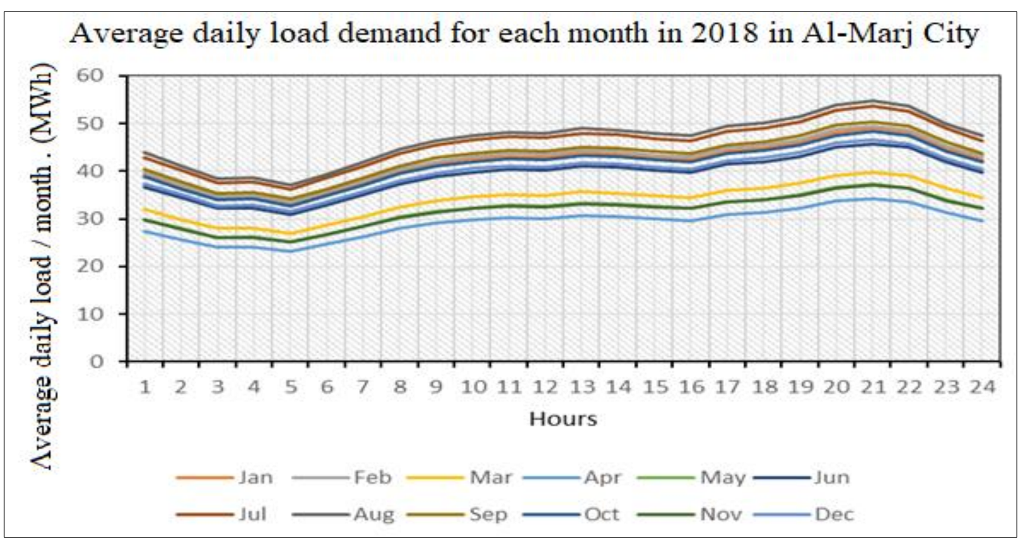

Figure 4. 5 Average daily load demand for each month in 2018 in Al-Marj City.

- **Solar radiation**

In this study, the solar radiation data was obtained from NASA's weather reports. Figure 4.6 presents the average daily solar radiation values throughout the year at the project site under consideration. According to the location, the annual average solar radiation at the site is determined to be 5.4 kWh/m^2/day. To acquire this data, built-in weather database that includes solar radiation data obtained from NASA reliable sources is used from HOMER Pro. [98].

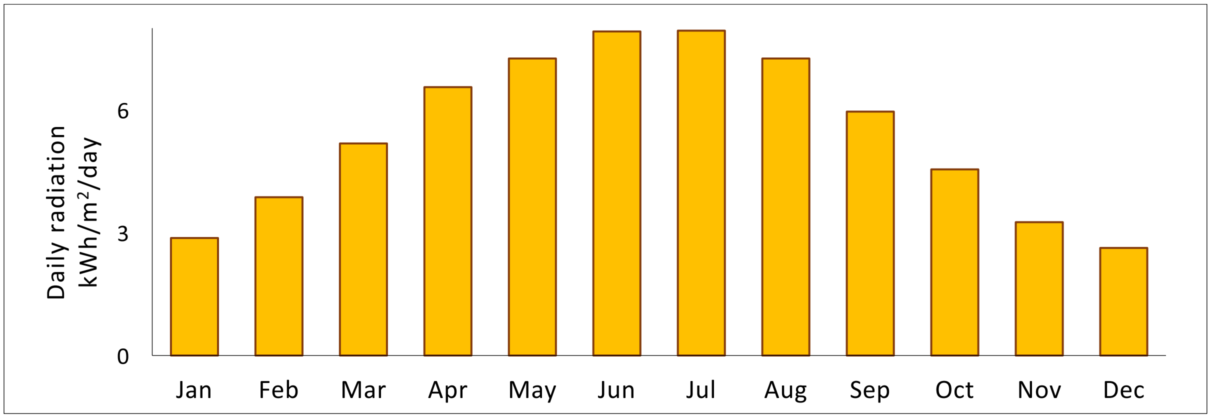

Figure 4. 6 The average daily solar radiation per month at the proposed site.

- **Wind speed**

Wind speed data was collected from Weather Base reports. Figure 4.7 provides is presenting the annual average wind speed at the proposed project site, revealing an average value of 4.3 m/s. This information is significant for the design and assessment of the renewable energy system. [99].

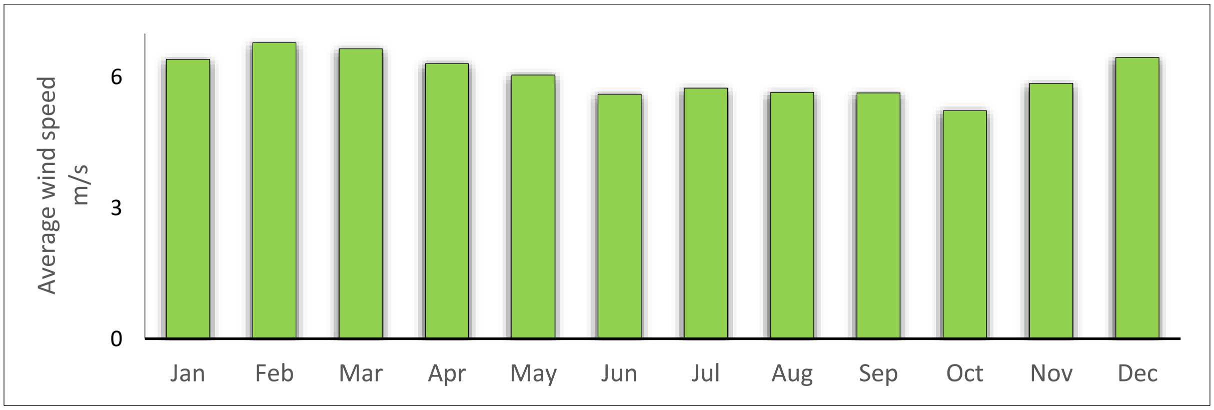

Figure 4. 7 Annual average wind speed in the proposed project site.

- **PV array**

The PV array model is a thin-film PV panel, which incurs a capital expenditure of $3,000 per kW. This cost encompasses the PV subsystem, which involves shipping, setup hardware, tracking system, wiring, project site transportation, and installation expenses. Additionally, the specified replacement cost of each PV panel model is $2,100. Table 4.2 provides further details regarding the specifications of the PV panel, and additional parameters can be found in Appendix A [100].

Table 4. 2 Specification of the PV panel

Rated capacity	200,000 kW
Temperature coefficient	-0.5
Operating temperature	45^0 C
Efficiency	15%

- **Wind turbine**

For the study case in the Al-Marj city, the general wind turbine recommended by HOMER Pro is considered. Wind turbine E-82 E2 is selected based on the following characteristics:

1. Based on the average wind speed of 4.3 m/s in the selected location there is potential of supply energy in surplus of 280 kW.

2. Opting for high-output capacity wind turbines, such as the E-82 E2, offers a distinct advantage when compared to smaller counterparts that necessitate additional land for installation, as highlighted in reference [101]. The technical specifications and cost details for the E-82 E2 turbine type can be found in Table 4.3 and Appendix A.

Table 4. 3 The technical parameters and cost values of the wind turbine

Technical specification E-82 E2	**Rotor**
Rated power	2,000 kW
Rotor diameter	82 m
Capital cost	1,642,500 $
Replacement cost	1,511100 $
Hub height	138 m
Lifespan	20 years

- **Batteries**

The energy storage in a hybrid system can be costly since the system depends on the battery if there is inadequate electricity generated from the system. A lead-acid battery (such as the 6CS25P battery model) is preferred in designing HRES as they have a high storage capacity, which is common requirement in systems with RES stochastic output. The valve regulates the lead-acid battery at a nominal voltage of 6 V with max charge/discharge current for a 1hr discharge of 278.8A, a capacity of 820Ah, and roundtrip efficiency of 80%. The capital cost required is 1,200$ and the replacement cost is 1,000$, whereas the operation and maintenance costs needed to maintain the battery are expected to be 5$ per year [101]. More specifications are presented in Appendix A.

- **Converter**

The converter, also known as an inverter, converts electricity from direct current (DC) to alternating current (AC). It is a significant component in the system, accounting for approximately 5% of the total installation cost. The cost of the converter was assumed within the range of typical costs. The capital cost was estimated at $700 per kilowatt (kW), and the replacement cost was assumed to be $550 per kW.

The operation and maintenance (O&M) cost of the inverter was estimated at $3 per kW per year. These cost assumptions were based on international pricing estimates, considering specific factors relevant to the project site, such as transportation to the location, shipping, and installation requirements. For all sizes considered in the system, the inverter efficiency was assumed to be 90%, while the rectifier efficiency was assumed to be 85%. It was also assumed that the inverter can operate simultaneously with the AC power. These assumptions and cost estimates are inputs for the economic analysis and optimization of the HRES, allowing for accurate evaluation of the overall system costs and performance [101].

- **Generators**

In Libya, most electricity is generated by diesel generators, such as in Al-Marj city. For this reason, the diesel generator was selected in the design instead of gasoline or natural gas [102]. In HOMER Pro software, the generator input was specified as AC mode with a minimum load ratio of 30%. The minimum load ratio was selected to this value for avoiding the generator running at a low load value, because if the generator is running below 25% of the load ratio this regime will increase the effect of corrosion, the lifetime, and the maintenance cost. Load ratios and lifetimes are obtained from HOMER Pro's online portal (year 2018) [101], which provides information about the distributed generators various capacities and expected life span as presented in Appendix A.

- **Diesel fuel**

Libya stands out as one of the most cost-effective places globally when it comes to fuel prices. This is mainly attributed to the substantial support provided by the Libyan government in subsidizing fuel, reaching an amount exceeding 6.3 B$ in recent times. Throughout the past few decades, diesel prices in Libya have remained remarkably low, not surpassing 0.031 dollars per Litre, and this trend has continued until 2023 in the present oil market situation [103][104].

These fuel prices are exceptionally low compared to the average diesel costs observed worldwide, making it significantly cheaper for consumers in Libya, even considering the actual production costs thus, the diesel prices considered are based on actual costs, taking into account transportation expenses, as the project area is located far from the diesel sources. Therefore, the fuel price was assumed to be 0.20 dollars per Litre. Furthermore, to assess the impact of potential variations in diesel costs, a sensitivity analysis was conducted. Different scenarios were examined by assuming increased diesel prices at 0.20, 0.40, 0.60, and 0.80 dollar per Litre. These variations allowed to evaluate the cost of energy under different diesel price conditions, providing valuable insights into the project's economic viability and sustainability.

4.3. Optimal Size of The System and Results

Two models were developed in HOMER Pro for the PV and wind turbine system. These models were analysed in two different scenarios: the island mode and the grid-connected mode. This comparison of results allows for a comprehensive understanding of their capabilities and efficiency under different operational conditions, aiding in making informed decisions for optimizing the system configuration based on specific energy requirements and project conditions.

4.3.1. The PV Hybrid Energy System Model

The schematic of the PV hybrid energy system is illustrated in Figure 4.8.

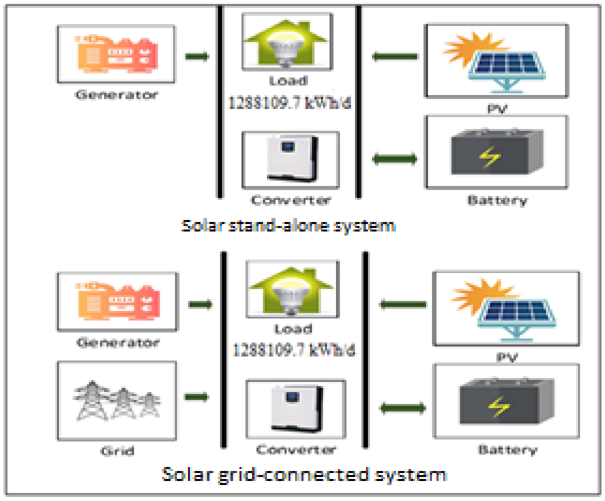

Figure 4. 8 Schematic diagram of the solar hybrid energy system configurations for both stand-alone and grid connected configurations.

Table 4.4 presents the results obtained from HOMER Pro simulations for the zero-percentage capacity shortage case. The corresponding configuration consists of a 160 MW PV array, a 60 MW diesel generator, an 80 MW inverter, and a 30 MWh battery storage system. The NPC for this configuration is calculated to be 2.27 B$, and the cost of energy is estimated to be 0.193 $/kWh. These results provide valuable information about the economic feasibility and performance of the proposed PV hybrid energy system under the specified conditions.

Table 4. 4 The Optimal size of the PV stand-alone system.

PV stand-alone system served load at lowest cost of energy						
Architecture				**Cost**		**System**
PV (MW)	Generator (MW)	Battery (MWh)	Converter (MW)	Life cycle cost ($)	Cost of energy ($/kWh)	Capacity shortage (%)
160	60	30	80	2.27B	0.193	0.02

The total annual electric power production of this system is 143,802 MWh/year from the PV array and 353,899 MWh/year from the diesel generator, of which 28.9% is produced by the PV array and the rest from the diesel generator. The monthly average power production is shown in Figure

4.9. The total energy consumption of the load is 470,160 MWh/year, leaving a very low excess electricity production of a 0.630% and no unmet load. The percentage of renewable fraction is 24.7%.

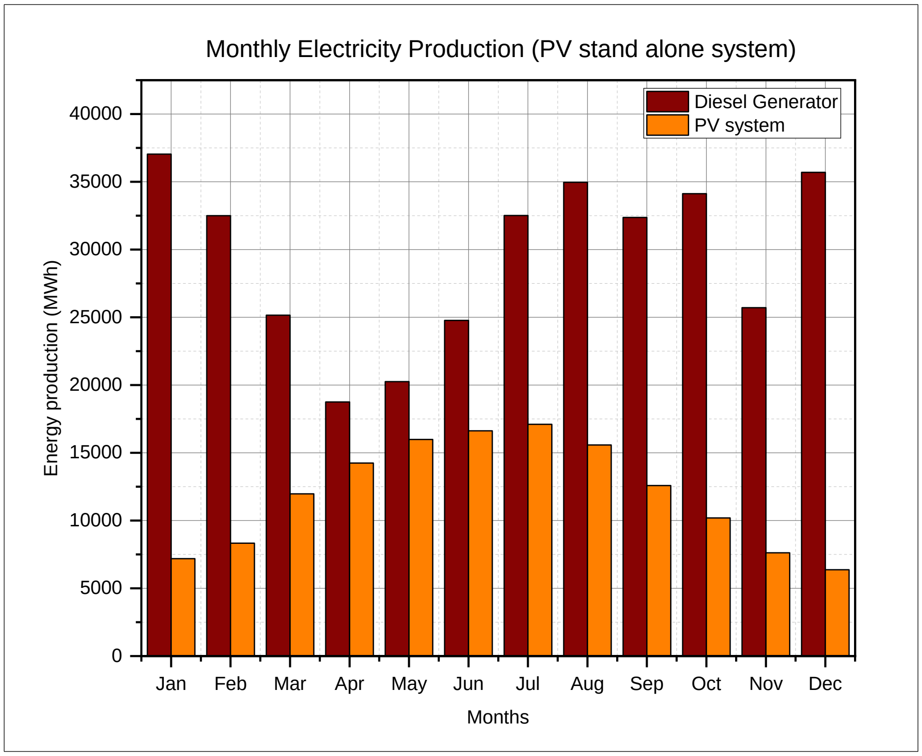

Figure 4. 9 The monthly electricity production for the stand-alone solar hybrid energy system.

During the sensitivity analysis, the optimization process revolves around variables assumed in the design, assessing their impact on the cost of energy. These variables encompass solar irradiation, with values considered at maximum, average, and minimum levels. Additionally, various fuel prices are taken into account, including the actual price of 0.2 US$/L, along with estimated prices of 0.4, 0.6, and 0.8 US$/L, to gauge their influence on the outcomes. Figure 4.10 displays the test results for sensitivity analysis of all system components in the stand-alone solar system design. This figure illustrates the impact of each sensitivity variable on the different components of the system. Notably, the results indicate that achieving a low cost of energy at 0.15 $/kWh is attainable under specific conditions: a solar radiation level of 7.9 kWh/m^2/day, a diesel fuel price of 0.2 $/L, and a renewable energy sharing percentage of 31.2%. These findings provide clear insights into how variations in these key parameters influence the overall performance and cost-effectiveness of the stand-alone solar system design.

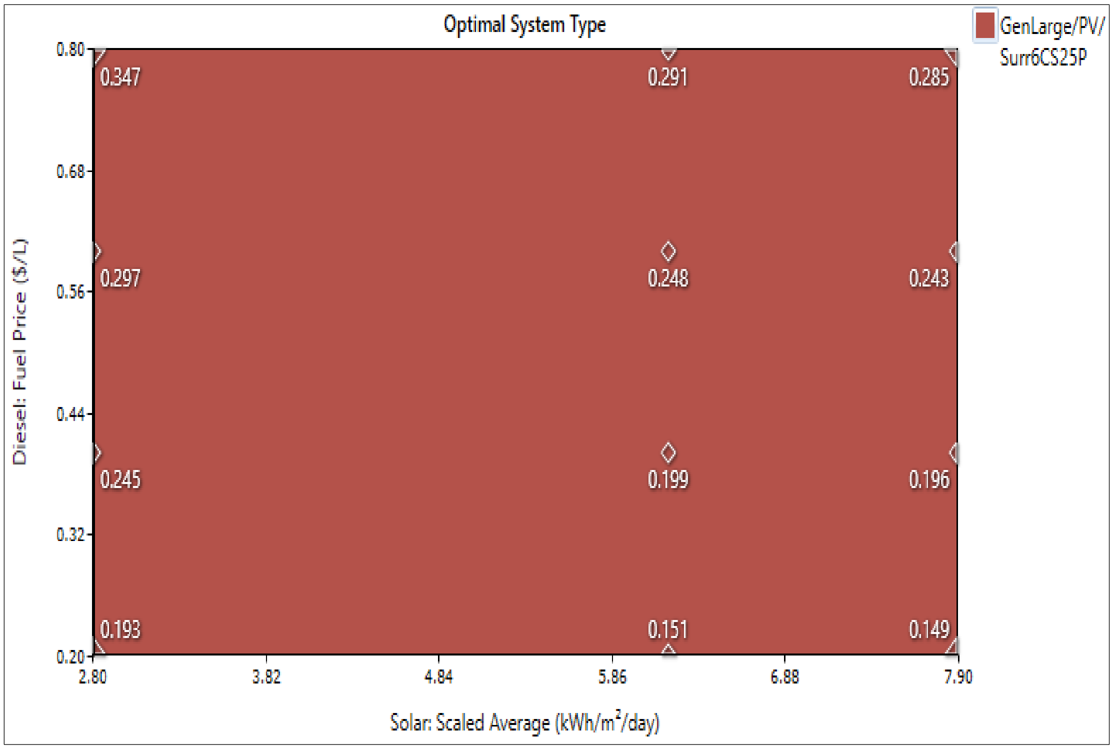

Figure 4. 10 Sensitivity outcomes of the optimal solar system operating in a stand-alone configuration.

In Figure 4.11, sensitivity results depict the impact of varying diesel fuel prices alongside solar radiation levels set at maximum, average, and minimum values. The analysis reveals a direct correlation between the escalating diesel rates and the increased cost of energy. Interestingly, despite fluctuations in total solar radiation and diesel costs, there were no discernible alterations in the sizes of system modules such as the battery, diesel generator, and converter. Noteworthy changes were only observed in the PV size, particularly when the cost of diesel surpassed 0.4 $/L. These observations underscore the substantial influence of diesel price fluctuations on the overall energy cost within the system and shed light on how these variations specifically affect the sizing of individual components, particularly the PV array, across different cost scenarios.

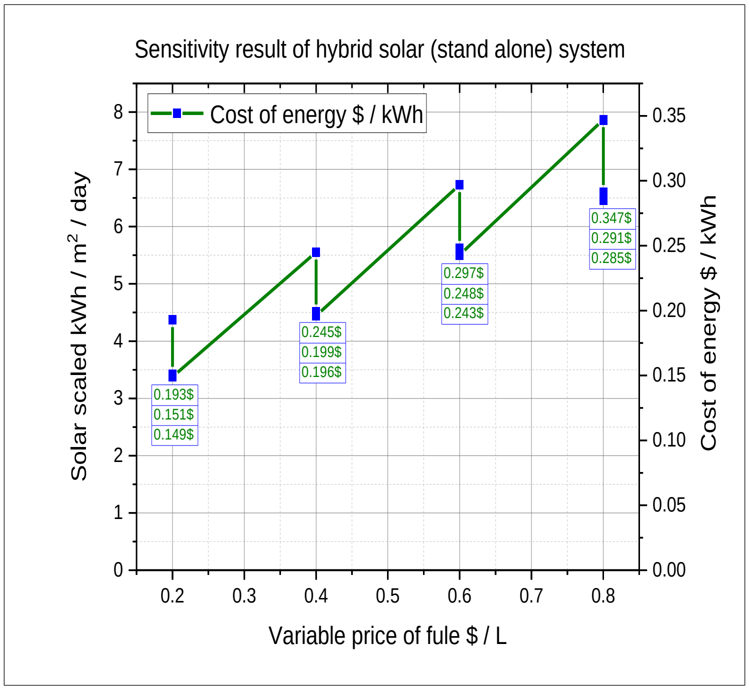

Figure 4. 11 Optimal system operation and sensitivity results for hybrid solar energy system in the stand-alone configuration.

Table 4.5 displays the results obtained from simulation results for the grid-connected case. The table presents the system configuration with a capacity of 60 MW for the PV array, 60 MW for the inverter, 10 MWh batteries, and an 80 MW grid connection. The Net Present Cost (NPC) for this configuration is calculated to be 1.58 billion dollars, with the lowest cost of energy recorded at 0.152 dollars per kilowatt-hour (kWh). These findings provide clear information about the economic feasibility and performance of the grid-connected PV hybrid energy system, highlighting its potential for delivering cost-effective electricity when connected to the grid.

Table 4. 5 The Optimal size of the PV in grid-connected system.

PV grid-connected system served load at lowest cost of energy						
Architecture				**Cost**		**System**
PV (MW)	Battery (MWh)	Converter (MW)	Grid (MW)	Life cycle cost ($)	Cost of energy ($/kWh)	Capacity shortage (%)
60	10	60	80	1.158 B	0.152	0.05

The annual total load demand amounts to 470,160 MWh. The total electric power production from this system exceeds the demand requirements, resulting in surplus energy generation. The entire system's annual production reaches 475,519.3 MWh, which is divided into 53,926 MWh from the PV array and 421,592 MWh from the utility grid. The PV array contributes around 11.3% of the total electricity production, while the majority, approximately 88.7%, is supplied by the utility grid. This clear analysis highlights the system's capability to effectively cover the load demand and demonstrates the potential for additional energy production, which can be harnessed for various purposes. Figure 4.12 illustrates the monthly average power production of the system. The total energy consumption of the load is 470,160 MWh/year. The surplus electricity value in the system is zero, indicating that all the energy produced is utilized effectively to meet the load demands without any surplus. Additionally, the system exhibits an unavailability capacity of 0.0543%, demonstrating its reliability and ability to fulfil the annual electrical load requirements efficiently.

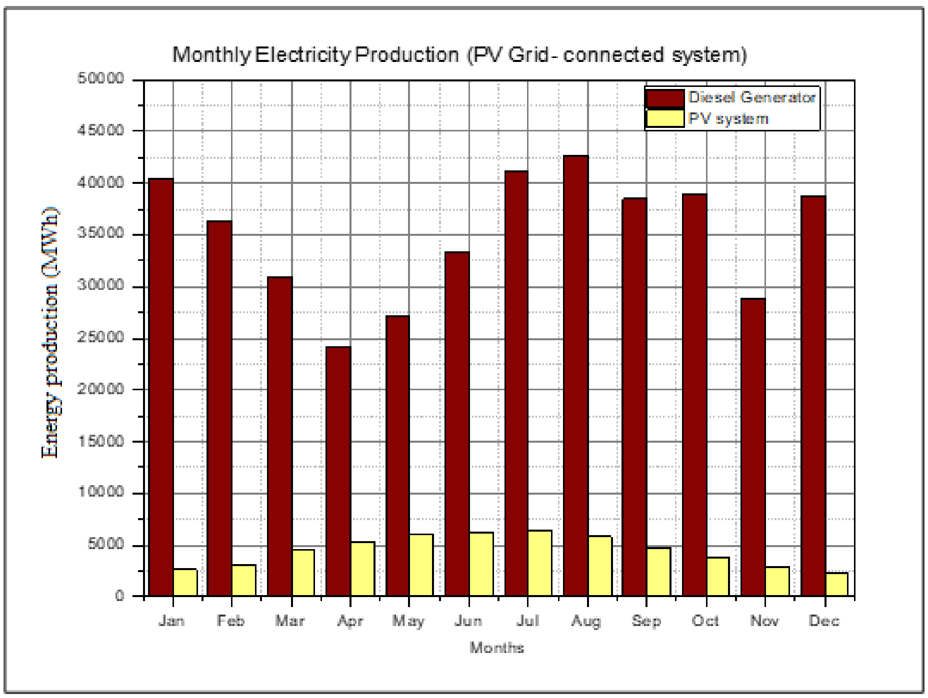

Figure 4. 12 The optimization outcomes for monthly average power production grid-connected solar energy system.

Figure 4.13 presents the sensitivity test results for the grid-connected solar system, illustrating the impact of the same sensitivity variable used in the stand-alone system on the system's components. The findings indicate that the low cost of energy, valued at 0.13 $/kWh, can be achieved under specific conditions: with a solar radiation of 7.9 kWh/m2/day and a diesel fuel price of 0.2 $/L, while maintaining a renewable energy sharing percentage of 26%.

These results offer valuable insights into the system's performance and cost optimization, enabling informed decision-making regarding the most economically advantageous configuration based on solar radiation and diesel price conditions, while considering the proportion of renewable energy integration into the system.

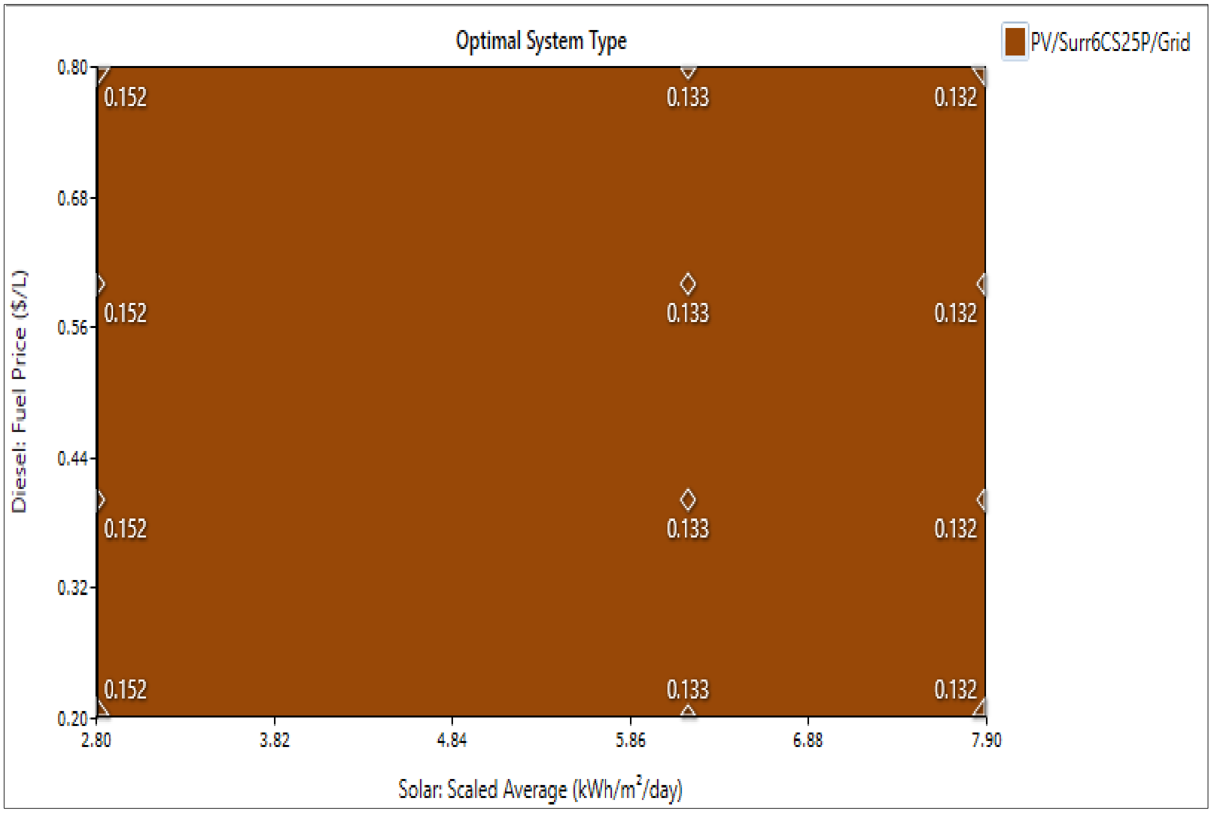

Figure 4. 13 Sensitivity outcomes and optimal solar system operation in the grid-connected configuration.

Additionally, the sensitivity findings depicted in Figure 4.14 reveal that the energy cost does not experience an upward trend with increasing diesel fuel expenses. As anticipated, the energy cost diminishes in accordance with the variations in solar irradiation, encompassing maximum, average, and minimum values.

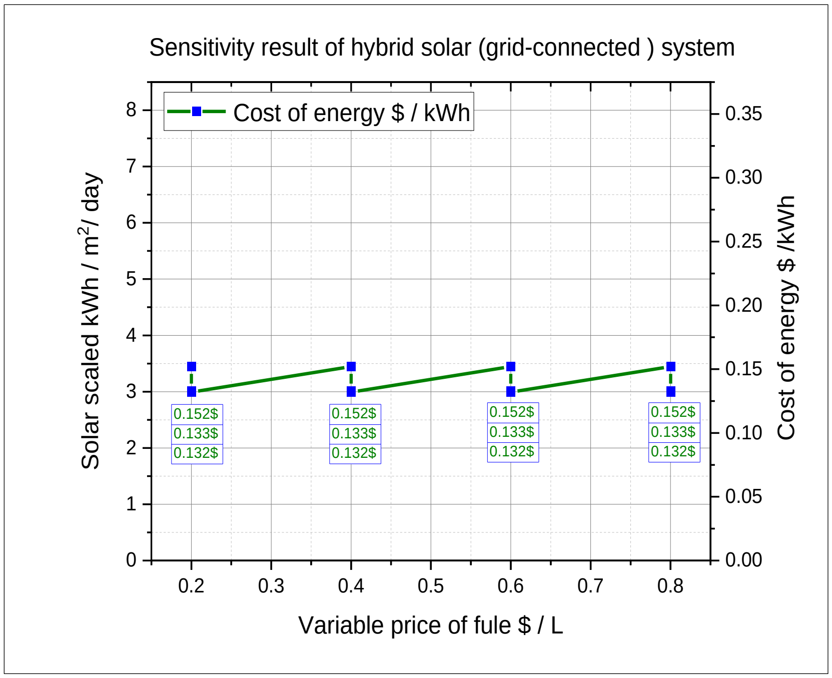

Figure 4. 14 Optimal system operation and sensitivity results for hybrid grid-connected solar energy system.

4.3.2. The Hybrid Wind Energy System Model

A schematic diagram for the wind energy system is shown in Figure 4.15.

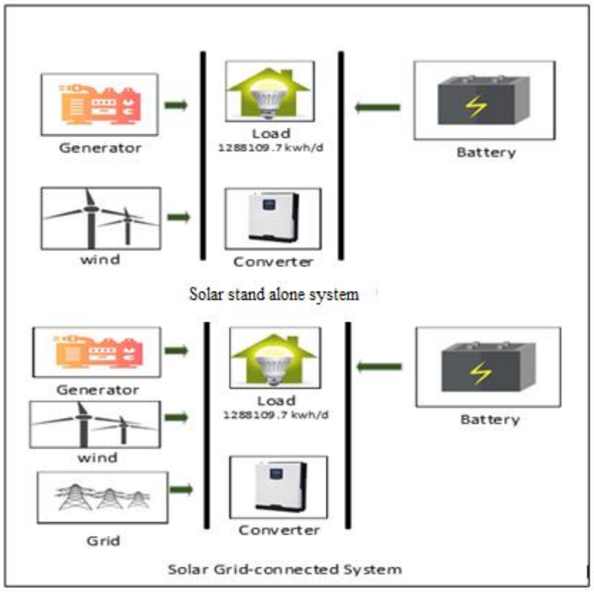

Figure 4. 15 Schematic diagram of the hybrid wind energy system for both stand-alone and grid connected configurations.

The optimization results for the stand-alone wind Hybrid Renewable Energy System (HRES) are presented in Table 4.6, indicating the optimal configuration of the wind turbine, diesel generator, battery, and converter. The cost of energy in this system is calculated to be 0.234 $/kWh with a life cycle cost 997 M$. In addition, the significant contribution of 37.8% from renewable energy sources and the capacity shortage 0.09 percent.

The total annual electric power production of this optimized system is 244,992 MWh/year from the wind turbine and 329,294 MWh/year from the diesel generator. This distribution shows that 45% of the total electricity production is generated by the wind turbine, while the remaining 55% is produced by the diesel generator. These results emphasize the system's capability to harness wind energy efficiently, significantly contributing to the overall electricity production while maintaining a substantial reliance on the diesel generator for additional power generation.

Table 4. 6 Optimal size of the wind turbine stand- alone system.

Wind turbine stand-alone system served load at lowest cost of energy						
Architecture				**Cost**		**System**
Wind turbine 2MW (Number)	Generator (MW)	Battery (MWh)	Converter (MW)	Life cycle cost ($)	Cost of energy ($/kWh)	Capacity shortage (%)
100	60	30	80	997 M	0.234	0.09

Figure 4.16 presents the average monthly power production of the system. The total energy consumption of the load amounts to 470,160 MWh/year. The system exhibits a very low excess electricity production of 9.3%, indicating that it efficiently meets the load demands with only a minor surplus. Moreover, the unmet load percentage is very low, at 0.0371%, underscoring the system's reliability in fulfilling the electrical load requirements.

These findings highlight the system's effective performance in achieving a well-balanced energy production. However, it is important to note that the Cost of Energy (COE) in the wind stand-alone system has been observed to be higher compared to the COE in the PV stand-alone system. Despite the system's efficiency in harnessing wind energy, factors such as the initial investment cost and operational expenses of the wind turbine contribute to the higher COE when compared to the PV system. It is important to carefully consider these cost factors and assess their implications while making decisions regarding the most suitable renewable energy system for the specific requirements and constraints of the project.

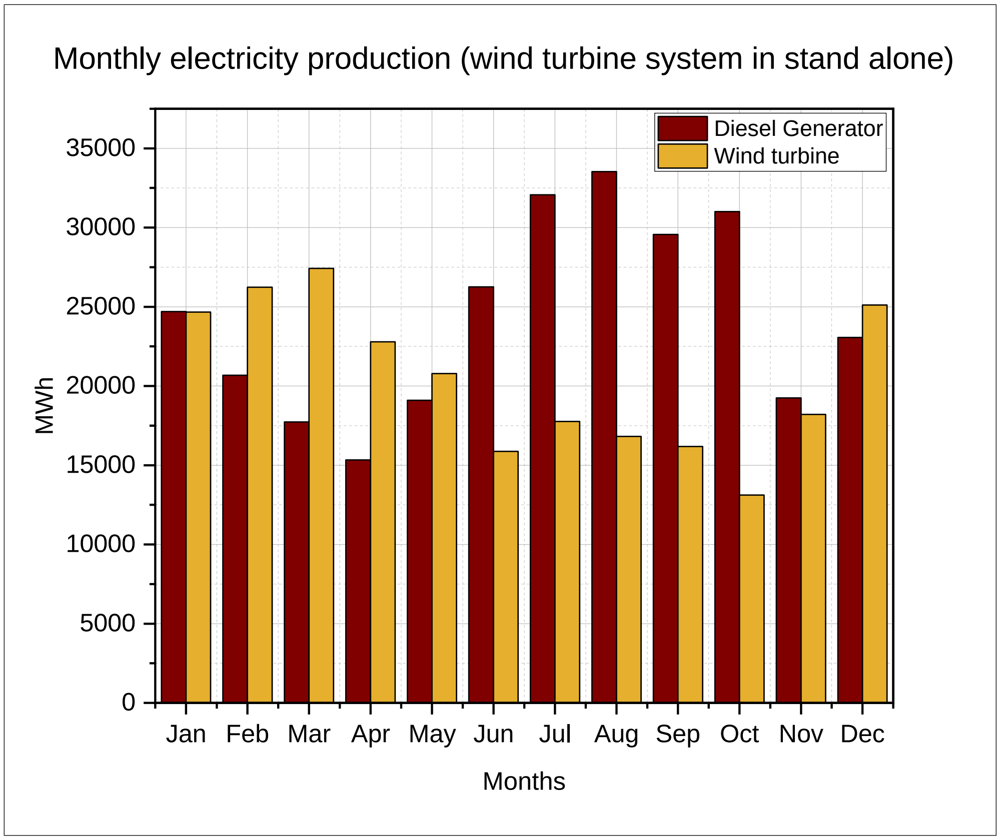

Figure 4. 16 The optimization outcomes for the hybrid stand-alone wind energy system.

During the sensitivity analysis in the wind system, the variables of price fuel are the same as applying the PV system, but the variable of wind speed has added as maximum, average, and minimum value. the optimization process revolves around variables assumed in the design, assessing their impact on the cost of energy. Figure 4.17 presents the minimum cost of energy, which is 0.186 $/kWh. This minimum cost occurs under specific conditions: a wind speed of 5.70 m/s and a diesel price of 0.20 $/L, while maintaining a renewable energy share of 52%.

Notably, these figures reflect favourable conditions, with a combination of low diesel prices and maximum wind speed. As anticipated, the cost of energy is expected to increase when diesel prices rise and/or wind speeds decrease. These results underscore the sensitivity of the system's cost of energy to variations in both diesel prices and wind speed, highlighting the need for careful consideration of these factors when planning and optimizing the stand-alone wind HRES for optimal economic performance.

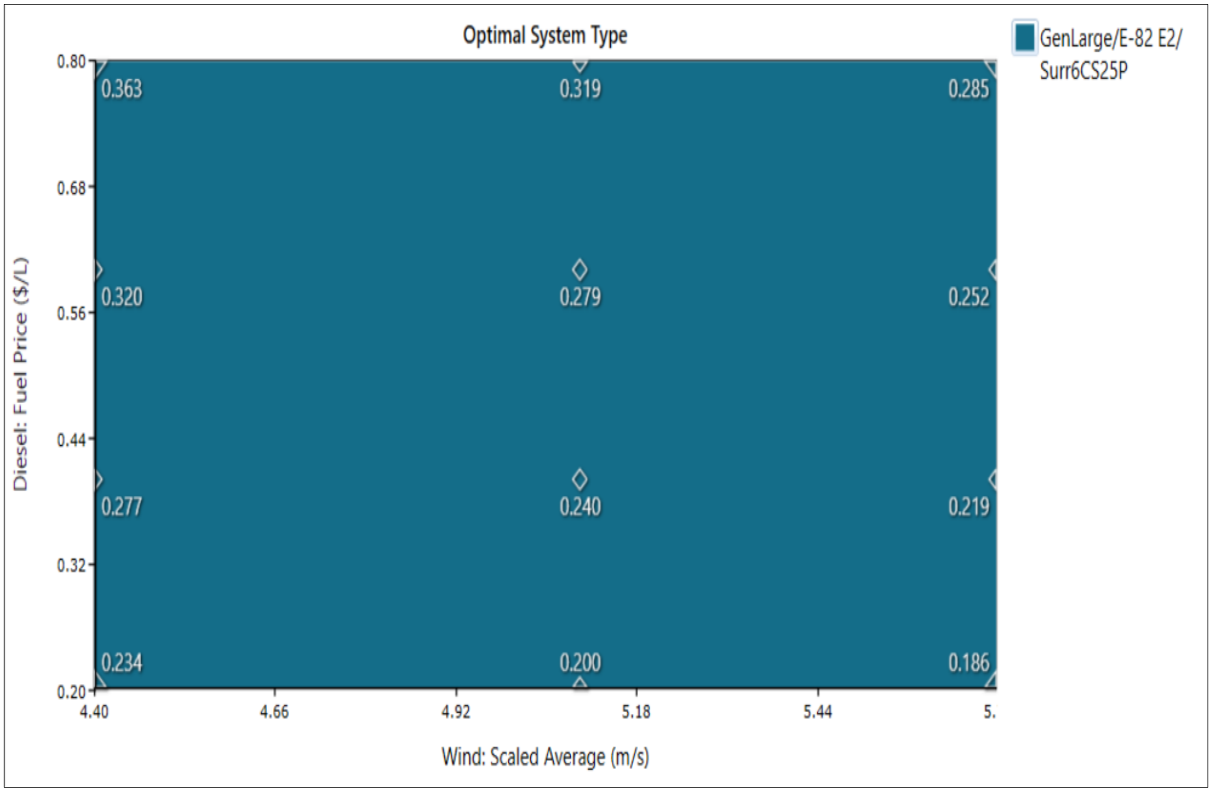

Figure 4. 17 The sensitivity outcomes and optimal operation of the grid-connected wind energy system.

From sensitivity results, most system configuration aspects, such as the number of turbines, remain the same for variable wind speed values. Only the number of hours during which the diesel generators are running decreases dramatically with increasing diesel prices. The amount of diesel required decreases as the average wind speed with variables at maximum, average, and minimum increases, as illustrated in Figure 4.18.

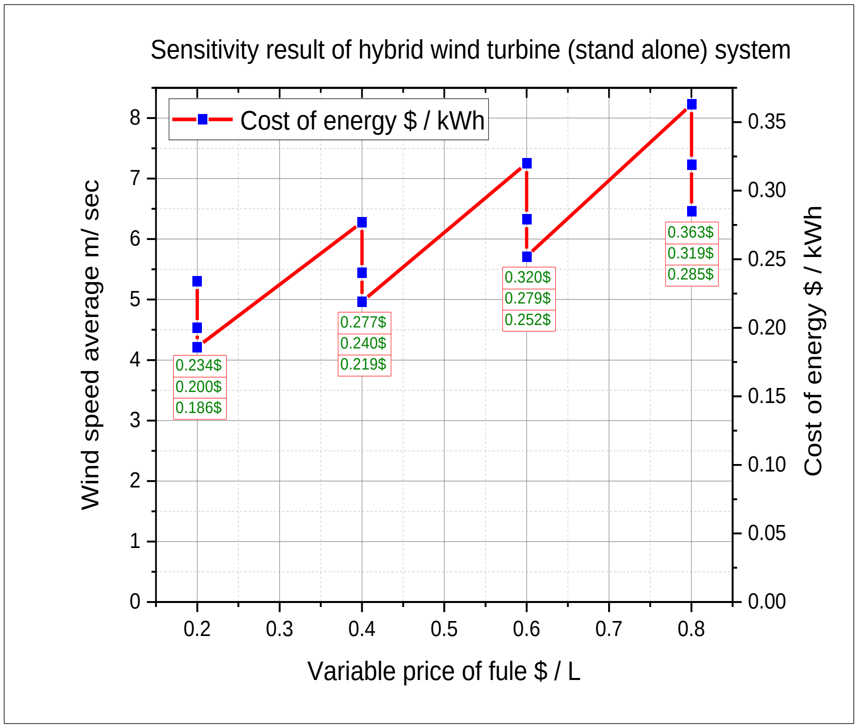

Figure 4. 18 The optimal system operation and sensitivity results for hybrid stand-alone wind energy system.

In the context of the operation technology for the grid-connected wind Hybrid Energy System in Al-Marj City, the system configuration is set as a grid, wind, and diesel generator. The COE for this configuration is calculated to be 0.16 $/kWh and the NPC is 960 M$. Notably, the system effectively meets the load demand with no capacity shortage, ensuring a reliable power supply. Figure 4.19 and Table 4.7 illustrate that 20.8% of the total energy is produced by the wind turbine (E-82), emphasizing the significant contribution of the utility grid. The power excess of the system's components is very low, indicating that the system operates efficiently with minimal excess of energy. This analysis underscores the successful integration of wind energy into the grid-connected system, showcasing its significant contribution to overall electricity production. However, it is important to acknowledge that the cost-effectiveness of the grid-connected wind system was slightly higher compared to the PV grid-connected system.

Table 4. 7 Optimal size of the wind turbine grid-connected system

PV grid-connected system served load at lowest cost of energy							
Architecture					Cost		System
Wind turbine 2MW (Number)	Battery (MWh)	Generator (MW)	Converter (MW)	Grid (MW)	Life cycle cost ($)	Cost of energy ($/kWh)	Capacity shortage (%)
40	10	60	60	76	960 M	0.16	0

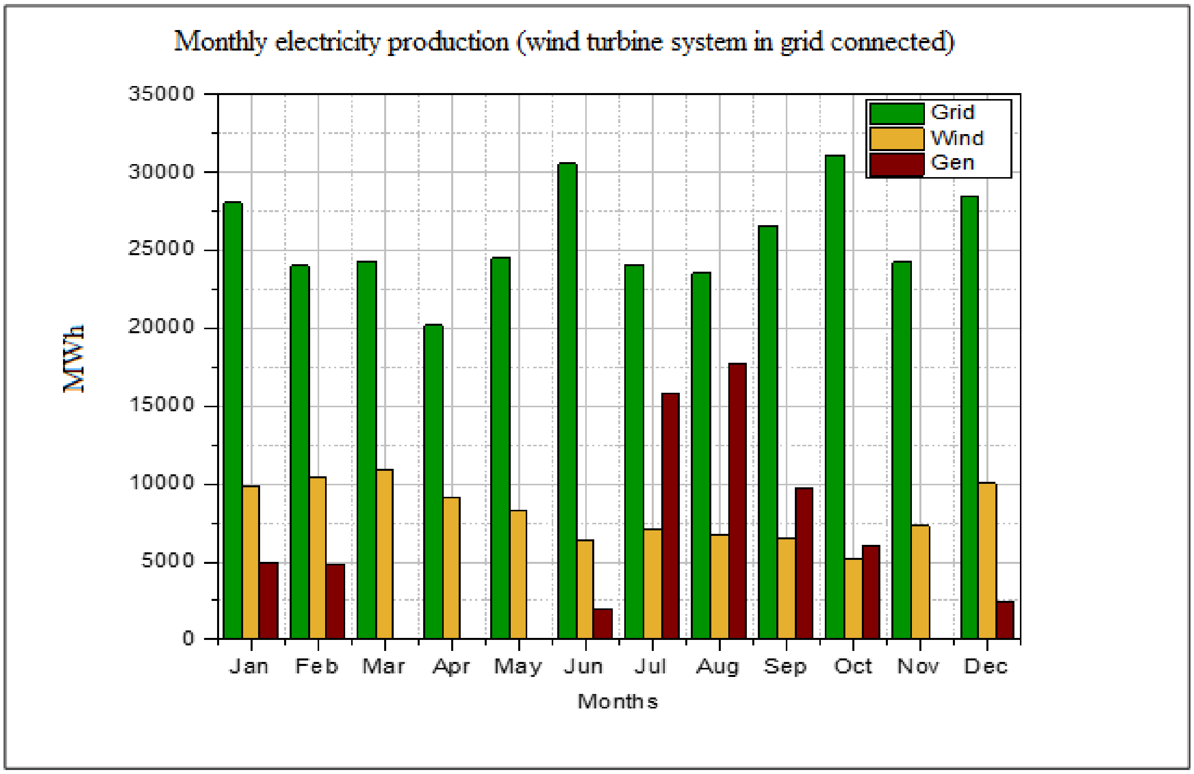

Figure 4. 19 Optimization outcomes for monthly average power production grid-connected solar energy system.

The total energy consumption of the load is recorded at 470,160 MWh/year. The power production of the system is distributed among three sources, with the diesel generator contributing 13.5%, the wind turbine contributing 20.8%, and the utility grid contributing 65.7%. The total production from the system amounts to 471,209 MWh/year. The excess of electricity generated by the system is very low, representing only 0.0114% of the total energy produced in a year. This indicates that the system is operating with high efficiency. The sensitivity analysis results for the grid-connected wind HES indicate that the optimal system configuration considers the same sensitivity variables used in the stand-alone system. As shown in Figure 4.20. This finding implies that an increase in fuel price and wind speed at the site does not influence the system's configuration. The chosen configuration represents the optimal size and arrangement that aligns with the load requirements. The lowest cost of energy is achieved at 0.134 $/kWh, and this favourable outcome occurs under specific conditions: a wind speed of 5.70 m/s, a diesel price of 0.20 $/L, and a renewable energy share set at 52%. These results affirm the cost-effectiveness and efficiency of the grid-connected wind HES, showcasing its ability to harness wind energy effectively and balance it with conventional diesel generation while delivering reliable and economically viable power supply to Al-Marj City.

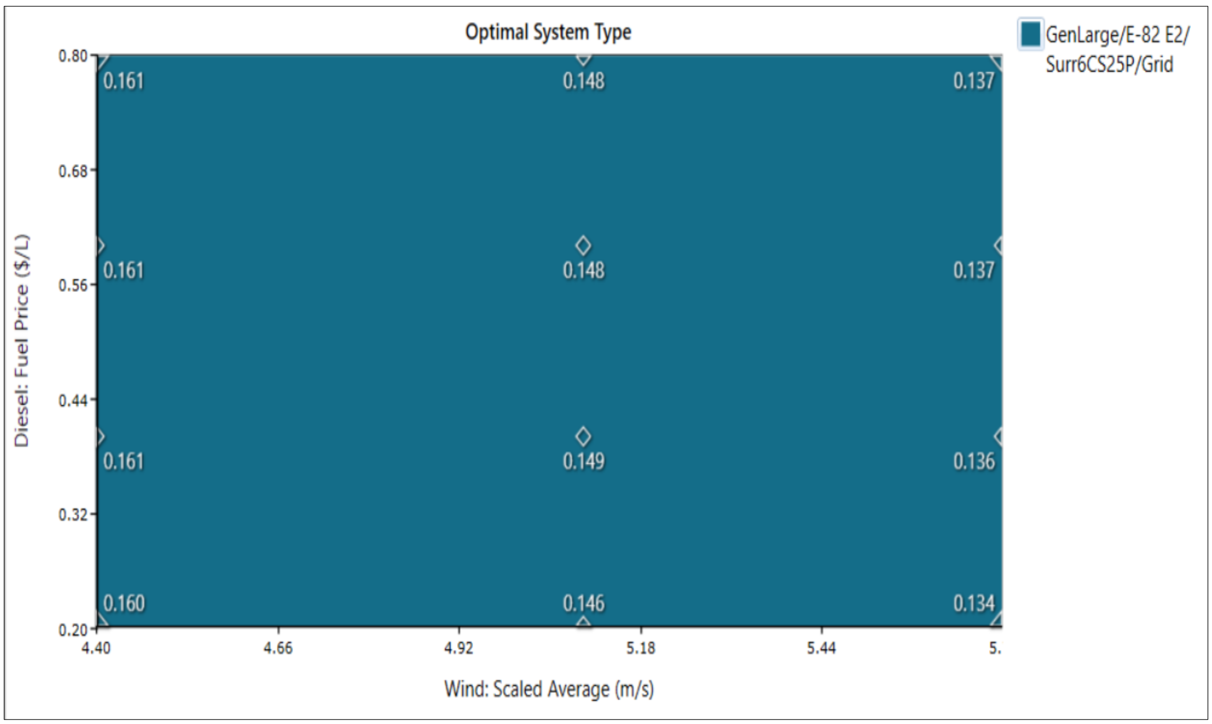

Figure 4. 20 Sensitivity outcomes and optimal wind system operation in the grid-connected configuration.

The outcomes of the sensitivity simulation emphasize that while the cost of energy is minimally influenced by diesel prices, it experiences a decrease due to the fluctuations in wind speed at maximum, average, and minimum values, as illustrated in Figure 4.21.

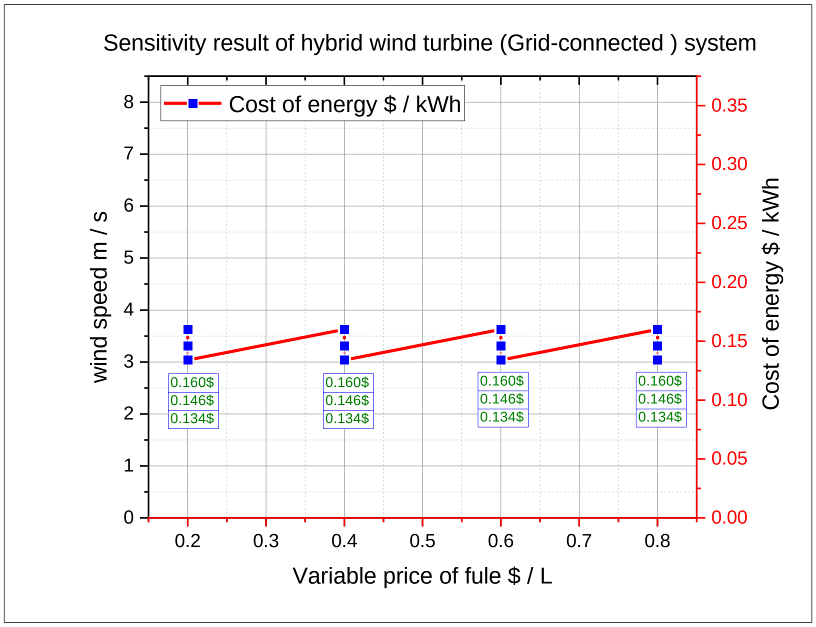

Figure 4. 21 Optimal system operation and sensitivity results for the hybrid wind energy system in the grid-connected configuration.

4.4. Design Comparison and Results Analysis of The Solar and Wind Energy Systems

The analysis of the results for both scenarios demonstrates a high feasibility for utilizing solar HES in the region, whether in the form of a stand-alone system or a grid-connected one. The solar HES exhibits superior cost-effectiveness, resulting in a lower cost of energy production compared to the wind energy system. In the stand-alone configuration, the cost of energy for the PV system is 0.19 $/kWh, while it is 0.23 $/kWh for the wind energy system. Similarly, in the grid-connected setup, the cost of energy for the solar HES is 0.15 $/kWh, whereas it is 0.16 $/kWh for the wind energy system. Sensitivity analysis conducted for both systems explored future changes in diesel prices, solar radiation values available at the Al-Marj site, and wind speeds experienced throughout the year. The results obtained for the two systems are compared in Figure 4.22, clearly demonstrating that the cost of energy in the solar energy system remains consistently cheaper than that of the wind energy system across all variables and scenarios studied. These findings reaffirm the economic viability and attractiveness of solar HES as a sustainable and cost-effective energy solution for Al-Marj City, outperforming the wind energy system in terms of lower energy costs and enhanced overall efficiency.

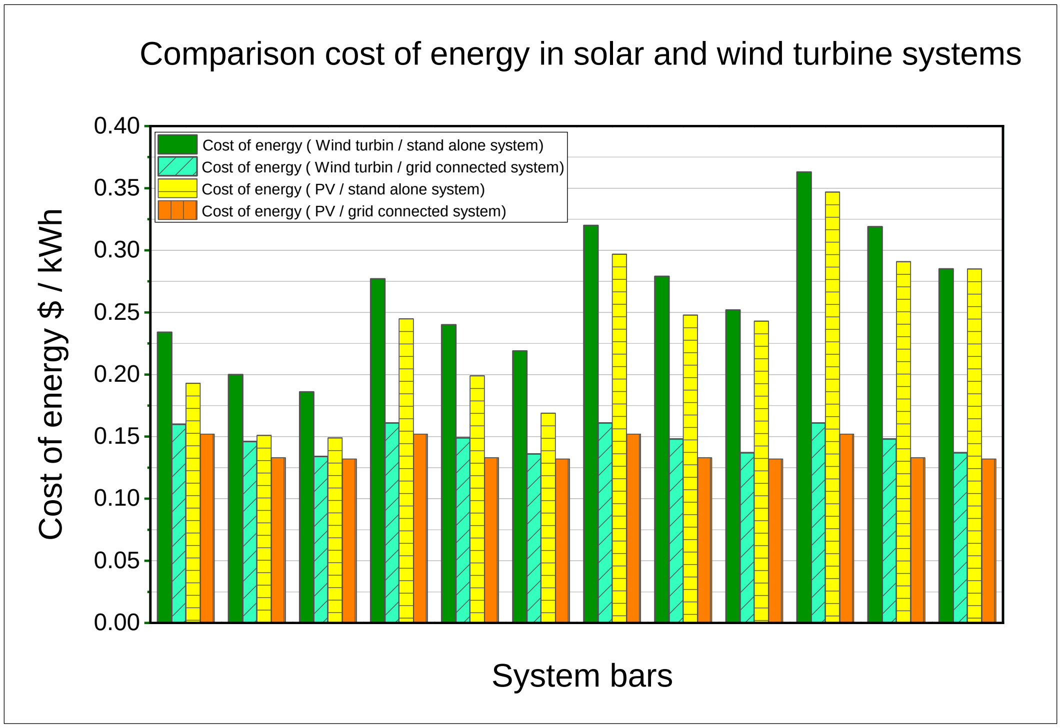

Figure 4. 22 Comparison of the simulation results of solar energy and wind turbine hybrid energy systems.

4.5. Summary

The aim of this chapter is to study the feasibility of implementing RE technologies in the Libyan energy production system to overcome the problem of frequent power outages. This issue is caused by the insufficient energy capacity currently produced, which does not meet the Libyan society's demands, resulting in excessive electricity outages, lasting hours and sometimes days in some of the country's regions. To achieve these objectives, an investigation of alternative means of energy production instead of the fossil energy resources currently used has been conducted. As a case study, a hybrid energy system in the Al-Marj City has been designed, with several scenarios and system configurations studied and analysed. The study considered the stand-alone and grid-connected configurations for a PV energy system and a wind energy system. The analysis of the results showed that a solar energy system is the more optimal option in terms of the cost of energy. As the alternative option of designing a wind energy the Al-Marj City HRES did not prove cost-effective or efficient to be considered for implementation. The shares of solar energy in the system vary from 35.9% to 11.3% for all possible configurations examined, resulting in the cost of energy being 0.15 $/kWh and 0.13 $/kWh for the stand-alone system and the grid-connected system, respectively. On the other hand, the shares of wind energy vary from 20.6% to 52.2% and the resulting cost of energy is 0.18 $/kWh and 0.13 $/kWh for the stand-alone system and grid-connected system, respectively. Thus, all indications point to the superiority of a solar energy production system as the more cost-effective and competitive option to the current cost of energy than the wind energy production system.

In summary, the results of this study conclude that there is a high prospect of feasibility for establishing a PV hybrid energy system in this region of Libya, whether as a stand-alone system or a grid-connected one. The study also recommends renewable energy technology as the most sustainable way of developing the Libyan energy sector and addressing its current energy shortage crisis.

CHAPTER 5

Optimal Design of Renewable Energy Integration for LSTM-Based Load Demand Forecasting in Al Marj City for year 2030

5.1. Introduction

Time series forecasting is a crucial task in various domains, including energy planning and finance [105]. Accurate forecasting can help organizations and decision-makers to make informed decisions, optimize resource utilization, and reduce costs. However, traditional statistical methods are limited in their ability to model complex and dynamic time series data, which often contain long-term dependencies, seasonality, and trends. Machine learning techniques, particularly neural networks, have shown promising results in forecasting time series data [106]. Among the various types of neural networks, Long Short-Term Memory (LSTM) networks have emerged as a powerful approach for time series forecasting [107]. LSTM networks have the ability to learn long-term dependencies and capture non-linear relationships between data points [108]. They utilize feedback connections, which allow them to analyse entire data sequences rather than just single data points. LSTM networks have shown accurate results in various applications, including speech recognition, natural language processing, and time series forecasting.

The development of LSTM networks for time series forecasting has received significant attention in recent years. For example, in [109] a hybrid LSTM network was proposed to forecast the hourly electricity load demand. The proposed model combined LSTM networks with autoencoders to extract the most relevant features from the input data. The model outperformed traditional forecasting methods, including ARIMA and SVM. Similarly, in [110] a LSTM network was used to predict air quality in Beijing.

This study introduces LSTM neural network model that successfully forecasts load demand data for AL Marj city in 2030. The model utilizes key variables such as population, primary energy consumption, and consumption per capita to make accurate predictions. To ensure optimal performance, the input and output data are first normalized before training the neural network with the available training data. Following the training phase, the model is employed to predict load demand for future years, and its performance is assessed by computing the R-square value. Hence, the future load data acquisition offers valuable insights for analysing the stand-alone system scenario presented in Chapter 4. This study aims to identify the optimal system configuration considering the impact of load demand growth expected in 2030, utilizing the forecasted load demand results specific to this city.

5.2. Methodology

Data normalization is a crucial step in preparing a dataset for machine learning models, and it is especially important for the LSTM neural network model used in this study. Normalization involves rescaling the numerical columns of the dataset to a common scale. This is necessary when the range of values for each feature in a dataset differs significantly, as it may cause some features to dominate the model training, leading to poor performance. Normalization aims to standardize the numerical values of the dataset and make them more comparable to each other. This study used the popular method of normalization which involves computing the mean and standard deviation of the numerical columns in the dataset. The process of normalization involves subtracting the mean value from each observation and dividing the result by the standard deviation. The mathematical expression (5.1) for the normalization equation used in this study is:

$$X_{norm} = \frac{X-\bar{X}}{std(X)} \tag{5.1}$$

Where:

X is the original dataset

$\bar{X}$ represents the mean of the dataset.

std(X) denotes the standard deviation of the dataset.

By applying this normalization technique to the dataset, it can transform the numerical values to a standard scale, making them easier to work with in the LSTM neural network model. The normalized data is then used as input to the LSTM model, which can learn from the historical data to forecast future values accurately. The normalization of data is a common pre-processing step in machine learning, and it has been shown to be effective in improving model performance in a variety of applications. Once the dataset was normalized, a new variable was created to store the normalized values of both the response and target variables. the response and target variables are referring to the key elements under consideration in the predictive modelling process. The response variable, often known as the dependent variable, represents the outcome or result that the model aims to predict. On the other hand, the target variable is the variable being forecasted. In the context of the LSTM neural network model, the newly created variable after normalization holds the scaled values for both the response and target variables, streamlining their integration into the model's training and forecasting procedures. This allowed to feed the pre-processed data into the LSTM neural network model. The creation of the neural network model involved defining the neural network layers, training the model, and performing prediction. The LSTM neural network belongs to the family of Recurrent Neural Networks (RNNs), which are types of artificial neural networks that allow connections between nodes to form cycles. LSTM networks address the challenge of limited capacity in learning longer-term dependencies. They achieve this by incorporating additional gates that regulate the flow of information within the hidden cell and between hidden states. These extra gates enhance the ability of LSTM networks to effectively capture and learn long-term relationships in sequential data. Compared to simple RNNs, LSTM networks exhibit reduced sensitivity to time gaps, making them highly suitable for analysing sequential data. In addition to the hidden state present in traditional RNNs, an LSTM block typically includes a memory cell, input gate, output gate, and forget gate as shown in Figure 5.1.

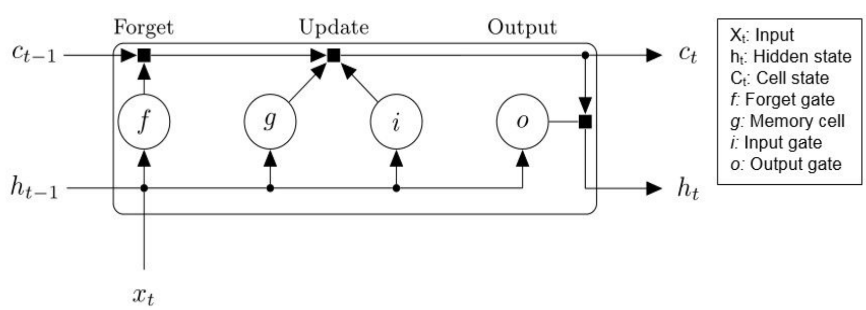

Figure 5. 1 The architecture of the LSTM network [111].

Overall, the LSTM architecture's integration of memory cells and gated mechanisms empowers the network to retain and selectively process relevant information across extended sequences. This capability significantly enhances its performance in tasks involving the analysis of sequential data.

As a result, the output from certain nodes can influence subsequent input to the same nodes, leading to temporal dynamic behaviour. For this study, the neural network layers were defined to consist of 256 hidden layers and a regression layer to predict the data. After defining the neural network layers, the next step involved training the model by utilizing the ADAM algorithm to optimize the weights and biases of the network. The training process involved feeding the pre-processed dataset into the neural network model and adjusting the weights and biases to minimize the difference between the predicted and actual responses. To avoid overfitting, a maximum of 2000 epochs was set for the training process in the final step and predictions were made using the trained LSTM neural network model. The predicted results were then compared with the actual responses. To visualize the accuracy of the predicted results, the comparison was plotted on the same figure. Additionally, the performance of the LSTM neural network model was evaluated by computing the R-squared value, which is a common metric used for assessing the accuracy of fitted data.

5.2.1. Neural Network

The neural network model used in this study is a RNN consisting of LSTM layers. These layers enable the retention of information from earlier stages for use in later stages. The arrangement of recurrent layers determines the type of RNN that can be created. Various RNN architectures with different cell designs can be developed due to the distinct cells and internal connections they possess. In [112] it is proposed the LSTM cell to address the issue of long-term dependency. They were able to increase the memory capacity of the typical recurrent cell by adding a "gate" to it. The LSTM network architecture includes an input gate, an output gate, and a forget gate which controls the flow of information through the network. These gates allow the network to selectively store, retrieve, or discard information from the previous time steps, making it well-suited for time series analysis and forecasting tasks. By utilizing this architecture, the LSTM neural network model can effectively capture the complex temporal dependencies and seasonality present in the data.

5.2.2. Dataset Description

The dataset consists of 31 data points spanning from 1990 to 2020 [113], as depicted in Table 5.1. It includes three types of data: population, primary energy consumption measured in MWh, and consumption per capita measured in kWh. The objective is to utilize this data to make predictions for future responses.

Table 5. 1 Data set of Al Marj city for population, Primary energy consumption (GWh) and Consumption per capita kWh

Year	Population	Primary energy consumption (MWh)	Consumption per capita (kWh)
1990	56675	89376	1577
1991	58050	96246	1658
1992	59412	104149	1755
1993	60744	109885	1809
1994	62018	112872	1820
1995	63218	111959	1771
1996	64334	115029	1788
1997	65379	117878	1803
1998	66385	138014	2097
1999	67396	164721	2177
2000	68444	152082	2222
2001	69534	156868	2256
2002	70656	195858	2772
2003	71799	2150.38	2948
2004	72944	226564	3106
2005	74074	253925	3428
2006	75201	285237	3793
2007	76324	237334	3756
2008	77397	243181	3142
2009	78358	263439	3362
2010	79000	266093	3361
2011	79807	271557	2839
2012	80296	280576	3516
2013	80738	289657	3596
2014	81271	299047	3678

2015	81990	308751	3762
2016	82933	318776	3848
2017	84065	329128	3936
2018	85314	339734	4025
2019	86578	383021	4825
2020	87776	396923	4525

For this study, a LSTM based neural network was developed using MATLAB. The neural network was constructed by adding a sequence layer as the first layer, followed by an LSTM layer and a fully connected layer. Finally, a regression layer was added to predict the values based on the input year. The sequence layer is used to ensure that the input data is in sequence form for the LSTM layer, while the LSTM layer is responsible for retaining important information from the past that can be used for future predictions. The fully connected layer was used to connect the output of the LSTM layer to the regression layer, which generated the final predictions. The developed neural network architecture is shown in Figure 5.2, indicating the flow of input through the various layers, processing, and output.

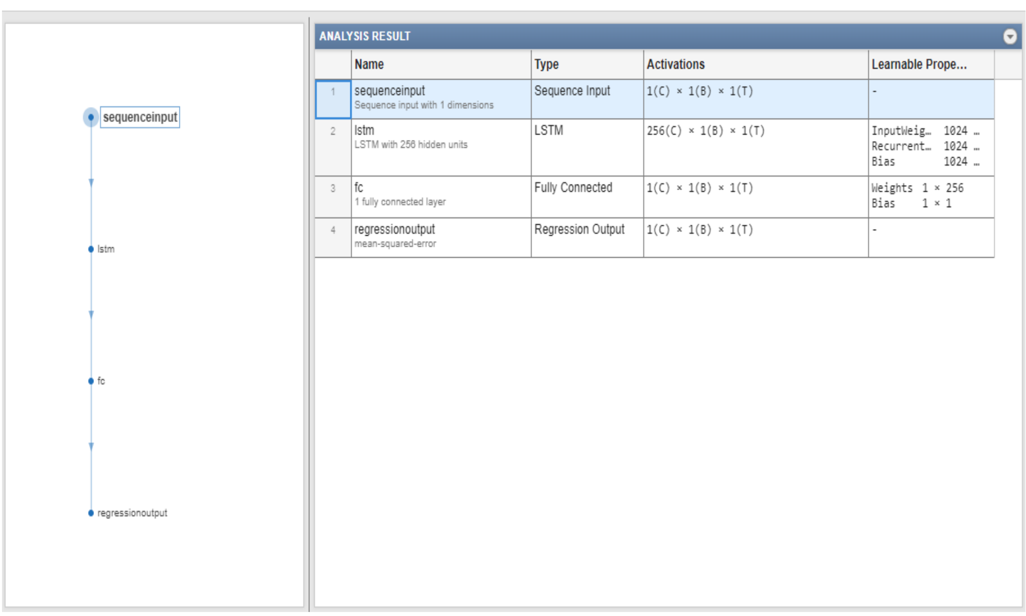

Figure 5. 2 LSTM model for trained network usage analysis

Figure 5.2 illustrates a four-layer LSTM model for trained network usage analysis (Analyse the network: displays an interactive plot of the network architecture and a table containing information about the network layers.). In addition, the LSTM network has 256 hidden layers which were trained using MATLAB. During the training process, the model was trained with the option to display the training progress of losses and root mean square error (RMSE). The RMSE is a widely used metric to evaluate the accuracy of regression models. A lower RMSE value indicates better performance of the trained model in predicting the response variable. To ensure that the developed LSTM network was accurately trained and capable of making precise predictions of the future response variable, the training progress of losses and RMSE was monitored in this study. This helped in assessing the accuracy of the trained model and identifying the optimal number of epochs required for the model to converge.

5.2.3. Training Network

To train a neural network, various hyperparameters need to be set, such as the optimization algorithm, the number of epochs, the learning rate, and the batch size. In this study, the ADAM algorithm was chosen for optimization, and the number of epochs was set to 2000 to obtain accurate results. To evaluate the accuracy of the model, the R-squared value was computed, which measures the proportion of variance in the predicted results that can be explained by the model. A perfect fit is indicated by a value of 1, while values closer to 0 indicate poor performance. The first step to train the LSTM neural network involved splitting the dataset into training and testing sets. The training set was used to optimize the model, and the testing set was used to evaluate its performance. During training, the model adjusted its weights and biases to minimize the loss function, which measured the difference between the predicted and actual values. Backpropagation was used to calculate the gradients and update the parameters using the Adam algorithm. After each epoch, the R-squared value was calculated using the testing set, and the progress of the model was tracked. This allowed for the detection of overfitting, where the model performs well on the training set but poorly on the testing set. Overall, the training process of the LSTM neural network involved fine-tuning various hyperparameters and monitoring the performance of the model using appropriate evaluation metrics.

5.2.4. PV System Stand-Alone Design

The system design aspect of this investigation involved utilizing the HOMER Pro software to identify the most suitable system configuration, considering the projected rise in load demand by

2030. The objective of this investigational study was to identify financial viability in terms of COE and NCP in the case of a stand-alone system for Al Marj City as identified in Chapter 4.

5.3. Results and Discussion

5.3.1. Predict Consumption Per Capita

The developed MATLAB code implements a time series forecasting model for predicting consumption per capita and primary energy consumption. The code begins by importing data from an Excel file named *"ALMAR DATA SINCE 1990-2020"*. Subsequently, the data is normalized to obtain two variables, namely *XTrain* and *TTrain*. These variables serve as the input and target variables, respectively, in the neural network model. The neural network model is constructed using the LSTM architecture, comprising an input layer, one LSTM layer, a fully connected layer, and a regression layer. The training options are configured to utilize the Adam optimization algorithm, with a maximum of 2000 epochs for training. Following the training process on the trained data, the model predicts the consumption per capita. To evaluate the accuracy of the model, the predicted consumption per capita is compared with the actual data, and the R-Square value is calculated. In this case, the R-Square value is determined to be 0.99988, indicating a high level of accuracy, as depicted in Figure 5.3. Lastly, the code predicts the consumption per capita for the year 2030, yielding a value of 5860 kWh per capita, as shown in Figure 5.4.

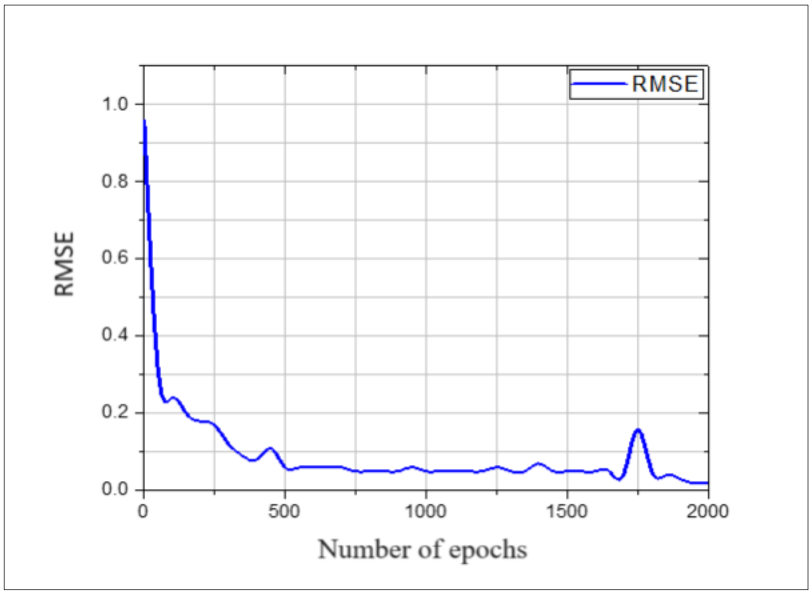

Figure 5. 3 Root Mean Squared Error of predicted data of consumption per capita.

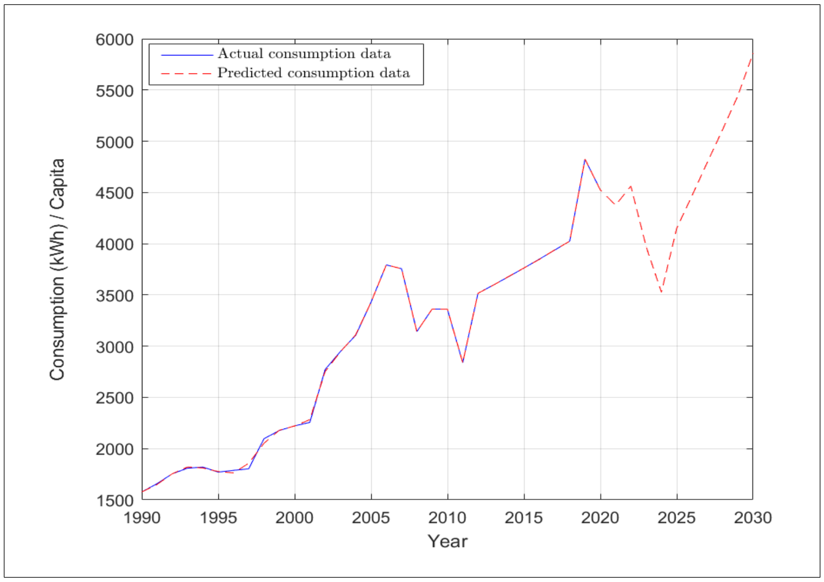

Figure 5. 4 Actual data and the predicted data of the consumption per capita.

5.3.2. Predict Primary Energy Consumption

The developed MATLAB code trains an LSTM neural network to predict primary energy consumption (see Appendix C). It pre-processes the data by normalizing it and then trains the neural network using the normalized data. The network is trained using the Adam optimizer for 2000 epochs, and the training progress is plotted. After training, the network is used to predict primary energy consumption for the year 2030, yielding a prediction of 517,292 MWh, and the predicted data is plotted along with the original data. Finally, the code computes the R-squared value of the predicted data which is 0.99993. The R-squared value indicates the goodness of fit of the predicted data to the original data. A value of 1 indicates a perfect fit, while a value of 0 indicates no correlation between the predicted data and the original data. The R-squared value of the predicted data is printed to the console and shown in Figure 5.5. Finally, the primary energy consumption for the year 2030 and old data are illustrated in Figure 5.6.

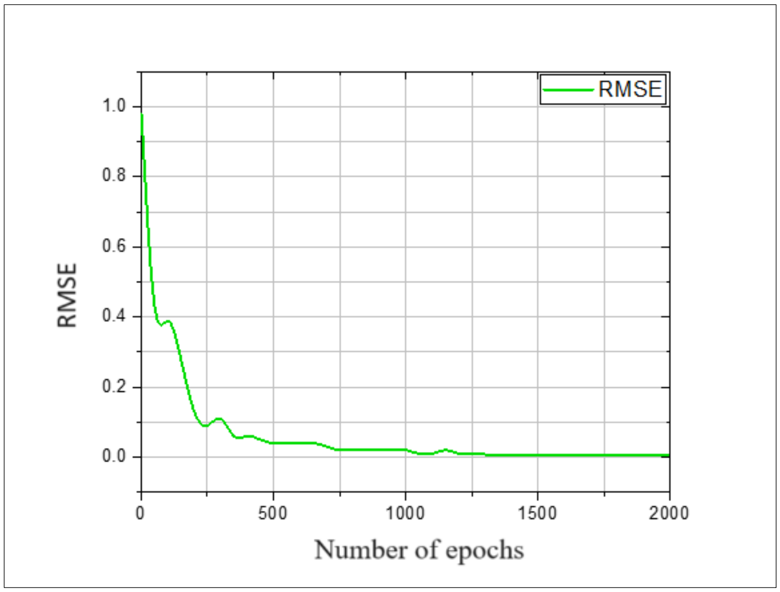

Figure 5. 5 The Root Mean Squared of predicted data of primary energy consumption.

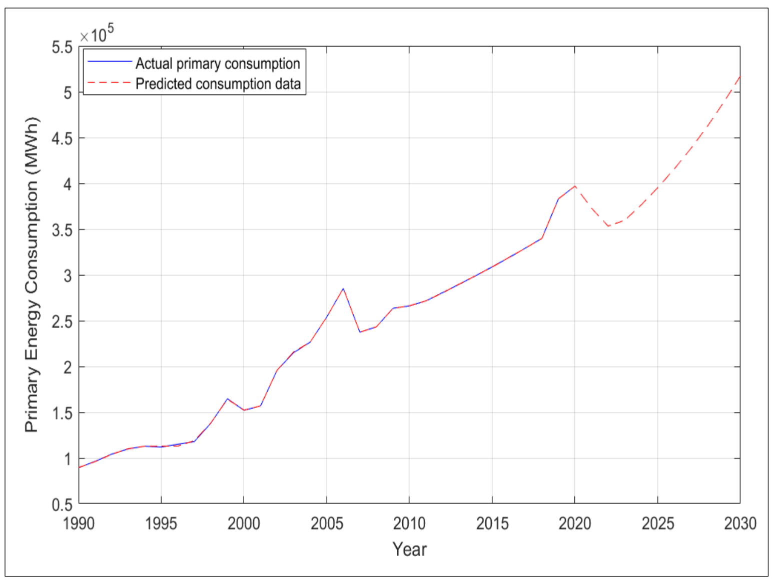

Figure 5. 6 The energy consumption for the year 2030 in Al Marj city.

5.3.3. Predicting The Population

Predictions of the population in a future year can be made using a neural network with LSTM layers. The script pre-processes the data by normalizing both the input and output data, and then trains the neural network using the training data, these data is presented in Appendix C. After training, the script predicts the population for 2030 as 94,404 capita and computes the R-squared value which is 0.99999 to evaluate the model's performance. Finally, it plots the RMSE, and the actual and predicted population values as shown in Figure 5.7 and 5.8.

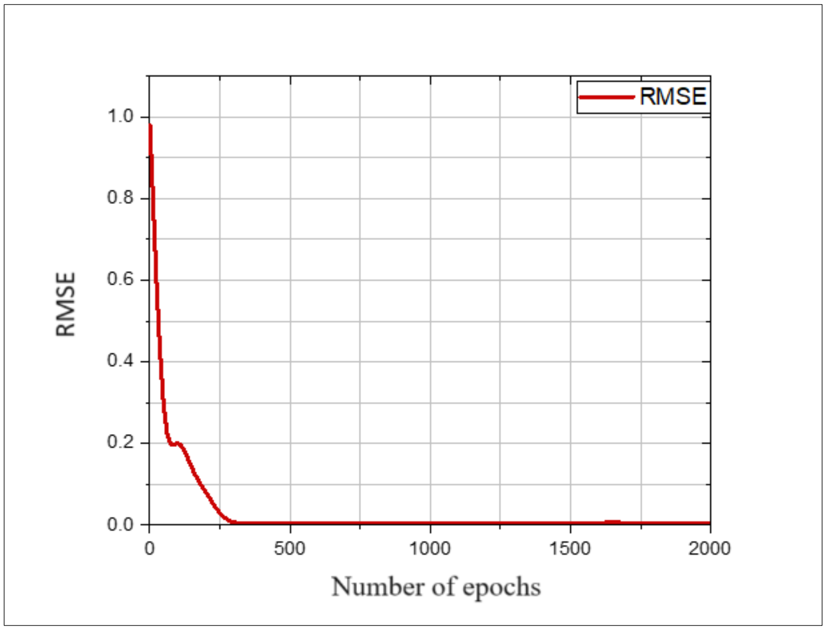

Figure 5. 7 The Root Mean Squared of predicted data of primary energy consumption.

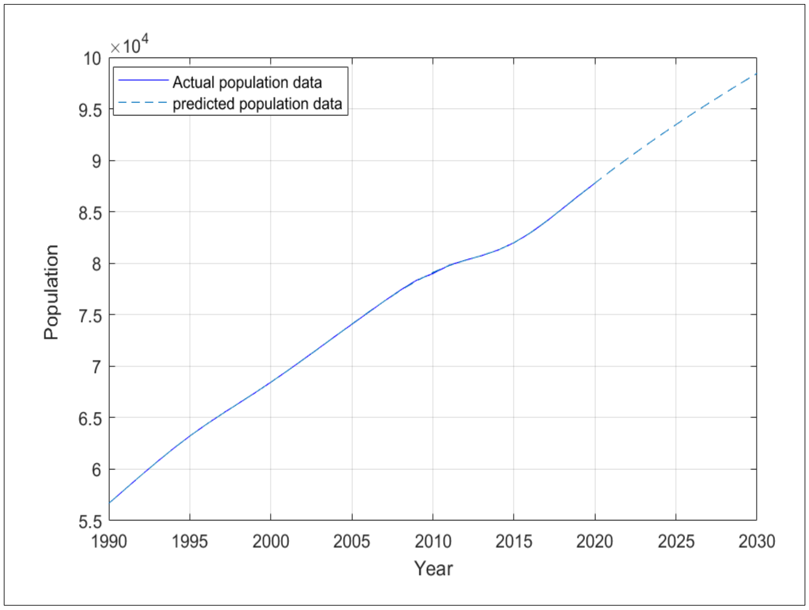

Figure 5. 8 The actual and predicted population values 2030.

The results presented in Figure 5.4. 5.6 and 5.8 show that the proposed method was able to predict the data with great accuracy. By comparing the actual and forecasted results, it was observed that they matched with each other. This observation is further supported by the computed R-squared values, which indicate the fitting accuracy of the results. A value closer to one suggests good forecasting and the ability to predict future results. It should be noted that having a higher number of past datasets could result in more accurate results. During the training process for the LSTM network, the RMSE value of the model decreased and converged, indicating a good forecasting model.

5.3.4. Simulation Results of Optimal Size Configuration In 2030

- **Electricity load calculation for Al Marj city 2030**

Based on a forecasting study, the projected population for Al Marj city in 2030 is expected to reach 94,404 individuals. The study also predicts a per capita consumption of 5860 kWh and estimates the total energy consumption for Al Marj city in 2030 to be 517,292 MWh. To calculate the monthly and daily load demand, it follows the methodology outlined in Chapter 3, which utilizes the latest available data collected by the General Electricity Company of Libya (GECOL). This methodology takes into account the real population growth rate and the load ratio derived from the most recent documented data. By applying this methodology, it can estimate the monthly and daily load demand for Al Marj City in 2030. These estimates are then used to model a stand-alone system scenario using HOMER Pro software, which helps determine the optimal system configuration to meet the anticipated load demand growth in 2030. Table 5.2 presents the predicted data used to assess electricity system loads for Al Marj in 2030.

Table 5. 2 Predicted data of Al Marj city in 2030.

Description	Values
Population estimate, Al Marj city for 2030.	94,404 people
The expected annual average of electricity consumption per capita in 2030	5860 kWh/ann./capita
Energy demand required by the system in 2030 to meet Al Marj electricity demands	517292 MWh/year
The average monthly energy demand for Al Marj city.	43,108.16 MWh/month

- **COE and NPC analysis**

The findings derived from the HOMER Pro simulations for the scenario where there is no capacity shortage are presented in Table 5.3. The results are based on a system configuration consisting of a 160 MW PV array, an 80 MW diesel generator, an 80 MW inverter, and a 30 MWh battery bank.

According to the simulation results, the system exhibits a net present cost (NPC) of 1.17 $ billion and an energy cost of 0.247 $/kWh.

Table 5. 3 Optimal size of the PV stand- alone system in 2030

PV stand-alone system served load at lowest cost of energy						
Architecture				**Cost**		**System**
PV (MW)	Generator (MW)	Battery (MWh)	Converter (MW)	Life cycle cost ($)	Cost of energy ($/kWh)	capacity shortage (%)
160	80	40	60	1.17 B	0.247	0

The system total production is 22,0921.40 MWh/year, which is a combination of the power generated by the PV system and diesel generator. The PV system produces 71,901.05 MWh/year, while the diesel generator produces 14,9020.3 MWh/year. Out of the total power generated, 32.5% is contributed by the PV system, while the remaining 67.5% is produced by the diesel generator.

To achieve an optimal balance between the cost of energy (COE) and the net present cost (NPC), the HOMER Pro software recommended upgrading the system configuration in 2018, as outlined in Chapter 4. The recommended upgrade involves increasing the power production from the diesel generator while keeping the power output from the PV system unchanged. The monthly electric power production of the system is illustrated in Figure 5.9. The total energy consumption of the load is estimated to be 18,8813.77 MWh/year, resulting in an excess electricity production of only 1.72 %. Furthermore, there is no unmet load and capacity shortage observed. The renewable generation contribution is determined to be 21.1%.

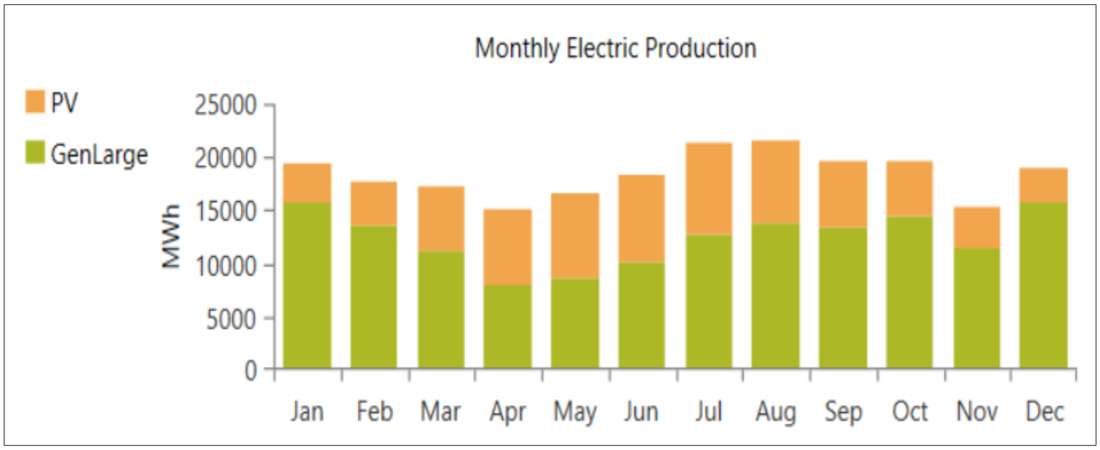

Figure 5. 9 Monthly electricity production for the stand-alone solar hybrid energy system.

- **Sensitivity analysis**

The sensitivity analysis results for all components of the stand-alone solar system design are presented in Figure 5.10 which illustrates the impact of each sensitivity variable on the COE of the system. The analysis reveals that the lowest cost of energy is achieved with a solar radiation of 7.9 kWh/m^2/day, a diesel fuel price of 0.2 $/L, and 34.6% renewable energy sharing, resulting in a COE of 0.193 $/kWh. Moreover, the study shows that there is no need to modify the system module size, battery, diesel generator and converter despite variations in total solar radiation and diesel cost.

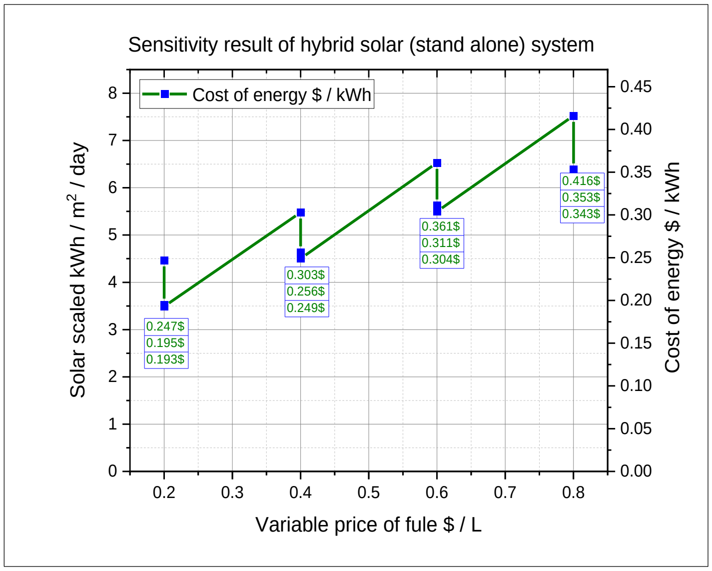

Figure 5. 10 Sensitivity analysis of the optimal COE in a solar system operating in a stand-alone configuration.

In Figure 5.11, the sensitivity analysis results for the Net Present Cost (NPC) of the stand-alone solar system are presented. The NPC is a measure of the total cost of the system over its lifetime, taking into account factors such as initial investment, operating costs, and revenue generated. The analysis indicates that the NPC is minimized under certain conditions. Specifically, the lowest NPC value of 0.90 B$ is achieved when the solar radiation level is 7.9 kWh/m^2/day, the diesel fuel price is 0.2 $/L, and there is no capacity shortage. This implies that the system is most cost-effective when it operates under these specific circumstances. However, as the diesel fuel price increases, the NPC of the system also increases. This suggests that higher fuel costs have a direct impact on the overall cost of the stand-alone solar system. It is important to note that the NPC is influenced by the price of diesel fuel because the system is designed to rely on a combination of solar power and diesel generators.

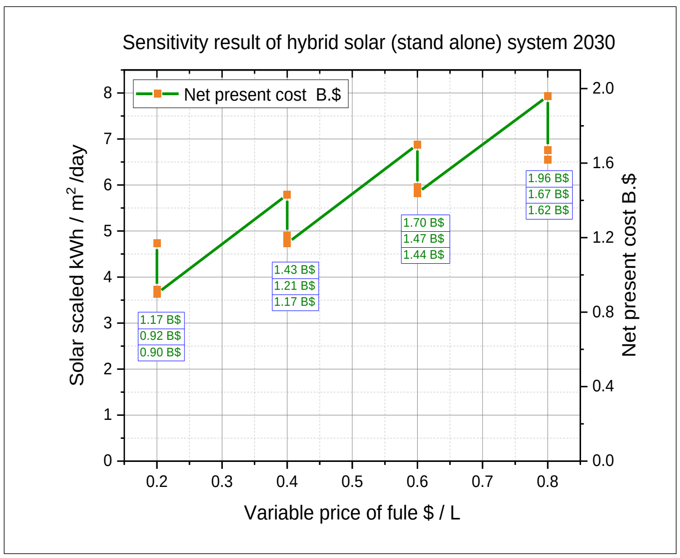

Figure 5. 11 Sensitivity analysis of the optimal NPC in a solar system operating in a stand-alone configuration.

The sensitivity analysis further reveals that variations in solar radiation levels significantly affect NPC. This indicates that changes in the amount of sunlight received by the solar panels have a notable impact on the system's overall cost. Higher solar radiation levels lead to a lower NPC, while lower radiation levels result in a higher NPC. Based on these findings, it is inferred that the design of the stand-alone solar system is highly sensitive to fluctuations in solar radiation and diesel fuel price. This means that small changes in these factors can have a considerable influence on the system's financial performance. However, the analysis suggests that modifying the size of the system's components may not be necessary to optimize its cost-effectiveness.

5.4. Summary

This chapter focuses on utilizing LSTM layers to create a neural network that can predict three critical indicators: Consumption per capita, Primary energy consumption, and Population, for load demand forecasting in AL Marj City. The process started by importing the dataset and normalizing the input and output data to make it suitable for neural network training. The neural network architecture included LSTM layers with 256 hidden units, chosen for their demonstrated ability to provide accurate forecasts. The model was then trained and evaluated using the R-squared value, which showed high accuracy, with values of 0.99988, 0.99993, and 0.99999 for Consumption per capita, Primary energy consumption, and Population, respectively. Additionally, the model's RMSE value decreased and converged during training, indicating its strong forecasting ability. The forecasted values for population, energy per capita consumption, and total energy consumption were employed to calculate the monthly and daily load demand. These load demand values were then utilized in the HOMER Pro software to create a model of a stand-alone system scenario. The purpose of this modelling was to determine the optimal system configuration that would effectively cater to the expected growth in load demand by the year 2030.

CHAPTER 6

Optimal Location and Sizing of DGs
Investigating Power, Frequency, and Voltage Dynamics
Analysis of Optimum Storage System

6.1. Introduction

Traditional electric power systems heavily depend on large-scale generating plants, often fueled by combustion or nuclear technology, situated far away from population centers. This setup necessitates the use of long-distance transmission networks, leading to environmental problems like greenhouse gas emissions and nuclear waste disposal challenges. As the demand for electricity continues to rise, there is a pressing need to significantly expand electricity generation. In 2012, a staggering 70% of the 22,200 TWh of electricity produced globally came from fossil fuels [114]. To address the drawbacks of conventional energy systems, Distributed Generation (DG) technologies have gained popularity. DG involves decentralized power production through smaller generators connected to distribution networks. This approach helps mitigate issues related to power losses, security vulnerabilities, greenhouse gas emissions, and the finite nature of fossil fuel resources. Among the various renewable energy sources suitable for DG, solar panels stand out as a promising solution. Their advantages include easy installation, scalability, low operational costs, and minimal emissions. Additionally, continuous technological advancements and decreasing prices make solar power an increasingly viable option for widespread adoption. Looking ahead, smart grids hold the key to revolutionizing the electricity distribution landscape. These advanced grids enable more efficient control and management of energy distribution, optimizing resource utilization. In this context, Medium Voltage (MV) islanding systems are expected to play a crucial role in the future. These systems can operate autonomously from the main grid, offering economic advantages [115][116]. Over recent years, solar energy has seen remarkable progress, becoming more affordable, widespread, and accessible. The cost of solar PV panels reduced significantly of nearly 80%. In the United States, solar PV installations reached a significant capacity of 96.18GW in 2020, making solar energy responsible for 11% of the country's renewable energy consumption.

Despite these advancements, solar energy does present challenges, including fluctuations and issues with power quality. However, Energy Storage Systems (ESS) offer a viable solution to address these concerns. ESS can effectively mitigate peak demand by absorbing surplus energy during periods of excess generation and injecting it back into the grid during peak demand, thereby ensuring a more stable power supply. To maintain the quality of the supply, particularly in terms of frequency and voltage magnitude, and to prevent overloading of any single resource, it is important to coordinate between Distributed Generators (DGs) and Battery Energy Storage Systems (BESS). Various control strategies have been proposed to enhance system stability and manage the intermittent nature of DGs [117][118]. Power electronic converters play an important role in connecting PV plants to the grid, regulating active power output while maintaining a unity generation power factor. Meanwhile, BESSs function as slack nodes, actively monitoring and regulating voltage and frequency to maintain energy balance and overall system stability. For stand-alone PV generation plants, Valve Regulated Lead Acid (VRLA) batteries are commonly used as they offer a cost-effective and readily available storage technology [119].

This chapter aims to assess the optimal placement and capacity of distributed generation technologies, utilizing Sensitivity and Particle Swarm Optimization algorithms within MATLAB software to minimize power losses in the system. Furthermore, the chapter includes simulations of the microgrid operating in island mode to analyze its behavior during abrupt load changes. Based on the results obtained from HOMER simulations, it was concluded that second-life electric vehicle batteries (SL-EV) offer the most appropriate and economically viable storage solution for achieving optimal performance in a zero decarbonization scenario. The simulation findings provide robust evidence in favor of using SL-EV batteries as the preferred option in this specific system.

6.2. Identification of the Case Study

6.2.1. Background of Study

This case study focuses on the medium voltage distribution network in Al Marj City, Libya, and its investigation and proposed control strategy. Al Marj is situated in the eastern part of Libya and experiences an annual Direct Solar Irradiance ranging from 1972 kWh/m^2 to 2800 kWh/m^2. The study aims to analyse the distribution network's performance and propose an effective control strategy to optimize its operations.

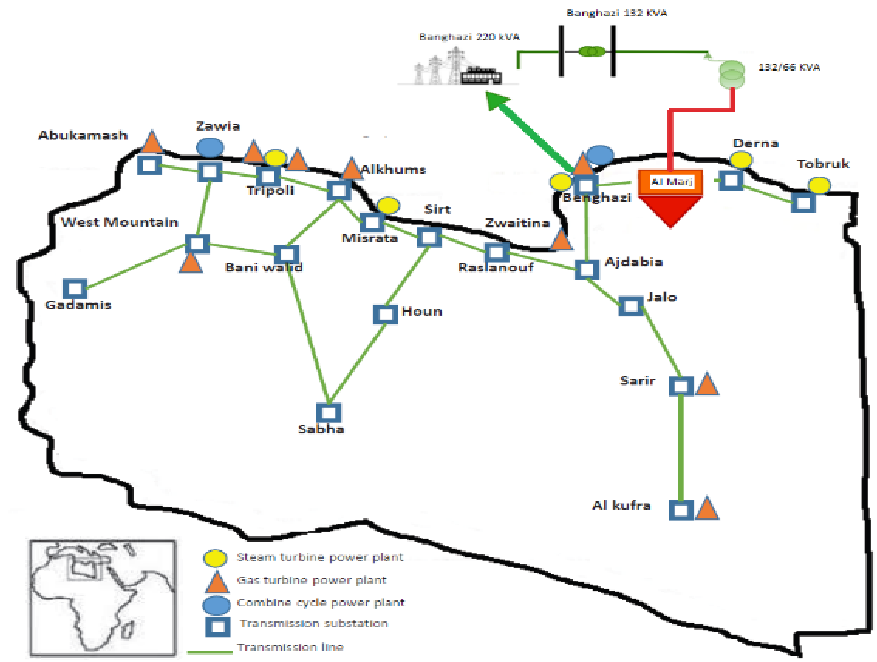

Figure 6. 1 The Gas power plant supplying Al Marj city via radial transmission line [120].

Despite the presence of plentiful energy resources in the region, the Al Marj area has been experiencing persistent and extended periods of power outages. The local gas power plant in the area is supplied through a 100 km radial transmission line that connects to the sub-transmission system, as depicted in Figure 6.1. The network configuration comprises of two step-down transformers with a capacity of 7.5 MVA each, which efficiently reduce the voltage from 66 kV to 11 kV. The system is equipped with a total of twenty-two bus bars that distribute power to twenty equivalent loads. The overall peak load demand is recorded at 2.3 MVA, and this power is transmitted to the loads via twenty overhead connection lines. At the far end of the network, step-down transformers rated at 11/0.4 kV are installed to further lower the voltage and transfer it safely to the loads. Refer to Figure 6.2 for a visual representation of the network setup.

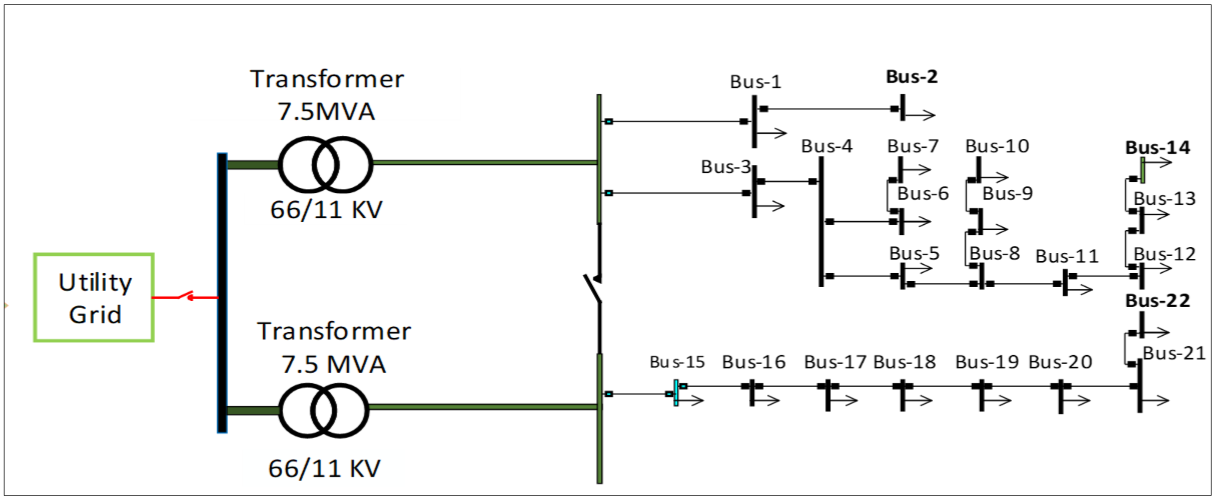

Figure 6. 2 Medium voltage distribution network diagram of Al Marj city.

6.3. Optimizing Distributed Generation Placement for Minimizing Power Loss

6.3.1. Methodology

- **Network power quality levels at steady-state conditions**

The installation of DGs in distribution systems offers numerous advantages, including enhanced reliability, reduced voltage sags, alleviated burden on sub-transmission systems, and the potential utilization of renewable energy sources. The integration of DGs has witnessed a significant rise attributed to these factors [121]. To assess the benefits of implementing DG technologies, specifically solar energy systems and battery storage, MATLAB simulations were conducted under steady-state conditions. These simulations aimed to investigate the effectiveness and potential advantages of deploying DG technologies in the distribution network.

- **Load flow study**

1. Voltage profile

In the case study, a load flow study was conducted to analyse the voltage profile of the network. The results revealed minor variations in voltage levels between nodes under normal operating conditions. Figure 6.3 illustrates the voltage profile of the Grid-connected system without any DGs. During this analysis, it was observed that Buses (12), (13), and (14) experienced the lowest voltage levels, which the voltage level in the 11kV Libyan distribution network kept at requirement limit (±6%).

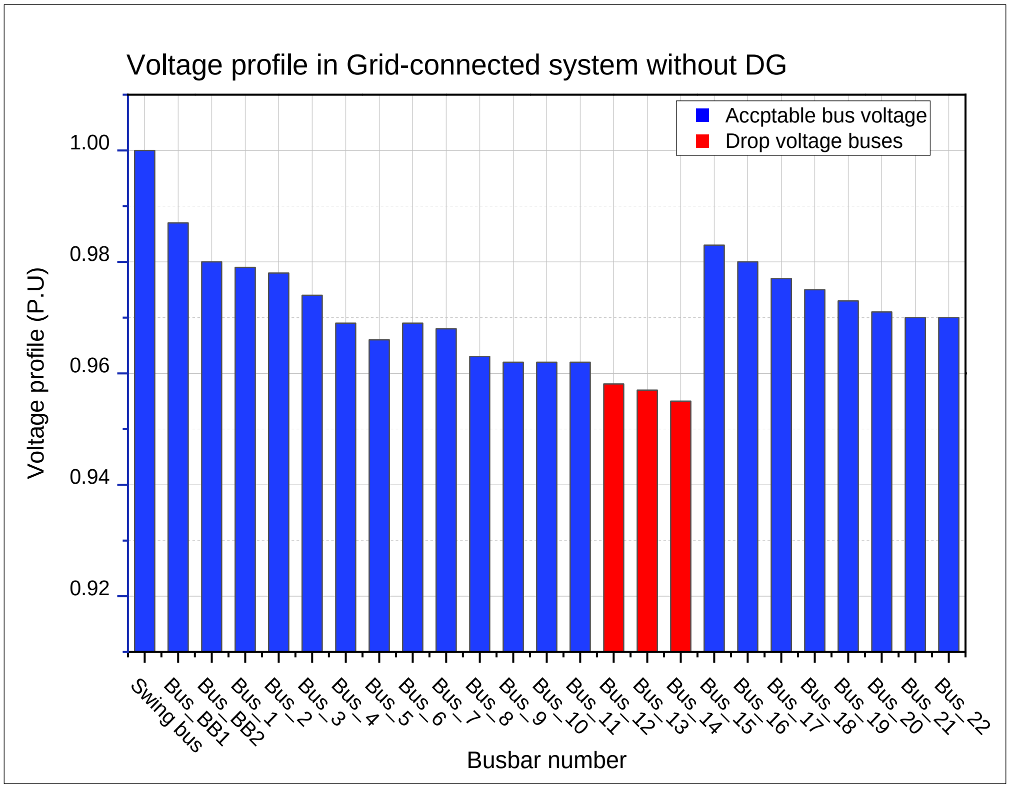

Figure 6. 3 Voltage profile of the grid- connected system without any DG.

2. Sensitivity analysis

In order to ensure optimal performance and minimize undesirable effects, careful consideration must be given to the placement of DG units within the distribution network. Poor positioning of DG units can lead to increased system losses, voltage flicker, and inadequate unit protection, resulting in outcomes contrary to the intended improvements. To address this concern, the case study employed a Sensitivity Analysis algorithm to determine the most suitable locations for DG placement. Additionally, Particle Swarm Optimization (PSO) was utilized to determine the appropriate size of the DG units, with the goal of minimizing power losses and enhancing the voltage profiles in the distribution networks [122][123].

To quantify the system's power losses, the study employed Equation (6.1), and the results were represented as illustrated in (6.2) and (6.3). By utilizing these approaches, it was aimed to achieve an efficient and optimized power system operation with reduced losses and improved voltage profiles in the radial distribution network [124]:

$$P_L = \sum_{i=1}^{n} \sum_{j=1}^{n} (\alpha_{ij} (P_i P_j + Q_i Q_j) + \beta_{ij} (Q_i P_j + P_i Q_j) \tag{6.1}$$

Where:

$$\propto_{ij} = \frac{r_{ij}}{|v_i||v_j|} \cos(\delta i - \delta j) \tag{6.2}$$

$$\beta_{ij} = \frac{r_{ij}}{|v_i||v_j|} \sin(\delta i - \delta j) \tag{6.3}$$

Where:

$\propto_{ij}$ is representing the active power loss coefficient between buses *i* and *j*.

β_{ij} is representing the reactive power loss coefficient between buses *i* and *j*.

δi and δj: are representing the phase angles of the voltage at buses *i* and *j*, respectively.

In the equation (6.1), P_i is active power and Q_i is reactive power injected at bus *i*. The term r_{ij} denotes the resistance between bus *i* and *j*.

The principle of the sensitivity method is based on linearizing the original non-linear equation around the initial operating point. This linearization process is essential in reducing the number of potential solution spaces within the equation, making the analysis more manageable and efficient.

For addressing the DG allocation problem in a system, the loss sensitivity factor is widely utilized. It can be calculated by dividing the differential real power loss by the differential real power injection of the DGs. The formula for the loss sensitivity factor is as follows:

$$\propto_i = \frac{\partial P_L}{\partial P_i} = 2 \sum_{j=1}^{n} (\alpha_{ij} P_j - \beta_{ij} Q_j) \tag{6.4}$$

This factor serves as a critical metric in determining the most effective placement of DG in the system to minimize power losses and optimize the performance of the DG units.

The relationship between the total power loss and the injected power in the system becomes parabolic, with the value reaching zero. This indicates that the power losses are minimized at this point

$$\propto_i = \frac{\partial P_L}{\partial P_i} = 2 \, \Sigma_{j=1}^{n} \; (\alpha_{ij} \, P_j \; - \beta_{ij} \; Q_j) = \; 0 \qquad (6.5)$$

Following this relationship, the real power injected at node i from distributed generation can be determined using equation (6.6):

$$Pi \; = \; \frac{1}{\alpha_{ii}} \; [\, \beta_{ii} \, Q_i + \; \Sigma_{j=1,j\neq i}^{n} \; \alpha_{ij} \, P_j \; - \beta_{ij} \; Q_j] \qquad (6.6)$$

Where:

Pi is Real power injection at bus i.

α_{ii} is Sensitivity factor associated with the real power loss at bus i concerning changes in real power injection at bus i.

β_{ii} is Coefficient associated with the squared term of the real power injection at bus i in the sensitivity analysis.

Q_i is Reactive power injection at bus i.

$\Sigma_{j=1,j\neq i}^{n} \; \alpha_{ij} \, P_j$ are the sum of the product of sensitivity factors α_{ij} and real power injections P_j for all buses j excluding bus i This part captures the influence of real power injections from other buses on bus i.

The difference between real power generation and real power demand at that node i is equal to the real power injected at that node as shown in Equation (6.7):

$$Pi \; = PDGi \; - \; PDi \qquad (6.7)$$

Where *PDGi* represents the real power injected from the DG unit placed at node *i*, and *PDi* is represents the power demand at node *i*. By combining Equations (6.4), (6.5) and (6.7), it can obtain relationship:

$$PDGi \; = \; PDi \; + \frac{1}{\alpha_{ij}} \; [\, \beta_i \, Q_j + \; \Sigma_{j=1,j\neq i}^{n} \; (\alpha_{ij} \, P_j \; - \beta_j \; Q_j) \,] \qquad (6.8)$$

This equation provides a method to calculate the real power injected by the DG unit at node *i* based on the loss sensitivity factor (α_i) and the power demand and generation at that node. It allows for effective optimization of the DG unit's placement and size to minimize power losses and enhance the system's efficiency. The process of sizing a Distributed Generation (DG) unit is performed using the equation (6.8). According to Equation 6.1, the bus with the highest ranking, determined by arranging the list in ascending order based on real power loss, is initially chosen as the location for the first DG unit. The next step involves repeating the process by placing the next DG unit at that specific location. This repetition continues until either the process returns to the same location, indicating that all possible locations have been evaluated, or until a minimum power loss is achieved. To calculate the sensitivity, an algorithm is employed as shown in figure 6.4. The first step involves running the base case load flow analysis. In the second step, the optimal size or number of DG units for each bus is determined using equation 6.6. This equation enables the calculation of the most suitable DG unit size for each bus, considering factors such as power loss minimization and system optimization. By implementing this algorithm, the sensitivity of the system to changes in DG unit sizes can be evaluated, providing valuable insights for decision-making in terms of DG placement and configuration.

The third step of the algorithm involves calculating the power loss for each bus in the distribution network based on the DG units of the optimal size determined in the second step. After determining the optimal size for the DG units, their injections at each bus are considered, and the load flow analysis is conducted using the base case variables as state variables. This analysis helps assess the system's performance with the DG units integrated. Finally, in the last step, the algorithm identifies the bus where the power loss is minimal after the placement of the DG units.

This particular bus is considered the optimal location for the DG unit. At this location, the DG unit achieves the most effective results in terms of minimizing power losses and enhancing the overall system efficiency. To obtain the final results, the load flow analysis is executed, considering the presence of DG units at the identified optimal locations. This comprehensive analysis allows for an evaluation of the system's performance under real operating conditions with the DG units in place. By observing the results of the load flow analysis with DG, the algorithm provides valuable insights into the effectiveness and benefits of DG placement and highlights the impact of DG on minimizing power losses and optimizing the distribution network's performance.

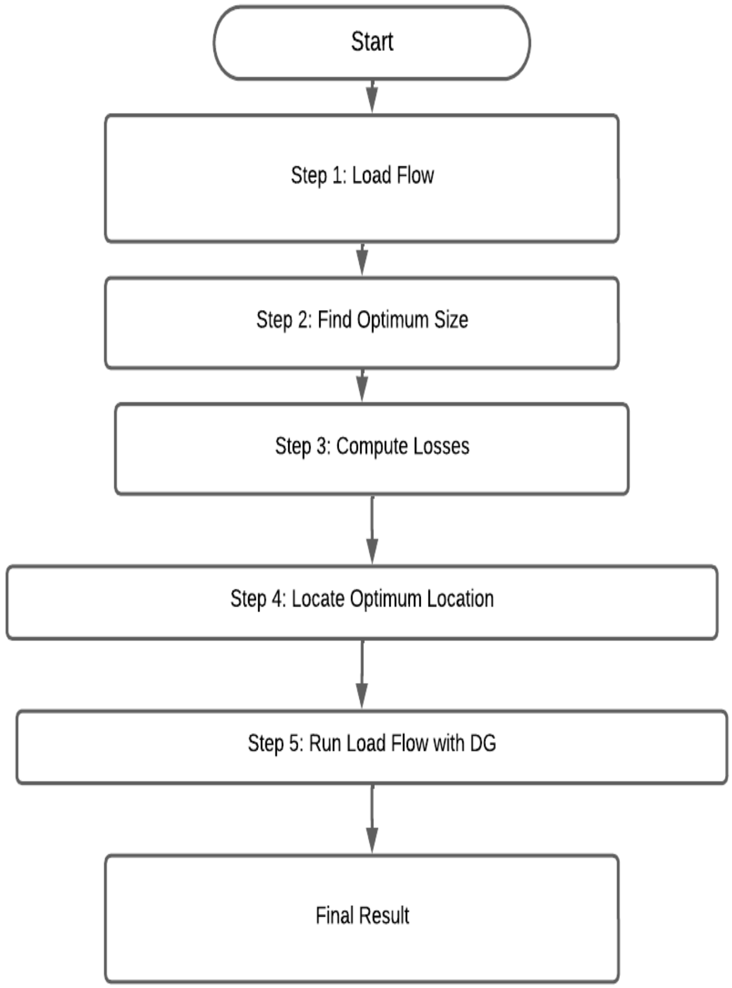

Figure 6. 4 Flowchart representation of the sensitivity analysis algorithm

3. Particle swarm optimization

Particle Swarm Optimization was first introduced in 1995, inspired by the collective behaviour of birds flocking and fish schooling [125]. It is an optimization technique that utilizes a population-based search algorithm, where individual particles dynamically change their positions (states) over time. These particles traverse a multidimensional search space, continuously adjusting their positions based on their individual experiences (Pbest) and the experiences of their neighbouring particles (Gbest). By leveraging the best positions, they have encountered, and the information shared by their neighbours, particles collectively explore and exploit the search space to find optimal solutions. The concept of a Searching Point in PSO is illustrated in Figure 6.5.

In PSO, each particle represents a potential solution to the optimization problem, and they "fly" through the search space looking for the best solution. The Pbest value for each particle represents the best solution it has found so far in its individual search history, while the Gbest value is the best solution found by any particle in the entire swarm. As particles communicate and share information about their best findings, they are influenced by the collective knowledge of the swarm, guiding them towards promising regions in the search space. By iteratively updating their positions and velocities based on their Pbest and Gbest values, the particles efficiently explore the solution space and converge towards optimal or near-optimal solutions. This study has chosen the PSO based on the literature review and emphasizes the importance of optimizing the size and location of distributed generators, particularly in existing power systems like Libya, where renewable energy integration is a novel and growing technology [126].

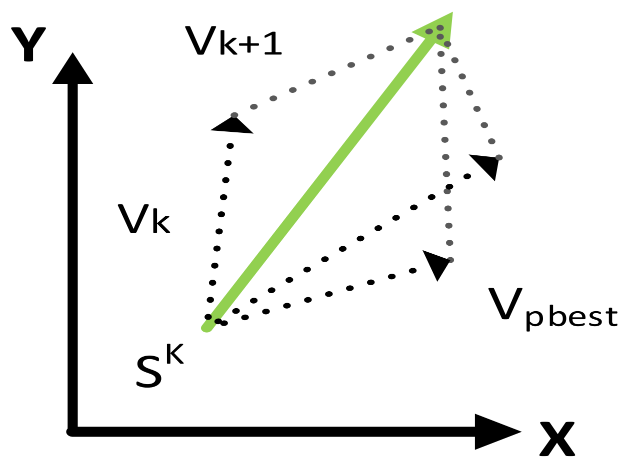

Figure 6. 5 Concept of a Searching Point by PSO.

The modification of particle positions in PSO can be effectively represented through the concept of velocity. The velocity of each particle (agent) is updated using the following equation:

$$(V_{id})^{K+1} = \omega V_{id}^{K} + c_1 rand * (pbest_{id} - S_{id}^{k} + c_2 rand) * (gbest_d - S_{id}^{k}) \quad (6.9)$$

Where:

$(V_{id})^{K+1}$ is the updated velocity of particle *(i)* in dimension *(d)* at iteration *k+1*.

Ω is the inertia weight that controls the impact of the previous velocity on the new velocity.

V_{id}^{K} is the current velocity of particle *(i)* in dimension *(d)* at iteration *k*.

C_1 and C_2 are acceleration coefficients that control the impact of the personal best ($Pbest_{id}$) and global best ($Gbest_d$) information, respectively.

rand is a random value between 0 and 1.

$Pbest_{id}$ is the personal best position of particle *(i)* in dimension *(d)*.

S_{id}^{k} is the current position of particle *(i)* in dimension *(d)* at iteration *k*.

$Gbest_d$ is the global best position among all particles in dimension *(d)* this velocity updte equation allows each practical to gradually approach its personal best position *(pbest)* and the global best position *(Gbest)*, promoting exploration and exploitation in the search space.

To obtain the modified solution space position, the following equation is applied:

$$S_{id}^{K+1} = S_{id}^{K} + V_{id}^{K+1} \tag{6.10}$$

4. Case Study

In this particular section, the main focus revolves around the distribution network of Al Marj City. The primary goal is to effectively tackle the challenge of determining the appropriate location and size of Distributed Generation (DG) sources. This analysis is performed on a network consisting of 22 buses, as illustrated in Figure 6.2 in section 6.2.1. The distribution network data for the system consists of 22 buses and 20 loads, which are presented in Table 6.1. This table provides an overview of the bus and load configurations within the distribution network.

Table 6. 1 Distribution network data of 22 buses and 20 loads in the distribution network system respectively.

Bus number	Sending end note	Receiving end note	Resistance (Ω)	Reactance (Ω)
1	1	2	0.0005	0.0048
2	1	15	0.0013	0.0110
3	1	3	0.0014	0.0513
4	3	4	0.0103	0.0586
5	3	15	0.0047	0.0321
6	4	5	0.0035	0.0967
7	4	6	0.0007	0.0054
8	5	8	0.0008	0.0240
9	6	7	0.0016	0.0207
10	8	9	0.0069	0.0300
11	9	10	0.0053	0.0306
12	8	11	0.0097	0.0570
13	11	12	0.0037	0.0222
14	12	13	0.0035	0.0660
15	13	14	0.0050	0.0900
16	15	16	0.0012	0.0069
17	16	17	0.0009	0.04229
18	17	18	0.0020	0.0180
19	18	19	0.0010	0.0493
20	19	20	0.0024	0.0132
21	20	21	0.0547	0.2360
22	21	22	0.0066	0.0160

Loads	P (MW)	Q (MVar)
1	0.0946	0.07095
2	0.0946	0.07095
3	0.0946	0.07095
4	0.0946	0.07095
5	0.0946	0.07095
6	0.0946	0.07095
7	0.0946	0.07095
8	0.0946	0.07095
9	0.0946	0.07095
10	0.0946	0.07095
11	0.0946	0.07095
12	0.0946	0.07095
13	0.0946	0.07095
14	0.0946	0.07095
15	0.0946	0.07095
16	0.0946	0.07095
17	0.0946	0.07095
18	0.0946	0.07095
19	0.0946	0.07095
20	0.0946	0.07095

6.3.2. Discussion of the Results

- **Scenario l: Grid-connected system**

During the load flow analysis of the grid-connected system, a real power loss of 0.747 MW was observed. This loss indicates inefficiencies within the system and highlights areas that may require attention for optimization. Additionally, the voltage profile of the system, as illustrated in Figure 6.3 of section 6.3.2, was thoroughly examined. The voltage profile provides valuable information about voltage variations across different nodes in the network, offering insights into the system's overall performance and stability. Analyzing both the real power loss and voltage profile results contributes to a comprehensive understanding of the system's operational characteristics, enabling system operators and engineers to make informed decisions to enhance its efficiency and reliability.

- **Scenario ll: Off-grid system**

The algorithm has been adjusted to account for the grid being offline when calculating the DG location and power loss. In the first iteration, the maximum loss savings are observed at bus 14. The optimal size for the DG at bus 14 is determined to be 4.8965 MW. If a DG of 4.9965 MW is connected at bus 14 in the base system, it serves as the base case. The program then identifies bus 22 as the next optimal location for a DG with a size of 2.0195 MW. Subsequently, a DG of 2 MW is placed at bus 22 to determine the subsequent optimal location. The analysis continues, and bus 2 is found to be the next optimal location with a recommended DG size of 0.9995 MW.

Further, a DG of 0.9995 MW is placed at bus 2 to identify the subsequent optimal location. This leads to bus 14 being identified with a size of (-2.8964 MW), indicating that the DG size at bus 14 has been reduced from 4.8965 MW to approximately 2 MW in order to minimize the real power loss in the islanded mode. These optimization steps are summarized in Table 6.2, providing a clear overview of the optimal DG locations and sizes for reducing power loss in the system under consideration.

Table 6. 2 The Size of DG and optimum location

Iteration No.	Location BUS No.	DG size (MW)	Loss Reduction (MW)
1	14	2	0.176
2	22	2.0195	0.169
3	2	0.9995	0.104
4	14	- 2.8964 MW	0.027

Consequently, DGs were installed at buses 14, 22, and 2 with capacities of 2 MW, 2.0195 MW, and 0.9995 MW, respectively. The total real power losses were then evaluated for both grid-connected and off-grid scenarios, and Table 6.3 presents a comparative analysis of these losses. Notably, the table showcases the considerable reduction in power losses achieved through DG installation in the off-grid system. The difference in total power losses between the grid-connected and off-grid configurations serves as a clear indication of the effectiveness of DGs in mitigating power losses and enhancing the overall performance of the system. This underscores the significance of incorporating DGs in power systems to optimize their efficiency and reliability.

Table 6. 3 Total power loss in grid-connected and off-grid system

	Grid connected system (MW)	Three DG Off-grid system (MW)
Real power loss	0.74786	0.271021

Through load flow analysis, the voltage profile of the off-grid system was thoroughly examined after integrating three distributed generators (DGs) at buses 14, 22, and 2. These DGs were installed with capacities of 2 MW, 2.0195 MW, and 0.9995 MW, respectively, as detailed in Table 6.2. Notably, the voltage profile exhibited significant improvement compared to the voltage profile observed in the grid-connected scenario. The visual representation of the system's single-line diagram can be found in Figure 6.6, while the results of the enhanced voltage profile are depicted in Figure 6.7. The remarkable improvement in the voltage profile highlights the effectiveness of

DG integration in the off-grid setup, signifying a substantial enhancement in the system's overall voltage stability and performance.

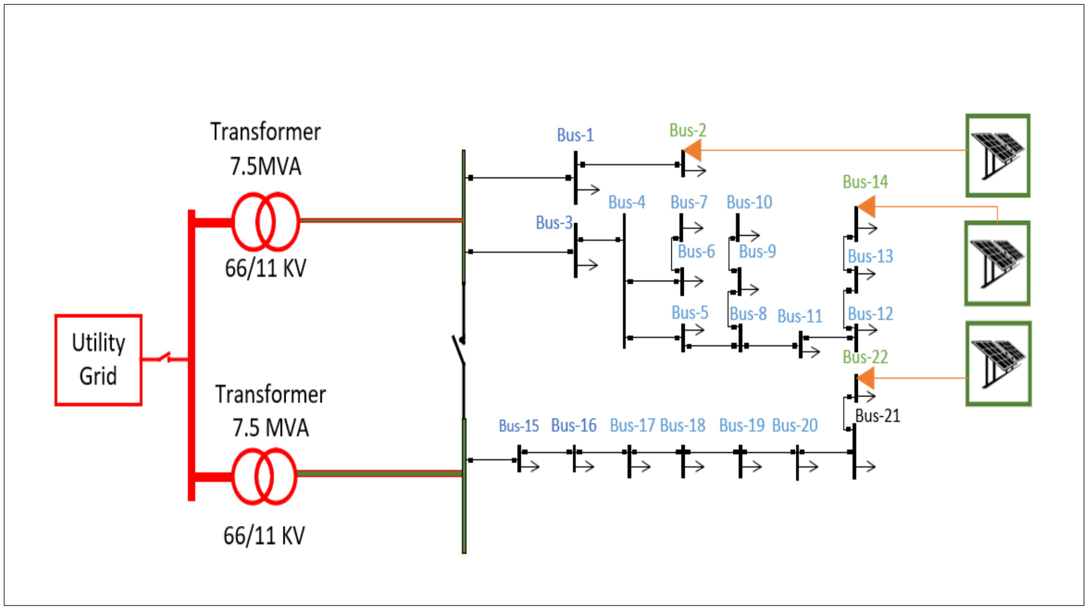

Figure 6. 6 Off-grid with DGs at buses 2, 14 and 22.

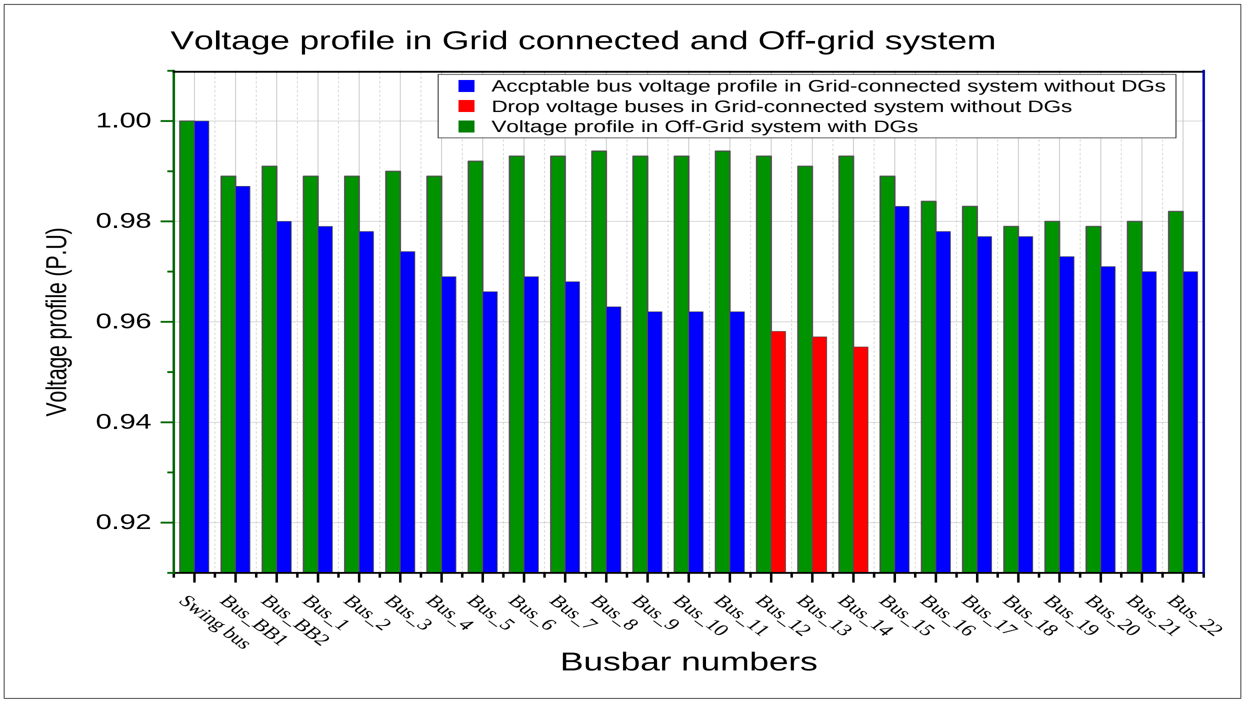

Figure 6. 7 Result of voltage profile as comparison off-grid with DGs and grid-connected.

6.4. Investigating Power, Frequency, and Voltage Dynamics through Modelling and Simulation

6.4.1. Microgrid Overview

The microgrid model for Al Marj City is depicted in Figure 6.8, illustrating its structure and components. The microgrids within the city are connected to medium voltage grids through breakers. Loads, such as electrical appliances and devices, are connected to the AC (alternating current) side of the microgrids, PV panels and BESS are connected to the DC (direct current) side. To facilitate the exchange of power between the AC and DC sides, a three-phase power electronic converter is employed. This converter utilizes six Insulated-Gate Bipolar Transistors (IGBTs), which are electronic switches, to control the flow of electricity and ensure efficient conversion and integration between the AC and DC systems of the microgrid.

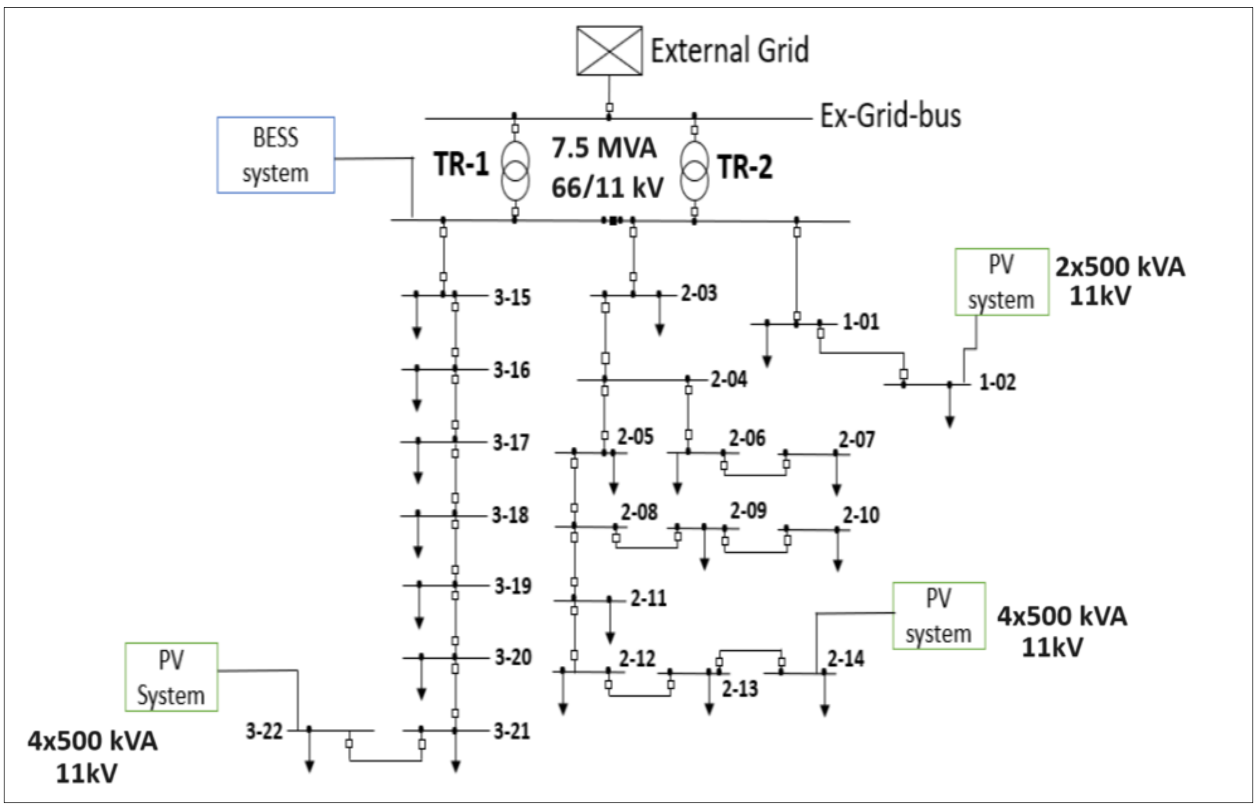

Figure 6. 8 Diagram of the microgrid model.

6.4.2. Battery Energy Storage System Model

Fuel cells have gained significant popularity as a distributed energy source, with applications ranging from hospitals and offices to residential areas and remote construction sites. On the other hand, battery systems utilizing lead-acid technology, although having lower energy density, are more cost-effective, making them a preferable choice for larger systems. While wind and solar power provide renewable energy, their intermittent nature often necessitates the incorporation of energy storage systems for standalone applications. Historically, batteries have been employed as backup power sources for solar and wind systems. Among the various electrochemical energy storage systems available, lead-acid batteries are the most widely employed [127][128].

Figures 6.9 and 6.10 illustrate the charge and discharge functions, respectively. It is important to note that this thesis does not focus on extensively covering the charge and discharge functions. In terms of the discharge curves these are represented in three primary sections. The first section shows an exponential voltage drop when the battery is fully charged. In the second section, the battery can be discharged until its voltage reaches a predetermined minimum level. Towards the end of this section, the total discharge is demonstrated by a rapid and steep slope in the voltage drop [129].

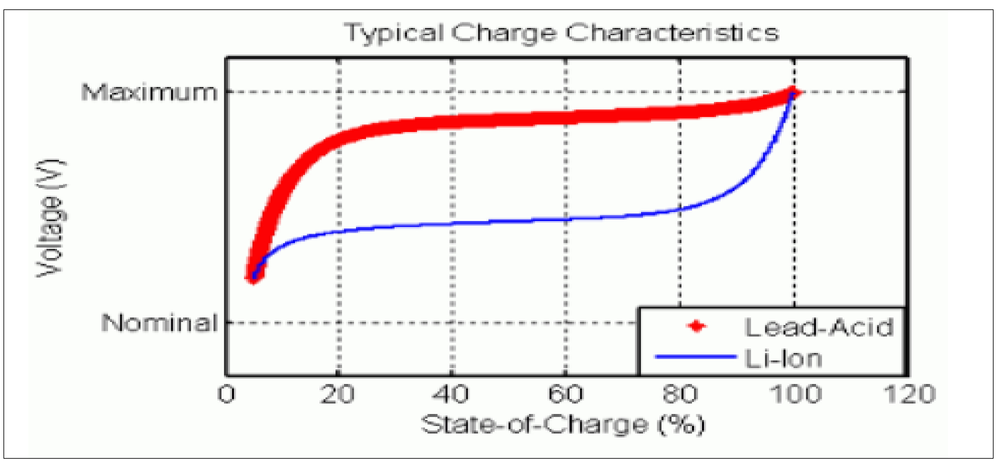

Figure 6. 9 Charge characteristic of the Lithium-Ion battery [129].

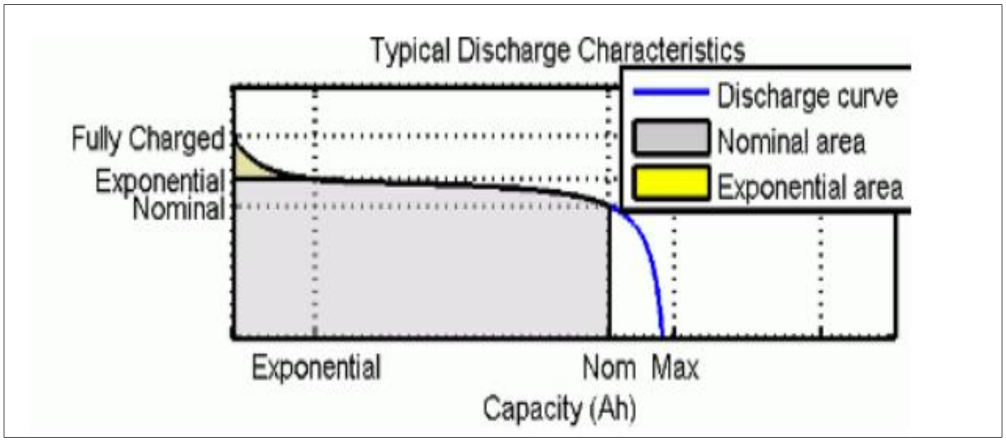

Figure 6. 10 Discharge characteristic of the Lithium-Ion battery [129].

6.4.3. Voltage Source Converter (VSC)

Recent advancements in power electronics and manufacturing processes have led to a significant increase in the switching frequency of Insulated-Gate Bipolar Transistors (IGBTs). IGBTs can be turned off by controlling their gate voltage, eliminating the need for external signals. This advantageous feature allows IGBTs to bridge AC and DC networks without the need for complex switching circuits like thyristors. The voltage on the DC side of the IGBTs can be regulated by modifying the switching signal at the IGBT gates. By incorporating a capacitor, the DC voltage can be stabilized [130]. In this study, a Voltage Source Converter (VSC) was implemented, utilizing six IGBTs to convert DC to AC in three phases. IGBTs can operate in both AC and DC states due to the inclusion of reverse diodes. The development of Voltage Source Converters (VSCs) has facilitated the seamless integration of renewable sources into power systems. VSCs offer a high degree of control flexibility, allowing them to be utilized in back-to-back or DC-to-AC converter systems for the integration of solar cells, wind turbines, and fuel cells into power systems. Given the time-variable nature of renewable resources, the incorporation of energy storage becomes essential in microgrids. Energy storage systems play a crucial role in reducing uncertainty in power generation and enhancing overall reliability. Among the preferred options for energy storage in microgrids, battery storage and supercapacitor storage stand out as two widely utilized technologies.

In order to interface with the power system, both supercapacitors and batteries require Voltage Source Converters (VSCs). As their outputs are in DC, an DC-to-AC inverter is necessary to connect them to AC grids. Within the VSC, monitoring of active and reactive power sets is performed as part of BESS. In this study, a frequency-active power and voltage-reactive power droop controller have been implemented on the VSC. This controller serves to prevent frequency and voltage deviations caused by load changes or disconnection from the utility grid. Each IGBT operates in parallel with the mentioned controller. Figure 6.11 displays the schematic representation of the VSC.

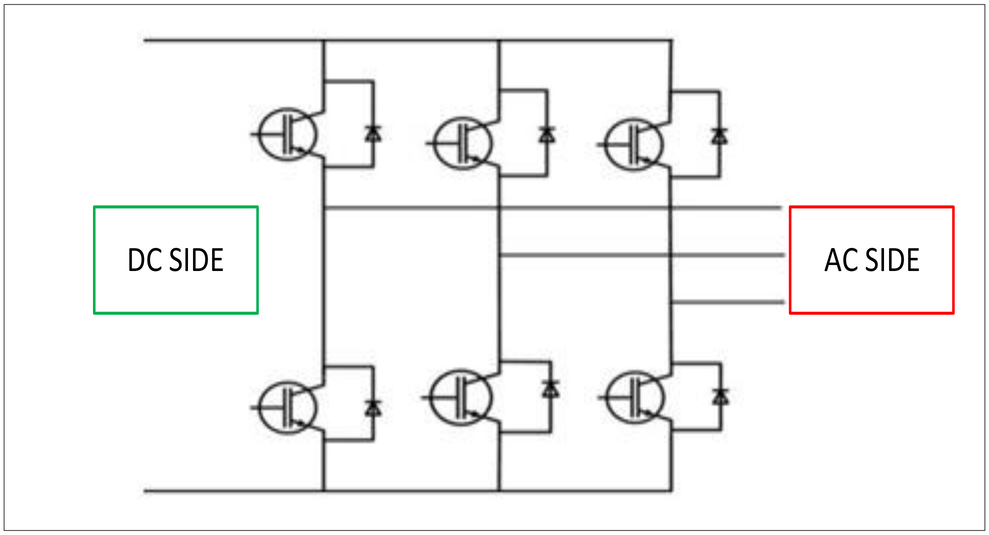

Figure 6. 11 Bidirectional VSC with IGBT switches.

6.4.4. Grid Model

The Simulink model representing the configuration of the case study is displayed in Figure 6.12 below. The configuration includes a three-phase source located at the utility plant, which is connected to a distribution line.

To simulate a microgrid system operating in island mode using MATLAB, it has commenced by modeling its fundamental components. This involves PV systems, battery storage systems (BESS), and loads. Also, model power electronics components such as inverters and converters to facilitate effective interfacing among renewable sources, storage systems, and loads as illustrated in Appendix B. During island mode operation, the microgrid is isolated from the main grid simulation, triggering the activation of islanded mode control strategies. These strategies ensure the stable operation of the microgrid in standalone mode by overseeing voltage, frequency, and power flow regulation within the system. Furthermore, performance monitoring and analysis are conducted to assess system stability. This approach allows us to simulate and scrutinize the operation of a microgrid system in island mode using MATLAB software.

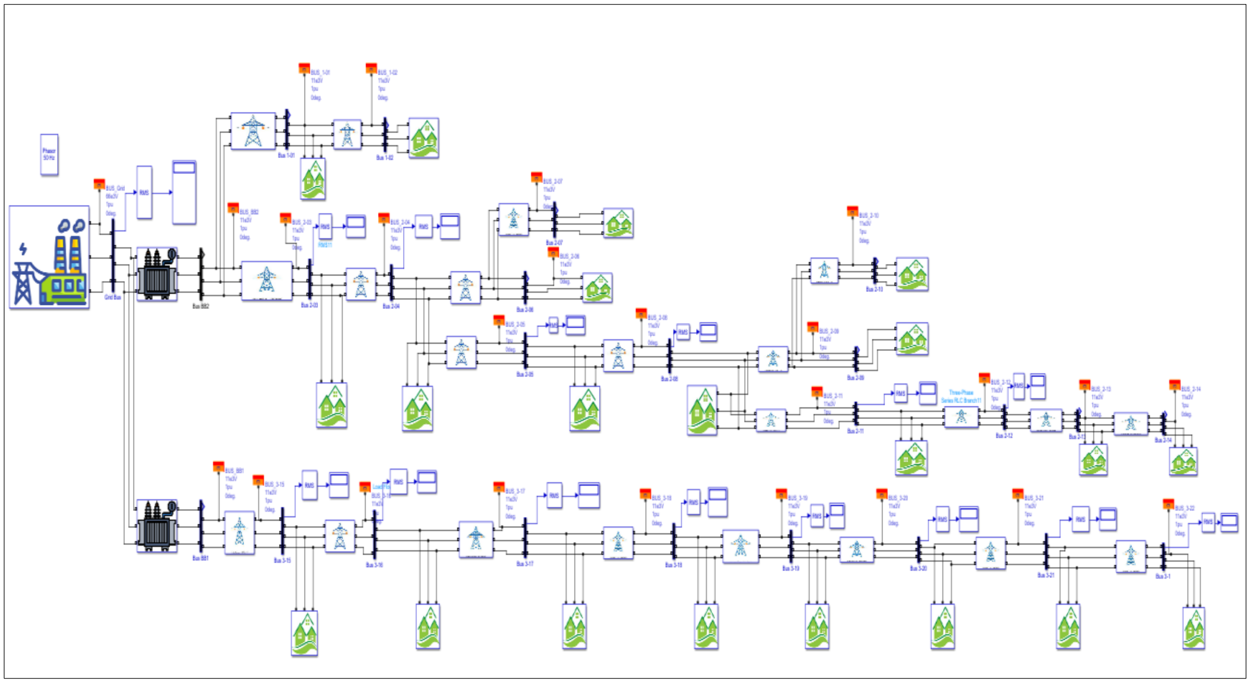

Figure 6. 12 Simulink model of the case study.

The microgrid is isolated from the main utility grid through the use of a three-phase breaker, as depicted in Figure 6.13. The substation in the microgrid configuration consists of a two-step-down transformer. The three-phase source in the configuration is designed as a swing generation type, with an RMS voltage of 66 kV across the phases. The frequency of the utility grid is set at 50 Hz, and the two-step-down transformer is rated at 66/11 kV.

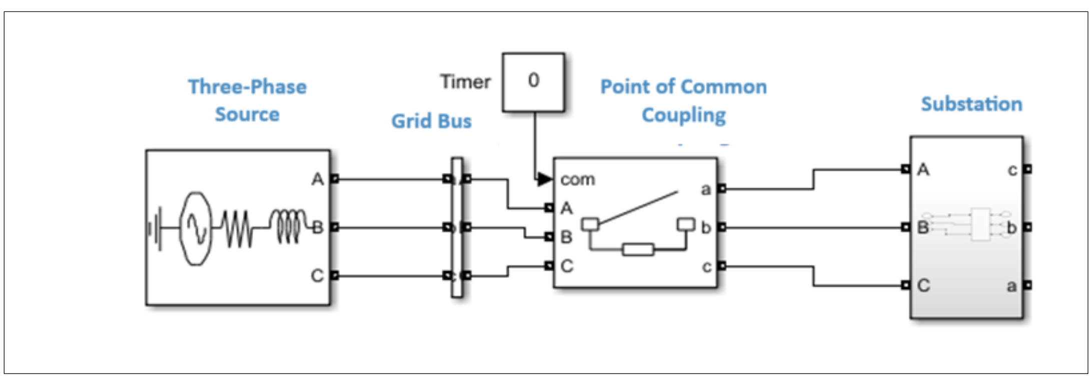

Figure 6. 13 Model of the three-phase breaker.

6.4.5. Load Model

Static loads and dynamic loads are the two types of loads that can be modelled in a microgrid. Static loads have constant power, current, and impedance characteristics. In this thesis, the sample loads are modelled using static loads with constant power type. Series RLC circuits are employed for load modelling. To evaluate the voltage and frequency response of the voltage source converter's control strategy, the loads are connected and disconnected from the microgrid. The load parameters are as follows:

- Equivalent of twenty loads.
- Each load consumes an estimated 0.0946 MW of active power.
- The voltage between the three phases is 11 kV at the line-to-line level.

6.4.6. PV Model

Due to the intermittent nature of solar irradiation, the power generated by solar panels cannot be guaranteed to meet the electricity demand of the microgrid when it is disconnected from the utility grid. Therefore, in the case of standalone mode, the PV panels alone cannot support the microgrid. In such cases, BESS is playing an important role in providing the necessary support. The BESS takes on the responsibility of supplying power to the microgrid. The model of PV with its control can be found in Appendix B.

6.4.7. Measurement Process

- ***dq* Transformation**

Park transformations or *dq* are vector space transformations of three-phase time-domain signals from stationary phase coordinate systems to rotating coordinate systems *(dq)*. The *dq* transformation essentially extends the Clarke transformation by applying an enable transformation to convert from a stationary to a synchronously rotating reference frame. In voltage source converters, the synchronous reference frame rotates with the voltage, while in current source converters, it rotates with the current. A mathematical model of a microgrid is derived using the dq transformation. A key advantage of the *dq* transformation is that it removes time-variant coefficients [131][132][133]. It is important to note that the transformation matrix and the inverse transformation matrix are defined in the following way [134]:

Park (*abc* to *dq*) $$A = \frac{2}{3}\begin{bmatrix} \cos\theta & \cos\left(\theta - \frac{2\pi}{3}\right) & \cos\left(\theta + \frac{2\pi}{3}\right) \\ -\sin\theta & -\sin\left(\theta - \frac{2\pi}{3}\right) & -\sin\left(\theta + \frac{2\pi}{3}\right) \\ \frac{1}{2} & \frac{1}{2} & \frac{1}{2} \end{bmatrix} \qquad (6.11)$$

Invers Park (*dq* to *abc*) $$A^{-1} = \begin{bmatrix} \cos\theta & -\sin\theta & 1 \\ \cos\left(\theta - \frac{2\pi}{3}\right) & -\sin\left(\theta - \frac{2\pi}{3}\right) & 1 \\ \cos\left(\theta + \frac{2\pi}{3}\right) & -\sin\left(\theta + \frac{2\pi}{3}\right) & 1 \end{bmatrix} \qquad (6.12)$$

The angle θ in the dq transformation is defined as $\theta = \omega t + \delta a$

Where:

ωt represents the angular frequency.

δa is the initial phase shift of the voltage.

Figure 6.14 provides a graphical representation of the corresponding vectors. In both the symmetrical components transformation and the *dq* transformation, the zero component is identical, denoted as $1/(3) * (Va + Vb + Vc)$. These transformations allow for the conversion of three-phase time-domain signals from the stationary phase coordinate system *(abc frame)* to rotating coordinate systems *(dq frame)*. By employing the *dq* transformation, the terminal voltage serves as the bridge between the variables in the *abc* frame and the new variables in the *dq* frame. This transformation simplifies the mathematical modelling of power systems and microgrids, providing a key advantage in the removal of time-variant coefficients, facilitating easier analysis and control.

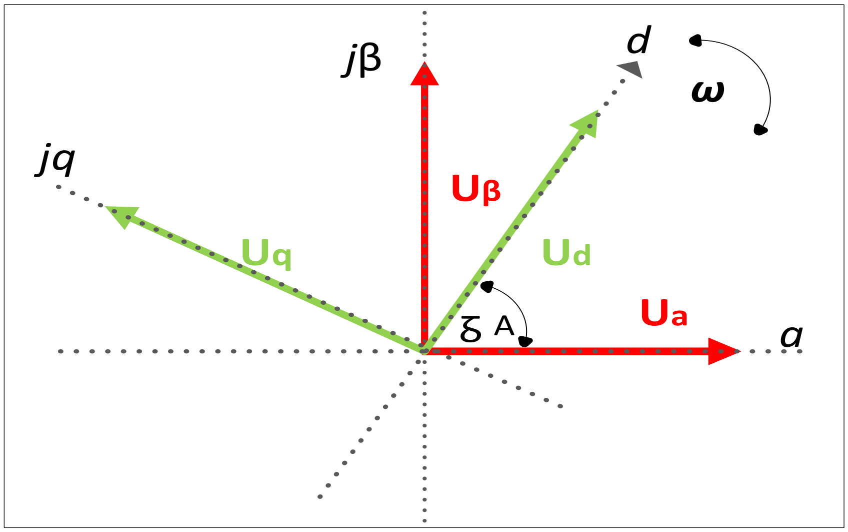

Figure 6. 14 dq0 transformation.

The *dq* transformation equations are given by:

Transformation from *abc* to *dq* frame:

$$V_{dq} = A.\ V_{dq} \tag{6.13}$$

Transformation from *dq* to *abc* frame:

$$V_{dq} = A^{-1}.\ V_{abc} \tag{6.14}$$

Where:

Vabc =[Va, Vb, Vc] represents the three-phase voltage vector in the *abc* frame.

Vdq represents the voltage vector in the *dq* reference frame.

A is the transformation matrix that converts *abc* frame quantities to *dq* frame quantities.

A^{-1} is the inverse of the transformation matrix, converting *dq* frame quantities back to abc frame quantities.

$$V_{abc} = \begin{bmatrix} Va \\ Vb \\ Vc \end{bmatrix},\ V_{dq} = \begin{bmatrix} Vd \\ Vq \\ V0 \end{bmatrix} \tag{6.15}$$

Vd and *Vq* represent the *d*- and *q*-components of the voltage, respectively, in the *dq* frame.

V0 represents the zero component of the voltage in the *dq* frame.

- **The instantaneous power in dq0**

The abc to dq0 block employs a Park transformation to convert a three-phase (abc) signal into a dq0 rotating reference frame. The angular position of this rotating frame is determined by the input wt, measured in radians. Similarly, the dq0 to abc block utilizes an inverse Park transformation to convert a dq0 rotating reference frame back to a three-phase (abc) signal. The angular position of this rotating frame is also determined by the input wt, measured in radians. When the alignment of the rotating frame at wt=0 lags 90 degrees behind the phase A axis, a positive-sequence signal with magnitude=1 and phase=0 degrees results in the following dq values: d=1, q=0.

In order to determine the instantaneous active and reactive power, the following equation is used.

$$p = V_d I_d + V_q I_q \tag{6.16}$$

$$q = V_q I_d - V_d I_q \tag{6.17}$$

Where:

V_d is the d-component of the terminal voltage in the *dq* frame.

V_q is the q-component of the terminal voltage in the *dq* frame.

I_d is the d-component of the current in the *dq* frame.

I_q is the q-component of the current in the *dq* frame.

When the synchronous frame is aligned to voltage the quadrature component is zero and the equations could be simplified as bellow.

$$p = V_d.I_d \tag{6.18}$$

$$q = - V_d.I_d \tag{6.19}$$

Whare:

p is the instantaneous active power.

q is the instantaneous reactive power.

The independent control of active and reactive power is achieved using the *dq* transformation. Moreover, Time constant version of the *dq* transformation means the instantaneous power in the *dq* frame is not equal to active or reactive power in the *abc* frame [134]. The definition of a power constant *dq* transformation is:

$$\begin{bmatrix} Vd \\ Vq \\ V0 \end{bmatrix} = \frac{2}{3} \cdot \begin{bmatrix} \cos\theta & \cos\left(\theta - \frac{2\pi}{3}\right) & \cos\left(\theta + \frac{2\pi}{3}\right) \\ -\sin\theta & -\sin\left(\theta - \frac{2\pi}{3}\right) & -\sin\left(\theta + \frac{2\pi}{3}\right) \\ \frac{1}{2} & \frac{1}{2} & \frac{1}{2} \end{bmatrix} \cdot \begin{bmatrix} Va \\ Vb \\ Vc \end{bmatrix} \quad (6.20)$$

The inverse transformation is given by:

$$\begin{bmatrix} Va \\ Vb \\ Vc \end{bmatrix} = \begin{bmatrix} \cos\theta & -\sin\theta & 1 \\ \cos\left(\theta - \frac{2\pi}{3}\right) & -\sin\left(\theta - \frac{2\pi}{3}\right) & 1 \\ \cos\left(\theta + \frac{2\pi}{3}\right) & -\sin\left(\theta + \frac{2\pi}{3}\right) & 1 \end{bmatrix} \cdot \begin{bmatrix} Vd \\ Vq \\ V0 \end{bmatrix} \quad (6.21)$$

6.4.8. Proposed Control Strategy

This study focuses on conducting main case studies to replicate the operation of controllers employed in the VSC connected to the battery banks. Specifically, a control strategy for the island mode is proposed. In this context, two primary control modes are discussed: the current-controlled mode and the voltage/frequency control mode for the islanded Al Marj city microgrid.

This section specifically focuses on the control of a VSC during stand-alone conditions, when the microgrid transitions to stand-alone mode and is disconnected from the utility grid. In this scenario, as the operating frequency of the VSC is no longer determined by the utility grid, the VSC controller assumes the responsibility of maintaining the frequency for the network. Consequently, the BESS incorporates a VSC with frequency control.

In stand-alone mode, microgrids are disconnected from the grid, resulting in a different role for the VSC controller. Instead of controlling active and reactive power, the VSC controller is now primarily focused on frequency regulation. Figure 6.15 provides an illustration of the connection between the VSC terminal of the BESS and the three-phase load through an *RLC* filter. In figure 6.15 the filter is containing *RL* series and connected parallel *Cf* which represents the shunt capacitor. Hence, C*f* produces *Qc* and VSC supplies active and reactive power (*Ps*, *Qs*) to the microgrid load.

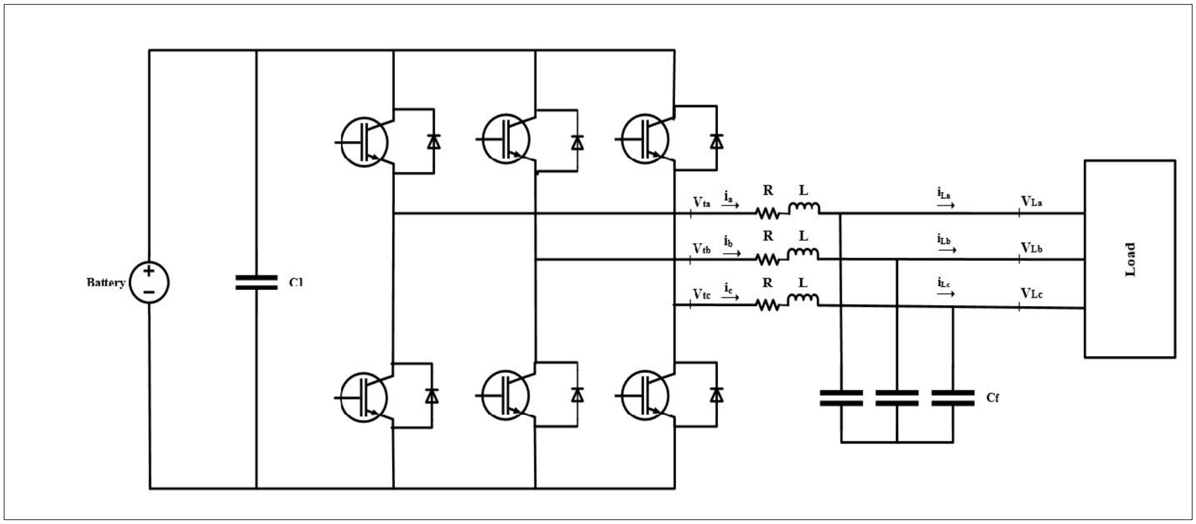

Figure 6. 15 VSC system with battery as a DC source connected to a three-phase load [127].

6.4.9. Analysis of Microgrid Performance in Stand-Alone Mode

A standalone controller is designed in accordance with Section 6.5.8. The utility grid frequency is not imposed at the PCC in this operating mode because the grid is disconnected using the three-phase breaker (see section 6.5.4), By regulating the voltage and frequency, the voltage/frequency controller ensures the loads have a stable voltage, and frequency, and the reactive and active power exchange is determined by the loads. After disconnecting 13 loads from the network during the starting run and waiting for 5 seconds, the simulation starts with 1.48505 MW of peak load. 11 kV and 50 Hz are selected as the reference voltage and frequency, respectively. *PL* and *QL* are the values of active power, and reactive power injected into the loads. Based on the simulation results, the microgrid operates stably in stand-alone mode. To evaluate the performance of the voltage/frequency controller, the simulation is run until it reaches 5 seconds then five loads are added to the previous loads to bring the power demand up to 2.07MW as shown in Figure 6.16.

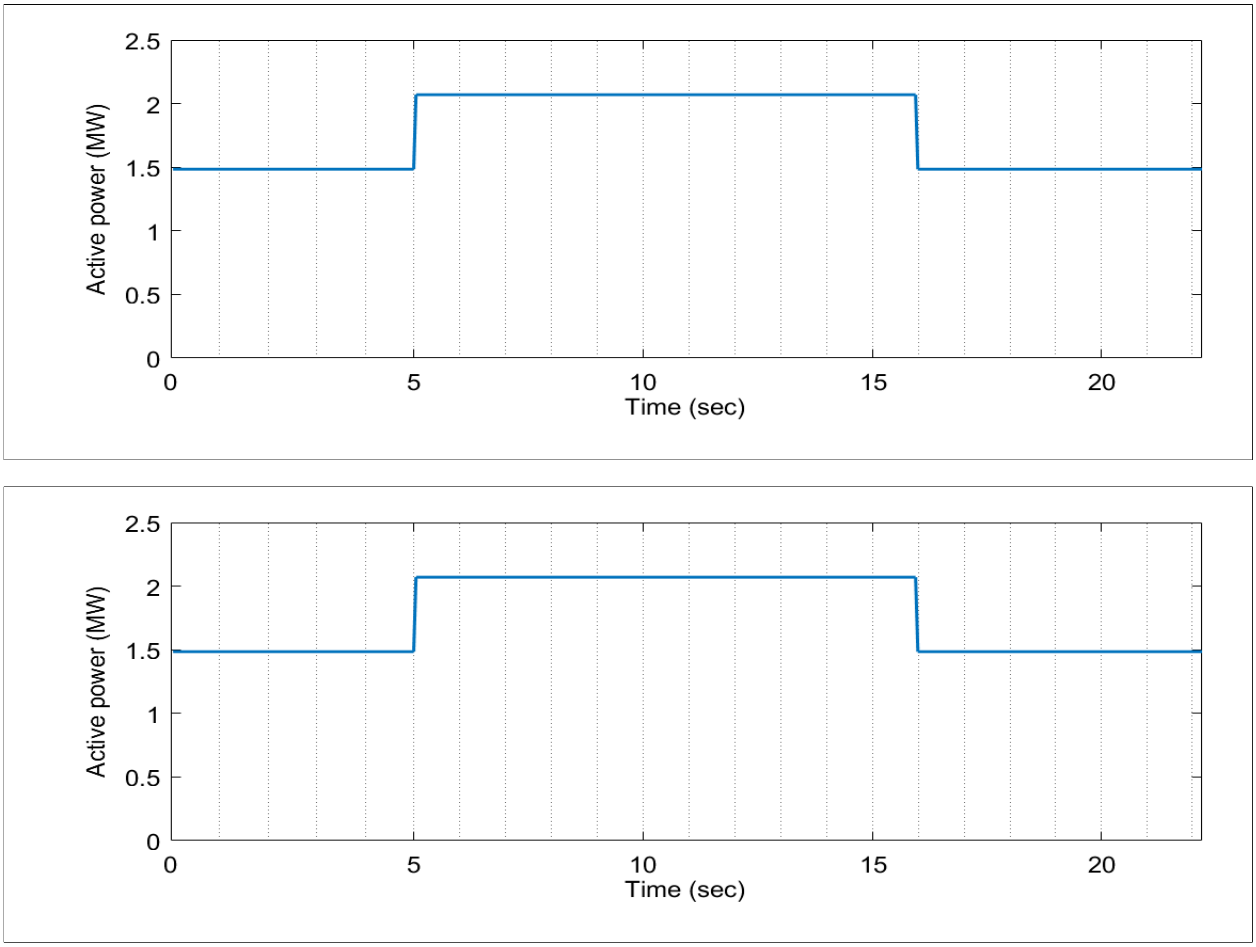

Figure 6. 16 Active power of load demand.

As expected, when the power demand exceeds the power injected into the loads by the battery inverter, the frequency of the microgrid drops. Additionally, the reactive power injected into the loads is insufficient to meet the demand, leading to a decline in the VSC terminal voltage V_t and subsequently, the load voltage V_L also drops. To address this issue, a PI (Proportional-Integral) controller is employed to sense the error between the actual load voltage V_L and the reference voltage V_{Lref} . Upon observing the error in voltage and frequency, the PI (Proportional-Integral) controller springs into action, initiating corrective measures to rectify the detected deviations and stabilize the voltage. Through its control actions, the PI controller adjusts the system parameters to ensure that the voltage and frequency return to their desired reference values, thus maintaining a stable and consistent power supply to the loads. Upon closer examination of the simulation results in Figures 6.17 and 6.18, it can be observed that the frequency variation is within an acceptable range compared to the standards set by the General Electric company of Libya, which is typically within +/- 5% of the nominal frequency (50 Hz). The frequency in the simulation results fell within the range of 50.048-49.96 Hz, demonstrating compliance with the specified standards. Overall, the use of the PI controller ensures that the microgrid operates within acceptable frequency limits and maintains stable voltage levels despite fluctuations in power demand and reactive power injection. This control mechanism is important for the reliable and efficient operation of the microgrid in stand-alone mode. After applying a disturbance at t = 16 seconds by disconnecting the same five loads, the demand becomes lower than the power injected to the loads by the battery, resulting in an increase in frequency. As reactive power demand decreases, the VSC inverter produces more reactive power than is consumed by the loads. As a result, VSC terminal voltage V_t and load terminal voltage V_L increase. The PI controller attempts to justifying for the error between V_L and V_{lref}. As a result of using the PI controller, the voltage shows several ripples before settling. If the PI controller is tuned more tightly, the response is faster. Similar to the first disturbance, V_L and f_L are maintaining their nominal values just a fraction of 0.1 second after the disturbance is applied to the loads and the controller sets them to 11 kV and 50 Hz, respectively.

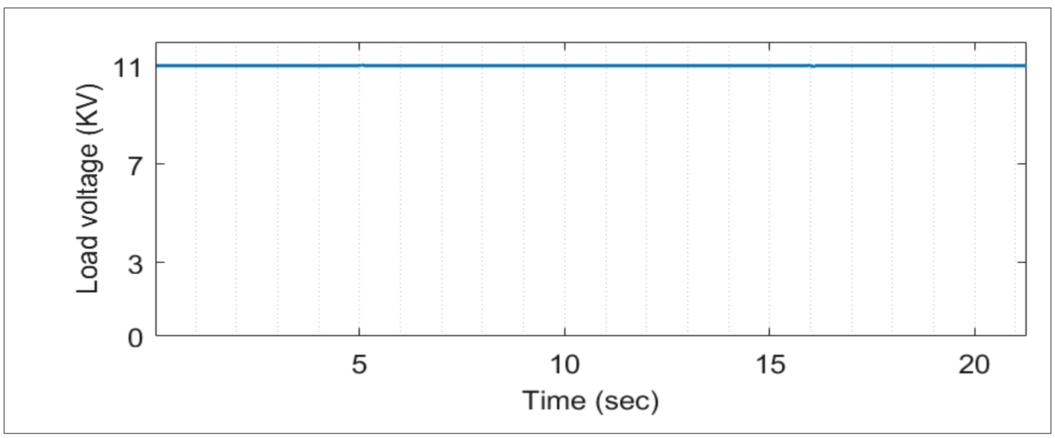

Figure 6. 17 Load voltage when the Microgrid is in the stand-alone mode operation.

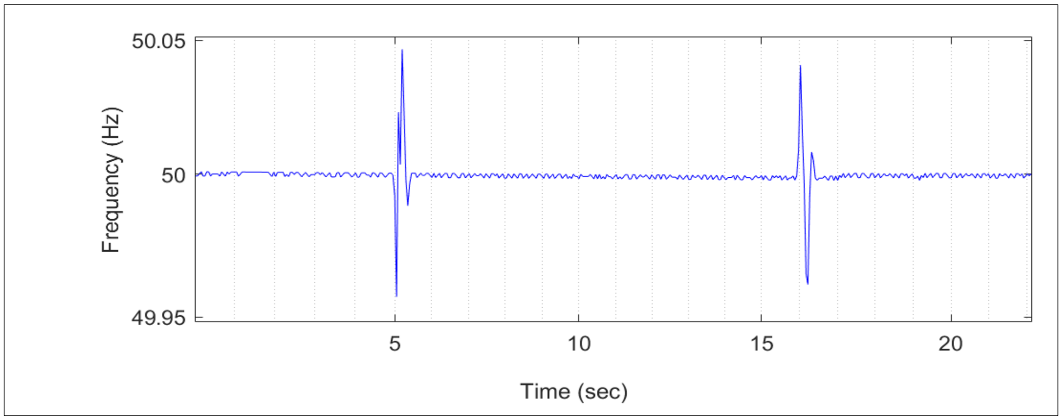

Figure 6. 18 Frequency when the Microgrid is in the stand-alone mode operation.

6.5. Analysis of The Economic Storge System

To conduct an optimal economy evaluation of two types of batteries, SL-EVB and Lead Acid, a methodology is employed as depicted in Figure 6.19. This flow chart outlines the steps taken to evaluate the economic viability of integrating these batteries into a microgrid system. The evaluation process utilizes HOMER-Pro simulation software and incorporates various input variables such as load profiles, solar radiation data, component economics, and other relevant parameters. A typical dataset is used to perform techno-economic optimization analysis. By running simulations with different scenarios and configurations, the methodology aims to determine the most cost-effective and efficient battery technology for the microgrid system. The evaluation considers factors such as battery performance, lifetime, maintenance costs, and overall system economics to arrive at an optimum solution.

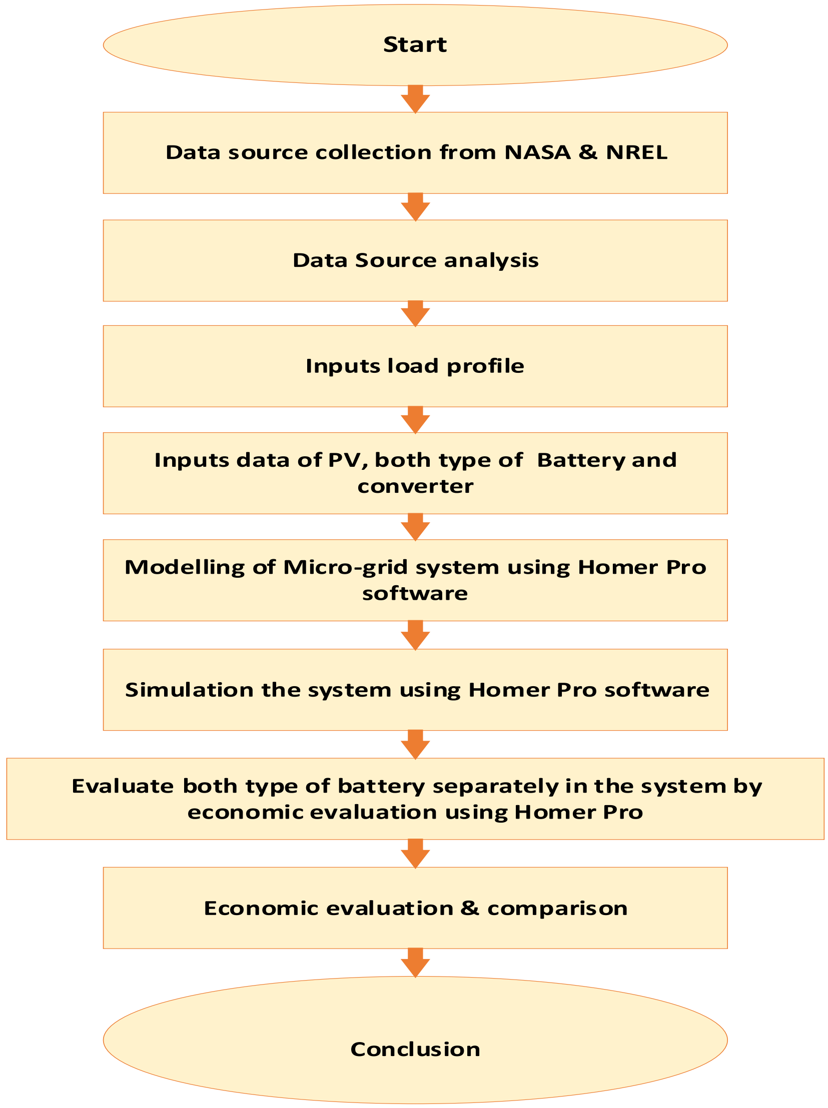

Figure 6. 19 Methodology used to conduct an optimum economy evaluation of both types of batteries.

6.5.1. HRES Configuration in Al Marj City Using HOMER Pro

In the context of Al Marj in Libya, a system based on the island model is implemented, taking into account design considerations such as sustainability and the optimization of solar energy utilization. To conduct the analysis, meteorological data provided by NREL and NASA for the geographical coordinates 32.28° N and 20.50° E are utilized. HOMER Pro's Microgrid models are employed to evaluate the system, considering the use of either SL-EVB or Lead-Acid batteries in islanded mode. Both battery technologies are examined to assess their suitability for the specific requirements of the standalone system. Figure 6.20 presents a schematic representation of the PV stand-alone system, outlining the configuration and components involved in the integration of solar energy for the microgrid.

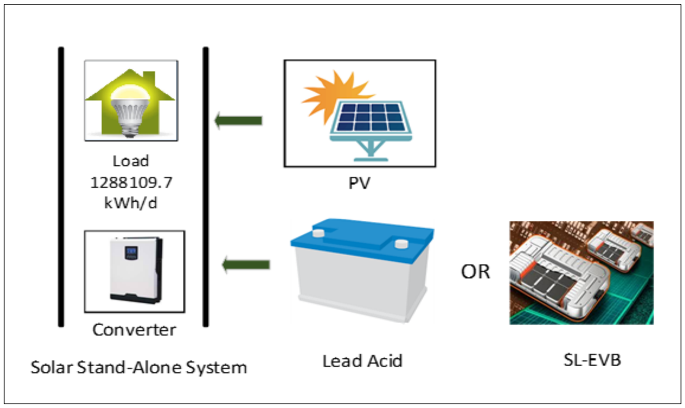

Figure 6. 20 Schematic diagram of the solar hybrid energy system configurations for both stand-alone.

- **Load profile**

HOMER Pro utilizes rescaled data for its calculations. The rescaled data involves multiplying the baseline data values by a common factor, which is determined by dividing the scaled annual average by the baseline annual average. This scaling process ensures that the shape and statistics of the data are preserved, although the magnitude may differ from the baseline data values. By default, the scaled annual averages are calculated based on the baseline data annual averages. When the scaled data set and the baseline data have equal values, there is no difference between them. To determine the load factor, the average load is divided by the peak load. Chapter 3 provides detailed information on the hourly average load in the specific study area, which is used in these calculations.

- **System configuration and components**

A proposed solution for meeting the energy requirements of Al-Marj, a city in east Libya, involves implementing a hybrid system. This system is designed to incorporate multiple components that work together synergistically. These components include PV panels, a converter, and a battery bank. The detailed functionalities and specifications of these components are presented in Chapter 4. It is important to note that in this proposed design, the diesel generator is not utilized, focusing primarily on the integration and optimization of solar PV, converter, and battery technologies to meet the energy needs of Al-Marj city. However, this particular section focuses on the storage system aspect of the proposed hybrid system. The evaluation aims to optimize the economic viability of the storage system by considering two types of batteries. The analysis involves comparing and assessing the performance, costs, and overall feasibility of using these batteries within the hybrid system to determine the most efficient and cost-effective battery technology for the specific requirements of the Al-Marj city's energy infrastructure.

- **Lead-acid batteries**

In a hybrid system, the energy storage component plays a significant role in ensuring uninterrupted power supply during periods of inadequate electricity generation. However, it is important to consider the cost implications associated with the energy storage system. In the design of HRES, lead-acid batteries are often preferred due to their high storage capacity, which is a common requirement in renewable energy systems. For instance, the 6CS25P battery model available in the HOMER Pro Library is a lead-acid battery commonly used in HRES. This battery is regulated at a nominal voltage of 6V and has a maximum charge/discharge current of 278.8A for a 1-hour discharge. It has a storage capacity of 820Ah and a roundtrip efficiency of 80%. The capital cost required for this battery is 1,200 $, and the replacement cost is 1,000 US$. Additionally, the operation and maintenance costs associated with maintaining the battery are estimated to be 5 US$ per year [135]. These cost considerations are important factors in the evaluation and selection of the appropriate battery technology for the hybrid system.

- **SL-EV battery**

For the optimization study, the SL-EV battery, specifically the Tesla Model S/X Module, has been selected. This module has a capacity of 6.4 kWh, 287Ah, and operates at a voltage of 22.8V. The module has been tested using the Deutronic diagnostic and conditioning system workshop tool, which applies the manufacturer's pre-defined high and low voltages for this module. The SL-EV battery module utilizes Panasonic 18650 cells and has a cell configuration of 6S86P (6 series 86 parallel) [136]. Each module consists of 516 cells, providing a nominal voltage of 22.8 V and an original capacity of 287Ah. In terms of costs, the SL-EV battery module requires a capital investment of 1,093 $, and the replacement cost is 1,000 $. The estimated operation and maintenance costs to maintain the battery are 5 $ per year [137]. These cost considerations are important factors in the optimization study, enabling the evaluation and comparison of the SL-EV battery with other energy storage options for the hybrid system.

6.5.2. Derivative Optimisation Using HOMER Pro

HOMER Pro is a versatile software tool that provides a complete solution for designing, optimizing, and evaluating energy systems, considering both technical and financial aspects. Through the use of optimization techniques, HOMER Pro finds the most suitable configuration for system components, while simultaneously minimizing the cost of energy (COE). This optimization process is facilitated by a specialized derivative-free algorithm, specifically designed for commercial applications, ensuring an efficient and effective search for the optimal system configuration without the need for derivative calculations. One significant aspect in system optimization is the battery charge size, which refers to the maximum energy that the battery can store and absorb. HOMER Pro considers this value to assess the potential surplus absorption from renewable energy sources. The calculation of the battery charge size is performed using the following equation [138]:

$$PP_{batt,cmax,kbm} = \frac{kQ_1 * e^{-K\Delta t} + Qkc(1 - e^{-K\Delta t})}{1 - e^{-K\Delta t} + c(k\Delta t - 1 + e^{-K\Delta t})} \quad (6.22)$$

Where:

Q1 represents the initial energy stored in the battery (measured in kilowatt-hours, kWh).

Q represents the total amount of energy (kWh) in the storage at the beginning of the time step

C represents the storage capacity ratio.

K represents the rate constant.

Δt represents the time step length.

This calculation helps to determine the battery's ability to absorb surplus energy from the renewable source. Additionally, HOMER Pro determines the discharge power size of the battery, which represents the maximum power that can be discharged from the storage bank. This calculation is essential for evaluating the battery's capacity to supply power to the load independently, without relying on other energy sources .

6.5.3. Stand-Alone System With SL-EVB Storge System

According to the simulation results, the system configuration with the highest ranking in terms of net present cost (NPC) and (COE). In this specific scenario, where a capacity shortage of 0.09% is allowed, the following values were determined a PV array with an annual energy generation of 237,255 MWh. An SL-EVB (SL-Electric Vehicle Battery) provides an annual energy storage capacity of 10,976 MWh. The net present cost (NPC) for this configuration is 6.81 B$. The cost of energy is calculated at 0.46 $/kWh. These results indicate that the proposed system configuration offers an efficient and cost-effective solution, optimizing energy generation, storage, and overall system performance. Figure 6.21 displays the outcomes of a sensitivity analysis performed on the various components of a standalone PV system design. The analysis considered three variables: solar radiation scaled average (kWh/m^2/day), cost of energy, and state of charge percentage for batteries. The figure shows the impact of each variable on the different components of the system. Based on the results of this sensitivity analysis, the lowest cost of energy achieved was 0.315 $/kWh. This was obtained assuming a solar radiation level of 7.9 kWh/m^2/day and a state of charge percentage of 70%.

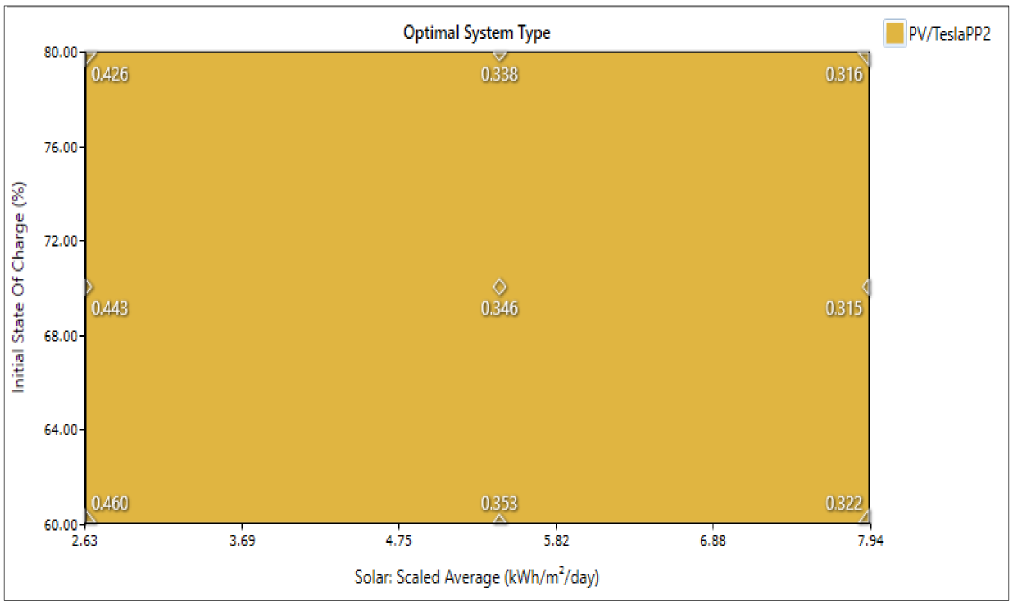

Figure 6. 21 Sensitivity analysis of the optimal PV system operating in a stand-alone using SL-EVB storge system.

6.5.4. Stand-alone system with Lead-acid storge system

In this case, the simulation results show the most economical net present cost and cost of energy configuration for the system. The capacity shortage percentage of 0.1 corresponding to a PV array that produces 307145 MWh per year with NPC of 7.5 B$, and cost of energy of 0.67 $/kWh. Considering the same variable sensitivity which applied in previous section, this analysis identified 0.483 $/kWh as a low cost of energy with solar radiation 7.9 kWh/m^2/day and an 80% charge state as illustrated in figure 6.22.

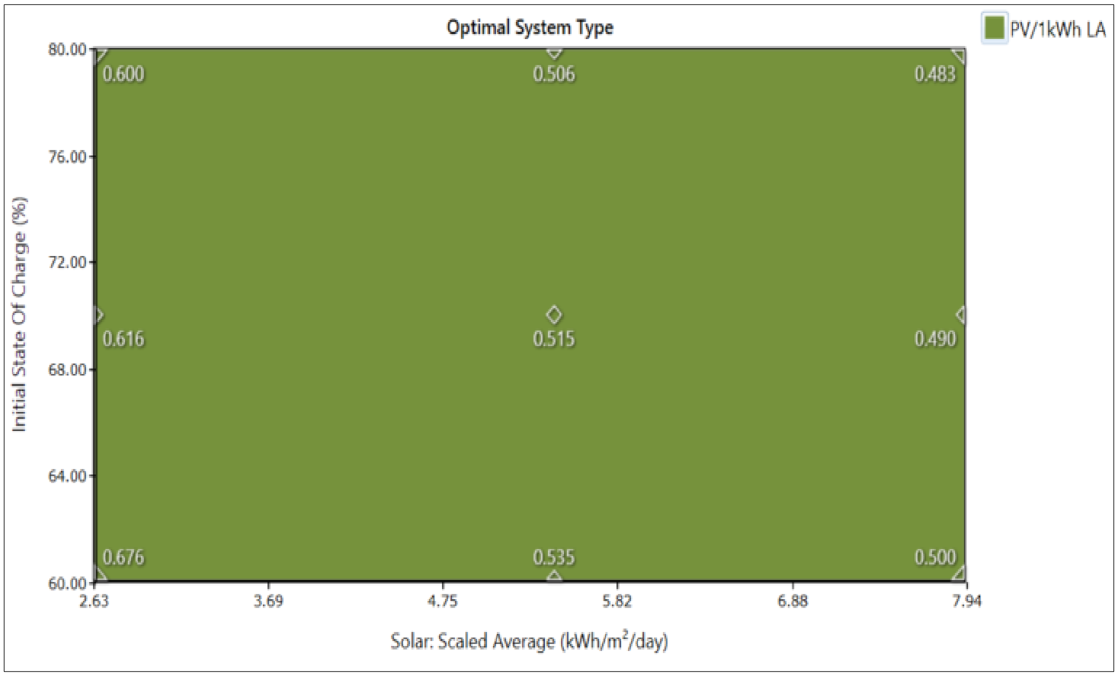

Figure 6. 22 Sensitivity outcomes of the optimal PV system operating in a stand-alone using SL-EVB storge system.

6.5.5. Simulation results

HOMER Pro simulations were carried out to determine the most optimal and economical storage system between SL-EV and lead-acid batteries. The present value of all costs incurred by the system over its lifetime was calculated to evaluate the impact of these battery types on consumer energy costs. Figure 6.23 (a) and (b) present a comparison between SL-EV and lead-acid batteries. According to the simulation results, the cost of energy (COE) for the system utilizing SL-EV batteries is estimated to be 0.46 $/kWh. On the other hand, the COE for the system employing lead-acid batteries is calculated to be 0.67 $/kWh. This comparison indicates that the SL-EV battery system offers a lower cost of energy, making it a more economical option for consumers. In terms of the net present cost (NPC), the system with SL-EV batteries has an allocation of 6.81 billion dollar, while the system with lead-acid batteries requires an allocation of 7.5 billion dollar. This further demonstrates that the SL-EV battery system is more cost-effective in terms of the overall investment required. Based on these findings, it can be concluded that the SL-EV battery system provides a more optimal and economical solution compared to the lead-acid battery system, offering lower cost of energy and net present cost for the system.

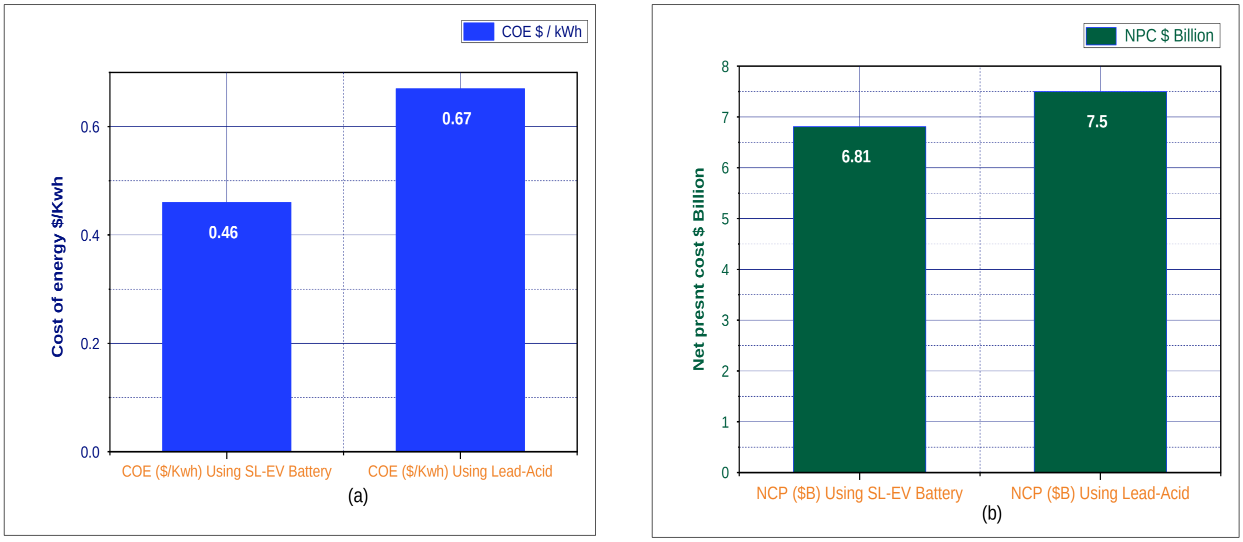

Figure 6. 23 Comparison of SL-EV batteries and Lead-acid batteries.

6.6. Summary

The integration of renewable energy sources in islanded systems has emerged as a viable option for supplying local networks with a weak connection to the main grid, in order to maintain end-user power quality during temporary blackouts. BESS play a crucial role in these systems, as they help to mitigate the fluctuations in PV output and maintain a balance between generation and load, thereby ensuring system stability. The effective placement and sizing of Distributed Generators within the distribution network, as well as the implementation of control strategies, have a significant impact on the coordination of BESS and renewable energy sources in islanded networks. This study aimed to investigate the use of distributed generation technologies that harness local renewable resources for the electrification of remote distribution networks. The location and size of the DGs were analysed using Sensitivity and Particle Swarm Optimization (PSO) algorithms, with the primary objective of minimizing the total real power losses and the number of DGs required. The response of the island mode microgrid to sudden changes in load was also analysed through simulation. The simulation results showed that the designed controller was able to run the system smoothly without any interruptions or voltage and frequency limits being exceeded. Finally, The HOMER simulation was utilized to identify the optimal and economically feasible storage system for achieving zero decarbonization in the system. The results revealed that SL-EV batteries emerged as the most suitable option, offering the best performance in terms of Net Present Cost (NPC) and Levelized Cost of Energy (COE). Furthermore, the study conducted an assessment of the present value of all costs associated with the system throughout its lifespan. This analysis provided insights into the economic implications of the chosen storage system. Overall, the HOMER simulation concluded that SL-EV batteries are the optimal choice for achieving zero decarbonization, considering their favourable results in terms of NPC, COE, and the economic evaluation of costs incurred by the system over time.

CHAPTER 7

Conclusions and Recommendations for Future Work

7.1. Introduction

This chapter reviews the conclusions of this research and summarises the key findings and the objective of the research. It provides several recommendations for power operators and policymakers in the context of the case study in Libya for future work. This chapter also summarises the main limitations and outlines the contributions of the work.

7.2. Conclusions of The Research

The objective of this research was to conduct a thorough evaluation of the implementation of renewable energy technology in Libya. This initiative stems from the nation's persistent challenges with electricity provision, largely stemming from historical conflicts and international embargoes. Focusing on the case study of Al Marj city, the study aims to offer a detailed and pragmatic assessment of the prevailing circumstances. Furthermore, it proposes a range of solutions to mitigate existing issues and prepare for future challenges, outlining a strategic vision for future planning endeavours.

The initial phase of this study involves devising a methodological framework to estimate the electricity load demand for Hybrid Renewable Energy Systems (HRES) in Al Marj city, Libya. This is crucial to address the existing gaps arising from the absence of monthly and daily load data since 2012 and 2008, respectively. The proposed methodology entails calculating the monthly and daily load demand for the year 2018 by leveraging the latest available data collected by GECOL. It incorporates a realistic population growth rate and adjusts electricity consumption per capita at the regional level. This approach can be extrapolated to estimate daily and monthly demand in other regions of Libya where data is lacking. Subsequently, the findings are utilized to explore alternative energy production methods aimed at alleviating the prevalent issue of frequent power outages. These outages, stemming from the current insufficient energy capacity, fail to meet the demands of Libyan society, resulting in prolonged electricity disruptions lasting for hours or even days in certain regions of the country. The data obtained from this estimation process is instrumental in evaluating the feasibility of integrating renewable energy technologies into Libya's energy production landscape.

The second phase of the study aimed to investigate alternative energy production methods to reduce reliance on fossil fuels. To accomplish this, a hybrid energy system was designed for Al-Marj City, and various scenarios and configurations for standalone and grid-connected photovoltaic (PV) and wind energy systems were analyzed. The results indicated that a solar energy system emerged as the most optimal choice in terms of cost efficiency, whereas the implementation of a wind energy system was not deemed cost-effective or efficient. The proportion of solar energy in the system ranged from 35.9% to 11.3% across all configurations, resulting in energy costs of 0.15 US$/kWh and 0.13 US$/kWh for standalone and grid-connected systems, respectively. Conversely, the share of wind energy ranged from 20.6% to 52.2%, with energy costs of 0.18 US$/kWh and 0.13 US$/kWh for standalone and grid-connected systems, respectively. In summary, the study concluded that a solar energy production system is the more cost-effective and competitive option compared to wind energy production. Ultimately, the findings suggest that implementing a PV hybrid energy system in Al-Marj, Libya, is highly feasible, whether as a standalone or grid-connected system. The study underscores the significance of renewable energy technology as the most sustainable solution to address the energy crisis in Libya. Furthermore, integrating renewable energy sources in isolated systems has emerged as a practical approach for supplying local networks with weak connections to the primary grid, ensuring the quality of power supply to end-users during temporary blackouts.

In the third phase of this research, the focus shifted to forecasting load demand for the year 2030 utilizing artificial intelligence algorithms. To anticipate future trends in three crucial indicators - Consumption per capita, Primary energy consumption, and Population - a neural network featuring LSTM layers was developed and trained on a dataset. Prior to training, the dataset was imported and normalized to ensure its suitability for neural network training. The architecture of the neural network comprised multiple layers, including LSTM layers equipped with 256 hidden units. The selection of the LSTM neural network was based on its demonstrated capability to provide accurate forecasts. The model's performance was evaluated using the R-squared value, which indicated a high level of fitting accuracy with values of 0.99988, 0.99993, and 0.99999 for Consumption per capita, Primary energy consumption, and Population, respectively. Furthermore, the root mean square error (RMSE) value of the model demonstrated a decreasing and converging trend during training, underscoring its robust forecasting capability. This study underscores the effectiveness of the LSTM neural network as a predictive tool for projecting future values of key indicators using historical data, offering significant potential for real-world applications in forecasting and decision-making.

Using the acquired load data, a stand-alone system scenario was simulated in HOMER Pro software to identify the optimal system configuration for the anticipated load demand growth in 2030. The simulations were conducted under the assumption of no capacity shortage. The results revealed that the most economical system configuration comprised a 160 MW photovoltaic (PV) array, an 80 MW diesel generator, and a 30 MWh battery bank. This configuration yielded a net present cost (NPC) of 2.63 US$B and a cost of energy (COE) of 0.204 US$/kWh. These findings indicate that this system configuration offers the optimal balance between cost-effectiveness and energy efficiency.

In conclusion, this research underscores the pivotal role of Energy Storage Systems (ESS) in Renewable Energy Systems (RES), as they effectively mitigate PV output fluctuations and uphold a balance between generation and load to ensure system stability. Furthermore, it explores the utilization of distributed generation (DG) technologies to electrify remote distribution networks, with a focus on minimizing total real power losses and optimizing the number and size of required DGs using Sensitivity and Particle Swarm Optimization algorithms. The study underscores the potential advantages of integrating renewable energy sources into islanded systems. By employing Sensitivity and Particle Swarm Optimization algorithms in MATLAB software to analyze the location and size of DGs, a notable reduction in total real power losses and the required number of DGs was demonstrated. A comparison between systems with and without DGs vividly showcased a significant decrease in power losses, with a remarkable reduction observed from 0.74786 MW in the grid-connected scenario to 0.27102 MW in the stand-alone system configuration. These findings underscore the effectiveness of leveraging local renewable resources for electrifying remote distribution networks, offering a viable solution for maintaining power quality for end-users during temporary blackouts. Consequently, this study yields valuable insights into optimizing distributed generation technologies, thus facilitating the transition toward a more sustainable and reliable energy system.

Utilizing HOMER Pro simulation, the research identified the most economically viable energy storage system to achieve zero decarbonization within the system. The results unequivocally favored SL-EV batteries over lead-acid batteries, demonstrating superior performance in terms of Net Present Cost (NPC) and Levelized Cost of Energy (COE). Specifically, the simulation showcased that the COE for SL-EV batteries is 0.46 US$/kWh, notably lower than 0.67 US$/kWh for lead-acid batteries. Moreover, the NPC for the SL-EV battery system was determined to be 6.81 billion dollars, compared to 7.5 billion dollars for the lead-acid battery system. Consequently, incorporating SL-EV batteries is projected to yield substantial cost savings and enhance efficiency within the stand-alone power system.

The study concludes by emphasizing the pivotal role of effective control strategies, as well as the importance of carefully determining the location and size of distributed generation (DG) systems and energy storage systems in maintaining system stability and mitigating fluctuations in renewable energy within islanded systems.

7.3. Recommendation for Future Work

The study has highlighted several significant challenges faced by the energy supply sector, particularly in terms of recurrent power outages during peak demand periods. To address these challenges, future research efforts should undertake a thorough exploration of various distributed generation (DG) technologies, combining photovoltaic (PV) systems and energy storage solutions. Additionally, there is scope for expanding the research to include the integration of advanced machine learning techniques to enhance optimization precision and control efficacy.

Furthermore, potential research trajectories could encompass:

1. **Demand-Side Management (DSM):** A detailed examination of methodologies for managing and optimizing consumer demand, leveraging smart grid technologies and incentive-driven initiatives. The goal would be to alleviate grid burdens during peak loads, promoting a balanced and harmonious energy ecosystem.
2. **Microgrid Development:** An in-depth investigation into establishing microgrids within specific geographical areas to enhance energy resilience, reduce transmission losses, and facilitate localized power generation and distribution.

3. **Innovation in Energy Storage:** A focused exploration of cutting-edge solutions in energy storage, including advanced battery technologies and compressed air energy storage. This aims to store surplus energy during periods of low demand and utilize it during times of increased demand, ensuring stability in the grid's operational dynamics.
4. **Demand Response Programs:** The strategic development and execution of demand response initiatives to incentivize consumers to adjust their energy consumption patterns during critical periods. This initiative holds the potential to effectively manage load surges and prevent disruptions.
5. **Grid Modernization:** A systematic investigation into adopting state-of-the-art grid infrastructure, such as smart meters, sensor arrays, and automated control systems, to enhance real-time monitoring capabilities and improve grid management efficiency.
6. **Hybrid Energy Systems:** An exhaustive examination of integrating multiple renewable energy sources alongside solar PV systems to create hybrid energy configurations that enhance reliability and efficiency.

By implementing these recommendations, the essence of the study's contribution can culminate in a comprehensive strategic plan to address Libya's energy deficit. Harmonizing these diverse approaches offers tangible prospects for mitigating local energy challenges while aligning with the global transition towards cleaner and more sustainable energy frameworks.

References

[1] S. H. Al-Behadili and W. B. El-Osta, "Life cycle assessment of Dernah (Libya) Wind Farm," *Renewable Energy*, vol. 83, pp. 1227–1233, 2015.

[2] "World Bank Climate Change Knowledge Portal," *Climate Change Knowledge Portal*. [Online]. Available: https://climateknowledgeportal.worldbank.org/download-data. [Accessed: 02-Jan-2019].

[3] "Is the union for the Mediterranean paving the way for sustainability?," *WWF*. [Online]. Available: https://wwf.panda.org/wwf_news/?193827%2FIs-the-Union-for-the-Mediterranean-paving-the-way-for-sustainability. [Accessed: 02-Jun-2020].

[4] "Libya - CO_2 emission 2021," *countryeconomy.com*, 19-Sep-2022. [Online]. Available: https://countryeconomy.com/energy-and-environment/CO_2-emissions/libya. [Accessed: 02-Jan-2021].

[5] "Electric Power Transmission and distribution losses (% of output)," *Data*. [Online]. Available: https://data.worldbank.org/indicator/EG.ELC.LOSS.ZS. [Accessed: 02-Jan-2023].

[6] J. W. Busby, K. Baker, M. D. Bazilian, A. Q. Gilbert, E. Grubert, V. Rai, J. D. Rhodes, S. Shidore, C. A. Smith, and M. E. Webber, "Cascading risks: Understanding the 2021 Winter Blackout in Texas," *Energy Research & Social Science*, vol. 77, p. 102106, 2021.

[7] S. M. Saad, K. I. Sharif, T. A. Mohamed, H. Y. Mustafa, N. El Naily, K. El-Arroudi, and F. A. Mohamed, "Modeling, simulation, and integration considerations of utility-scale solar PV to assess FRT detection-libyan sub-transmission grid case study," *2022 International Conference on Engineering & MIS (ICEMIS)*, 2022.

[8] O. A. Mohamed and S. H. Masood, "A brief overview of solar and wind energy in Libya: Current trends and the future development," *IOP Conference Series: Materials Science and Engineering*, vol. 377, p. 012136, 2018.

[9] W. El-Osta and Y. Kalifa, "Prospects of wind power plants in Libya: A case study," Renewable *Energy*, vol. 28, no. 3, pp. 363–371, 2003.

[10] S. Alweheshi, A. Abdelali, Z. Rajab, A. Khalil, and F. Mohamed, "Photovoltaic Solar Energy Applications in Libya: A survey," 2019 10th International Renewable Energy Congress (IREC), 2019.

[11] “Task A: Sector performance and structural sector reform - world bank.” [Online]. Available: https://documents1.worldbank.org/curated/en/315261527073425670/pdf/01-Task-A-Rapid-Assessment-of-the-Sector-Performance.pdf. [Accessed: 03-Jan-2023].

[12] Y. Aldali, D. Henderson, and T. Muneer, “A 50 MW very large-scale photovoltaic power plant for Al-Kufra, Libya: Energetic, economic and environmental impact analysis,” *International Journal of Low-Carbon Technologies*, vol. 6, no. 4, pp. 277–293, 2011.

[13] *General electrical company of Libya* . [Online]. Available: http://www.gecol.ly/gecol_en/Details_Adv_Ten.aspx?id=137083. [Accessed: 03-Jan-2020].

[14] Advances in grid-connected Photovoltaic Power Conversion Systems, 2019. doi:10.1016/c2016-0-05033-7.

[15] Z. Maheshwari and R. Ramakumar, “Smart Integrated Renewable Energy Systems (sires): A novel approach for sustainable development,” *Energies*, vol. 10, no. 8, p. 1145, 2017.

[16] elumtest2, “Major countries with load shedding,” *Elum Energy*, 14-Dec-2022. [Online]. Available: https://elum-energy.com/en/2022/11/04/major-countries-with-load-shedding/. [Accessed: 03-Jan-2021].

[17] “Download our energy transition outlook 2022,” *DNV*. [Online]. Available: https://www.dnv.com/energy-transition outlook/download.html?utm_source=Google&utm_medium=Search&utm_campaign=eto22&gclid=CjwKCAiAwc-dBhA7EiwAxPRylEfLgneadZWUyvNkyoRvuItj5OxkDQPcVnkiZCRkC2fciFG1lZxB4xoCdoQQAvD_BwE. [Accessed: 03-Jan-2022].

[18] M. Almaktar, A. M. Elbreki, and M. Shaaban, “Revitalizing Operational Reliability of the electrical energy system in Libya: Feasibility analysis of solar generation in local communities,” *Journal of Cleaner Production*, vol. 279, p. 123647, 2021.

[19] Hamad, W. Yaacob and A. Omran, "Quality Assessment of Groundwater Resources in the City of Al-Marj, Libya", Processes, vol. 9, no. 1, p. 154, 2021. Available: 10.3390/pr9010154.

[20] Electric power consumption (kWh per capita) - Libya | Data", Data.worldbank.org, 2022. [Online]. Available:

https://data.worldbank.org/indicator/EG.USE.ELEC.KH.PC?end=2010&locations=LY&name_desc=true&start=2003&type=shaded&view=chart. [Accessed: 16- Jun- 2022].

[21] Bureau of Statistics and Census >> globalEDGE: Your source for Global Business Knowledge", Globaledge.msu.edu, 2022. [Online]. Available: https://globaledge.msu.edu/global-resources/resource/16676. [Accessed: 23- May- 2022].

[22] Libya free map, free blank map, free outline map, free base map boundaries, divisions, names", D-maps.com, 2022. [Online]. Available: https://d-maps.com/carte.php?num_car=4724&lang=en. [Accessed: 20- Jun- 2020].

[23] The Political Economy of Migrant Detention in Libya: Understanding the players and the business models", *Global Initiative*, 2020. [Online]. Available: https://globalinitiative.net/migrant-detention-libya/. [Accessed: 10- Apr- 2020].

[24] N. America et al., "Libya Maps & Facts", *WorldAtlas*, 2020. [Online]. Available: https://www.worldatlas.com/webimage/countrys/africa/libya/lyland.htm. [Accessed: 10- Feb- 2020].

[25] 2018 African Economic Outlook, "2018 African Economic Outlook", Libya, 2020.

[26] "World Report 2018: Rights Trends in Libya", *Human Rights Watch*, 2020. [Online]. Available: https://www.hrw.org/world-report/2018/country-chapters/libya. [Accessed: 10- Sep- 2020].

[27] "Document Details", *World Bank*, 2020. [Online]. Available: http://documents.worldbank.org/curated/en/750661550977483586/Libya-Country-Engagement-Note-for-the-Period-2019-2021. [Accessed: 10- Sep- 2020].

[28] k. nationsonline.org, "Administrative Map of Libya - Nations Online Project", *Nationsonline.org*, 2020. [Online]. Available: https://www.nationsonline.org/oneworld/map/libya-administrative-map.htm. [Accessed: 10- Sep- 2020].

[29] Ibrahim, S., *Prospects of renewable energy in Libya*. Renew Energy, 1998. **14**: p. 135.

[30] *Documents.worldbank.org*, 2020. [Online]. Available: https://documents.worldbank.org/curated/en/750661550977483586/pdf/Libya-CEN-to-Board-final-01252019-636865562772741763.pdf. [Accessed: 11- Mar- 2020].

[31] "GENRAL ELECTRICAL COMPANY OF LIBYA", *Gecol.ly*, 2020. [Online]. Available: https://www.gecol.ly/GECOL_EN/Default.aspx. [Accessed: 11- Sep- 2020].

[32] "Electric power consumption (kWh per capita) - Libya | Data", *Data.worldbank.org*, 2020. [Online]. Available: https://data.worldbank.org/indicator/EG.USE.ELEC.KH.PC?end=2010&locations=LY&name_desc=true&start=2003&type=shaded&view=chart. [Accessed: 11- Apr- 2020].

[33] "Institutional Development and Performance Improvement of GECOL", gecol, LIBYA, 2017.

[34] A. Asrari, A. Ghasemi, and M. H. Javidi, "Economic evaluation of hybrid renewable energy systems for rural electrification in Iran—a case study," Renewable and Sustainable Energy Reviews, vol. 16, no. 5, pp. 3123–3130, 2012.

[35] Y. Cao, Y. Wu, L. Fu, K. Jermsittiparsert, and N. Razmjooy, "Multi-objective optimization of a PEMFC based CCHP system by meta-heuristics," Energy Reports, vol. 5, pp. 1551–1559, 2019.

[36] D. Yu, Y. Wang, H. Liu, K. Jermsittiparsert, and N. Razmjooy, "System identification of PEM fuel cells using an improved Elman Neural Network and a new hybrid optimization algorithm," Energy Reports, vol. 5, pp. 1365–1374, 2019.

[37] S. Diaf, D. Diaf, M. Belhamel, M. Haddadi, and A. Louche, "A methodology for optimal sizing of autonomous hybrid PV/Wind System," *Energy Policy*, vol. 35, no. 11, pp. 5708–5718, 2007.

[38] C. Brivio, M. Moncecchi, S. Mandelli, and M. Merlo, "A novel software package for the robust design of off-grid power systems," *Journal of Cleaner Production*, vol. 166, pp. 668–679, 2017.

[39] S. M. Sajed Sadati, E. Jahani, O. Taylan, and D. K. Baker, "Sizing of photovoltaic-wind-battery hybrid system for a Mediterranean island community based on estimated and measured meteorological data," *Journal of Solar Energy Engineering*, vol. 140, no. 1, 2017.

[40] M. Rizwan, G. Mujtaba, S. A. Memon, K. Lee, and N. Rashid, "Exploring the potential of microalgae for new biotechnology applications and beyond: A Review," *Renewable and Sustainable Energy Reviews*, vol. 92, pp. 394–404, 2018.

[41] G. Bekele and B. Palm, “Feasibility Study for a standalone solar–wind-based hybrid energy system for application in Ethiopia,” *Applied Energy*, vol. 87, no. 2, pp. 487–495, 2010.

[42] I. B. Askari and M. Ameri, “Techno-economic feasibility analysis of stand-alone renewable energy systems (PV/bat, wind/bat and hybrid PV/wind/bat) in Kerman, Iran,” *Energy Sources, Part B: Economics, Planning, and Policy*, vol. 7, no. 1, pp. 45–60, 2012.

[43] A. A. Moghaddam, A. Seifi, T. Niknam, and M. R. Alizadeh Pahlavani, “Multi-objective Operation Management of a renewable MG (micro-grid) with back-up micro-turbine/fuel cell/battery hybrid power source,” *Energy*, vol. 36, no. 11, pp. 6490–6507, 2011.

[44] T. Griffin, K. Tomsovic, D. Secrest, and A. Law, “Placement of dispersed generation systems for reduced losses,” *Proceedings of the 33rd Annual Hawaii International Conference on System Sciences*.

[45] M. A. Jafari and H. Afrakhte, “Effect of optimal placement and regulation of SSVR in Microgrid Island Operation,” *2014 19th Conference on Electrical Power Distribution Networks (EPDC)*, 2014.

[46] A. Ameli, S. Bahrami, F. Khazaeli, and M.-R. Haghifam, “A multiobjective particle swarm optimization for sizing and placement of dgs from DG Owner's and distribution company's viewpoints,” *IEEE Transactions on Power Delivery*, vol. 29, no. 4, pp. 1831–1840, 2014.

[47] G. Pepermans, J. Driesen, D. Haeseldonckx, R. Belmans, and W. D’haeseleer, “Distributed generation: Definition, benefits and issues,” *Energy Policy*, vol. 33, no. 6, pp. 787–798, 2005.

[48] R. H. A. Zubo, G. Mokryani, H.-S. Rajamani, J. Aghaei, T. Niknam, and P. Pillai, “Operation and planning of distribution networks with integration of renewable distributed generators considering uncertainties: A Review,” *Renewable and Sustainable Energy Reviews*, vol. 72, pp. 1177–1198, 2017.

[49] D. Q. Hung, N. Mithulananthan, and K. Y. Lee, “Optimal placement of dispatchable and nondispatchable renewable DG units in distribution networks for minimizing energy loss,” *International Journal of Electrical Power & Energy Systems*, vol. 55, pp. 179–186, 2014.

[50] R. Viral and D. K. Khatod, “An analytical approach for sizing and siting of dgs in balanced radial distribution networks for loss minimization,” *International Journal of Electrical Power & Energy Systems*, vol. 67, pp. 191–201, 2015.

[51] M. Kashyap, S. Kansal, and R. Verma, “Sizing and allocation of dgs in a passive distribution network under various loading scenarios,” *Electric Power Systems Research*, vol. 209, p. 108046, 2022.

[52] Y. Zhao, Y. An, and Q. Ai, “Research on size and location of distributed generation with vulnerable node identification in the active distribution network,” *IET Generation, Transmission & Distribution*, vol. 8, no. 11, pp. 1801–1809, 2014.

[53] A. J. Gil Mena and J. A. Martín García, “An efficient approach for the siting and sizing problem of distributed generation,” *International Journal of Electrical Power & Energy Systems*, vol. 69, pp. 167–172, 2015.

[54] F. Tooryan, E. R. Collins, A. Ahmadi, and S. S. Rangarajan, “Distributed generators optimal sizing and placement in a microgrid using PSO,” *2017 IEEE 6th International Conference on Renewable Energy Research and Applications (ICRERA)*, 2017.

[55] J. B. Dugan, S. J. Bavuso, and M. A. Boyd, “Fault trees and sequence dependencies,” *Annual Proceedings on Reliability and Maintainability Symposium*.

[56] M. Vatani, D. Solati Alkaran, M. J. Sanjari, and G. B. Gharehpetian, “Multiple distributed generation units allocation in distribution network for loss reduction based on a combination of analytical and genetic algorithm methods,” *IET Generation, Transmission & Distribution*, vol. 10, no. 1, pp. 66–72, 2016.

[57] Y. Abass, M. Abido, M. Al-Muhaini, and M. Khalid, “Multi-objective optimal DG sizing and placement in distribution systems using particle swarm optimization,” *2019 IEEE Innovative Smart Grid Technologies - Asia (ISGT Asia)*, 2019.

[58] V. Vemula, “Review on techniques of optimal placement and sizing of DG in distribution systems,” *PRZEGLĄD ELEKTROTECHNICZNY*, vol. 1, no. 12, pp. 3–8, 2021.

[59] T. K. A. Rahman, S. R. A. Rahim, and I. Musirin, “Optimal allocation and sizing of embedded generators,” *PECon 2004. Proceedings. National Power and Energy Conference, 2004.*

[60] M. A. Kashem, A. D. T. Le, M. Negnevitsky, and G. Ledwich, "Distributed generation for minimization of power losses in distribution systems," *2006 IEEE Power Engineering Society General Meeting*, 2006.

[61] R. S. Rao, K. Ravindra, K. Satish, and S. V. Narasimham, "Power loss minimization in distribution system using network reconfiguration in the presence of distributed generation," *IEEE Transactions on Power Systems*, vol. 28, no. 1, pp. 317–325, 2013.

[62] R. D. Zimmerman, C. E. Murillo-Sanchez, and R. J. Thomas, "MATPOWER: Steady-state operations, planning, and Analysis Tools for Power Systems Research and Education," *IEEE Transactions on Power Systems*, vol. 26, no. 1, pp. 12–19, 2011.

[63] T. Gözel and M. H. Hocaoglu, "An analytical method for the sizing and siting of distributed generators in radial systems," *Electric Power Systems Research*, vol. 79, no. 6, pp. 912–918, 2009.

[64] D. Gautam and N. Mithulananthan, "Optimal DG placement in Deregulated Electricity Market," *Electric Power Systems Research*, vol. 77, no. 12, pp. 1627–1636, 2007.

[65] N. K. Roy, H. R. Pota, and A. Anwar, "A new approach for wind and Solar Type DG placement in power distribution networks to enhance systems stability," *2012 IEEE International Power Engineering and Optimization Conference*, 2012.

[66] H. Manafi, N. Ghadimi, M. Ojaroudi, and P. Farhadi, "Optimal placement of distributed generations in radial distribution systems using various PSO and DE algorithms," *Electronics and Electrical Engineering*, vol. 19, no. 10, 2013.

[67] T. kumar and G. kesava Rao, "Analysis of IA and PSO Algorithms for Siting and sizing of DG in Primary Distribution Networks," *international jurnal of control theory and application*, vol. 10, pp. 341–350, Jun. 2017.

[68] J. A. Sneha and K. Kumar, "Optimal placement of different types of DG sources in distribution networks using PSO algorithm and Differential Evolution," *IOSR Journal of Electrical and Electronics Engineering*, vol. 9, no. 4, pp. 41–45, 2014.

[69] Pradeepa H., T. Ananthapadmanabha, S. Rani D.N., and Bandhavya C., "Optimal allocation of combined DG and capacitor units for voltage stability enhancement," *Procedia Technology*, vol. 21, pp. 216–223, 2015.

[70] U. Khaled, A. M. Eltamaly, and A. Beroual, “Optimal power flow using particle swarm optimization of renewable hybrid distributed generation,” Energies, vol. 10, no. 7, p. 1013, 2017.

[71] M. H. RIND, M. K. RATHI, A. A. HASHMANI, and A. A. LASHARI, “Optimal placement and sizing of DG in radial distribution system using PSO Technique,” *SINDH UNIVERSITY RESEARCH JOURNAL -SCIENCE SERIES*, vol. 51, no. 04, pp. 653–660, 2019.

[72] M. Dixit, P. Kundu, and H. R. Jariwala, “Optimal placement of PV array in distribution system for power loss minimization considering feeder reconfiguration,” *2016 IEEE 16th International Conference on Environment and Electrical Engineering (EEEIC)*, 2016.

[73] C. Divya and T. Manohar, “ Optimal Location of DG Units using Sensitivity Analysis,” *International Journal of Advance Technology and Innovative Research*, vol. 08, no. , pp. 4192–4196, Nov. 2016.

[74] E. Almeshaiei and H. Soltan, “A methodology for Electric Power Load Forecasting,” *Alexandria Engineering Journal*, vol. 50, no. 2, pp. 137–144, 2011.

[75] X. Zhang, J. Wang, and K. Zhang, “Short-term electric load forecasting based on singular spectrum analysis and support vector machine optimized by cuckoo search algorithm,” *Electric Power Systems Research*, vol. 146, pp. 270–285, 2017.

[76] G. Nalcaci, A. Özmen, and G. W. Weber, “Long-term load forecasting: Models based on Mars, ann and LR methods,” *Central European Journal of Operations Research*, vol. 27, no. 4, pp. 1033–1049, 2018.

[77] H. Wang, K. A. Alattas, A. Mohammadzadeh, M. H. Sabzalian, A. A. Aly, and A. Mosavi, “Comprehensive review of load forecasting with emphasis on intelligent computing approaches,” *Energy Reports*, vol. 8, pp. 13189–13198, 2022.

[78] M. A. Hammad, B. Jereb, B. Rosi, and D. Dragan, “Methods and models for Electric Load Forecasting: A comprehensive review,” *Logistics & Sustainable Transport*, vol. 11, no. 1, pp. 51–76, 2020.

[79] C. Kuster, Y. Rezgui, and M. Mourshed, “Electrical load forecasting models: A critical systematic review,” *Sustainable Cities and Society*, vol. 35, pp. 257–270, 2017.

[80] R. Adhikari and R. K. Agrawal, “An introductory study on time series modeling and forecasting,” *arXiv.org*, 26-Feb-2013. [Online]. Available: https://arxiv.org/abs/1302.6613. [Accessed: 26-Jan-2023].

[81] S. Siami-Namini, N. Tavakoli, and A. S. Namin, “The performance of LSTM and BiLSTM in forecasting time series,” 2019 IEEE International Conference on Big Data (Big Data), 2019.

[82] J. Cao, Z. Li, and J. Li, “Financial Time Series Forecasting Model based on CEEMDAN and LSTM,” *Physica A: Statistical Mechanics and its Applications*, vol. 519, pp. 127–139, 2019.

[83] S. Muzaffar and A. Afshari, “Short-term load forecasts using LSTM Networks,” *Energy Procedia*, vol. 158, pp. 2922–2927, 2019.

[84] A. Kumar Dubey, A. Kumar, V. García-Díaz, A. Kumar Sharma, and K. Kanhaiya, “Study and analysis of sarima and LSTM in forecasting time series data,” *Sustainable Energy Technologies and Assessments*, vol. 47, p. 101474, 2021.

[85] A. Narayan and K. W. Hipel, “Long short term memory networks for short-term electric load forecasting,” *2017 IEEE International Conference on Systems, Man, and Cybernetics (SMC)*, 2017.

[86] S. Atef and A. B. Eltawil, “Assessment of stacked unidirectional and bidirectional long short-term memory networks for electricity load forecasting,” *Electric Power Systems Research*, vol. 187, p. 106489, 2020.

[87] A. Haque and S. Rahman, “Short-term electrical load forecasting through heuristic configuration of Regularized Deep Neural Network,” *Applied Soft Computing*, vol. 122, p. 108877, 2022.

[88] Jian Zheng, Cencen Xu, Ziang Zhang, and Xiaohua Li, “Electric load forecasting in smart grids using long-short-term-memory based recurrent neural network,” *2017 51st Annual Conference on Information Sciences and Systems (CISS)*, 2017.

[89] A. Nespoli, E. Ogliari, S. Pretto, M. Gavazzeni, S. Vigani, and F. Paccanelli, “Electrical load forecast by means of LSTM: The impact of Data Quality,” *Forecasting*, vol. 3, no. 1, pp. 91–101, 2021.

[90] A. Khalil, Z. Rajab, M. Amhammed, and A. Asheibi, “The benefits of the transition from fossil fuel to solar energy in Libya: A street lighting system case study,” *Applied Solar Energy*, vol. 53, no. 2, pp. 138–151, 2017.

[91] A. Gawedar and R. Ramakumar, "Impact of Wind Energy System Integration on the Al-Zawiya Refinery Electric Grid in Libya", Journal of Power and Energy Engineering, vol. 04, no. 09, pp. 11-20, 2016. Available: 10.4236/jpee.2016.49002.

[92] “Population growth (annual %) - Libya,” Data. [Online]. Available: https://data.worldbank.org/indicator/SP.POP.GROW?locations=LY. [Accessed: 10-Mar-2019].

[93] Data.worldbank.org, 2022. [Online]. Available: https://data.worldbank.org/indicator/EG.USE.ELEC.KH.PC%5D. [Accessed: 23- May-2019].

[94] GECOL, 2010. GECOL. [Online] Available at: http://www.gecol.ly/ [Accessed 10 April 2019].

[95] Theme Mascot, “Company news,” General Electricity Company of Libya, https://www.gecol.ly/HomeEnglish (accessed Aug. 9, 2023).

[96] S. Bahramara, M. P. Moghaddam, and M. R. Haghifam, “Optimal planning of Hybrid Renewable Energy Systems using homer: A Review,” Renewable and Sustainable Energy Reviews, vol. 62, pp. 609–620, 2016.

[97] GPS coordinates of, Libya. Latitude: 0.0000 Longitude: 0.0000", Latitude.to, 2021. [Online]. Available: https://latitude.to/map/ly/libya/cities/al-mar. [Accessed: 30- May-2019].

[98] Homer pro 3.11,” Finding Data to Run HOMER, https://www.homerenergy.com/products/pro/docs/3.11/finding_data_to_run_homer.html (accessed Jul. 16, 2020).

[99] “Homer pro 3.11,” Finding Data to Run HOMER, https://www.homerenergy.com/products/pro/docs/3.11/finding_data_to_run_homer.html (accessed Jul. 17, 2020).

[100] “Homer pro 3.11,” Photovoltaic (PV) Library, https://www.homerenergy.com/products/pro/docs/3.11/photovoltaic_pv_library.html (accessed Jun. 09, 2020).

[101] "Library", Homerenergy.com, 2019. [Online]. Available: https://www.homerenergy.com/products/pro/docs/latest/library.html. [Accessed: 10-Feb- 2019].

[102] S. Alweheshi, A. Abdelali, Z. Rajab, A. Khalil and F. Mohamed, "Photovoltaic Solar Energy Applications in Libya: A Survey," 2019 10th International Renewable Energy Congress (IREC), Sousse, Tunisia, 2019, pp. 1-6, doi: 10.1109/IREC.2019.8754527.

[103] Abdullah BenIbrahim, "Report: The insoluble dilemma of fuel smuggling," The Libya Observer, https://libyaobserver.ly/economy/report-insoluble-dilemma-fuel-smuggling (accessed Jul. 16, 2023).

[104] "Libya gasoline prices, 10-jul-2023," GlobalPetrolPrices.com, https://www.globalpetrolprices.com/Libya/gasoline_prices/ (accessed Jul. 16, 2023).

[105] Petropoulos, F. et al. (2022) "Forecasting: Theory and practice," International Journal of Forecasting, 38(3), pp. 705–871. Available at: https://doi.org/10.1016/j.ijforecast.2021.11.001.

[106] A. Sagheer and M. Kotb, "Time series forecasting of Petroleum Production using Deep LSTM recurrent networks," Neurocomputing, vol. 323, pp. 203–213, 2019.

[107] B. B. Sahoo, R. Jha, A. Singh, and D. Kumar, "Long Short-Term Memory (LSTM) recurrent neural network for low-flow hydrological time series forecasting," Acta Geophysica, vol. 67, no. 5, pp. 1471–1481, 2019.

[108] W. Fang, W. Zhuo, Y. Song, J. Yan, T. Zhou, and J. Qin, Neurocomputing, vol. 526, pp. 180–190, 2023.

[109] R. Jiao, T. Zhang, Y. Jiang, and H. He, "Short-term non-residential load forecasting based on multiple sequences LSTM recurrent neural network," IEEE Access, vol. 6, pp. 59438–59448, 2018.

[110] J. Cui and Z. Li, "Prediction of upper limb action intention based on long short-term memory neural network," Electronics, vol. 11, no. 9, p. 1320, 2022.

[111] "Recurrent neural network with MATLAB," Recurrent Neural Network with MATLAB - MATLAB & Simulink, https://ww2.mathworks.cn/discovery/rnn.html (accessed Jul. 19, 2023).

[112] J. A. Pérez-Ortiz, F. A. Gers, D. Eck, and J. Schmidhuber, “Kalman filters improve LSTM network performance in problems unsolvable by traditional recurrent nets,” Neural Networks, vol. 16, no. 2, pp. 241–250, 2003.

[113] General electrical company of Libya . [Online]. Available: http://www.gecol.ly/gecol_en/about.aspx. [Accessed: 16-Feb-2022].

[114] M. E. Souza Junior and L. C. Freitas, “Power Electronics for Modern Sustainable Power Systems: Distributed generation, microgrids and smart grids—a review,” *Sustainability*, vol. 14, no. 6, p. 3597, 2022.

[115] W. Murray, M. Adonis, and A. Raji, “Voltage control in future electrical distribution networks,” *Renewable and Sustainable Energy Reviews*, vol. 146, p. 111100, 2021.

[116] *Smart Technologies for power and Green Energy: Proceedings of stpge 2022*. S.l.: SPRINGER VERLAG, SINGAPOR, 2022.

[117] B. D. Olaszi and J. Ladanyi, “Comparison of different discharge strategies of grid-connected residential PV systems with energy storage in perspective of optimal battery energy storage system sizing,” *Renewable and Sustainable Energy Reviews*, vol. 75, pp. 710–718, 2017.

[118] B. Mukhopadhyay and D. Das, “Multi-objective dynamic and static reconfiguration with optimized allocation of PV-DG and Battery Energy Storage System,” *Renewable and Sustainable Energy Reviews*, vol. 124, p. 109777, 2020.

[119] H. Rezzouk and A. Mellit, “Feasibility Study and sensitivity analysis of a stand-alone photovoltaic–diesel–battery hybrid energy system in the north of Algeria,” *Renewable and Sustainable Energy Reviews,* vol. 43, pp. 1134–1150, 2015.

[120] A. O. M. Maka, S. Salem, and M. Mehmood, “Solar photovoltaic (PV) applications in Libya: Challenges, potential, opportunities and future perspectives,” *Cleaner Engineering and Technology*, vol. 5, p. 100267, 2021.

[121] S. Azizi and M. Sanaye-Pasand, “A straightforward method for wide-area fault location on Transmission Networks,” *IEEE Transactions on Power Delivery*, vol. 30, no. 1, pp. 264–272, 2015.

[122] N. S. Rau and Yih-Heui Wan, “Optimum location of resources in Distributed Planning,” *IEEE Transactions on Power Systems*, vol. 9, no. 4, pp. 2014–2020, 1994.

[123] M. Gandomkar, M. Vakilian, and M. Ehsan, “Optimal distributed generation allocation in distribution network using Hereford Ranch algorithm,” *2005 International Conference on Electrical Machines and Systems*, 2005.

[124] D. Sai Krishna Kanth, Dr. M. Padma Lalita, and P. Suresh Babu, “Siting & Sizing of Dg for Power Loss & Thd Reduction, Voltage Improvement Using Pso & Sensitivity Analysis,” International Journal of Engineering Research and Development, vol. 9, no. 6, 2013.

[125] S. M. Mikki and A. A. Kishk, *Particle swarm optimization a physics-based approach*. San Rafael, Calif. (1537 Fourth Street, San Rafael, CA 94901 USA): Morgan & Claypool Publishers, 2008.

[126] K. Bhumkittipich and W. Phuangpornpitak, “Optimal placement and sizing of distributed generation for power loss reduction using particle swarm optimization,” *Energy Procedia*, vol. 34, pp. 307–317, 2013.

[127] M. Faisal, M. A. Hannan, P. J. Ker, A. Hussain, M. B. Mansor, and F. Blaabjerg, “Review of Energy Storage System Technologies in microgrid applications: Issues and challenges,” *IEEE Access*, vol. 6, pp. 35143–35164, 2018.

[128] M. Broussely, “Lithium-ion batteries for EV, HEV and other industrial applications,” *Lithium Batteries*, pp. 645–685.

[129] “AC voltage source,” *Generic battery model - Simulink*. [Online]. Available: https://www.mathworks.com/help/physmod/sps/powersys/ref/battery.html. [Accessed: 21-5-2022].

[130] T. Jing and A. S. Maklakov, “A review of voltage source converters for energy applications,” *2018 International Ural Conference on Green Energy (UralCon)*, 2018.

[131] Kyung-Hwan Kim, Nam-Joo Park, and Dong-Seok Hyun, “Advanced synchronous reference frame controller for three-phase ups powering unbalanced and nonlinear loads,” *IEEE 36th Conference on Power Electronics Specialists, 2005.*

[132] “ABC to DQ0, DQ0 to ABC,” *Perform transformation from three-phase (abc) signal to dq0 rotating reference frame or the inverse - Simulink - MathWorks United Kingdom*. [Online].Available:https://uk.mathworks.com/help/sps/powersys/ref/abctodq0dq0toabc.html. [Accessed: 22-5-2022].

[133] Y. Amirnaser, *Voltage - sourced converters in power systems: Modeling, control, and applications.* New Jersey: IEEE Press, 2012.

[134] C. J. O'Rourke, M. M. Qasim, M. R. Overlin, and J. L. Kirtley, "A geometric interpretation of reference frames and transformations: DQ0, Clarke, and Park," IEEE Transactions on Energy Conversion, vol. 34, no. 4, pp. 2070–2083, Dec. 2019. doi:10.1109/tec.2019.2941175

[135] Data to Run HOMER", Homerenergy.com, 2022. [Online]. Available: https://www.homerenergy.com/products/pro/docs/latest/finding_data_to_run_homer.html. [Accessed: 10- Jan- 2023].

[136] DBL1200HV (2023) Deutronic Elektronik GmbH. Available at: https://www.deutronic.com/produkte/dbl-diagnostic-and-conditioning-system-for-electric-vehicles/ (Accessed: 01 August 2023).

[137] "Tesla 6.2kWh modules: 24V: 270ah - tested used EV modules," *Second Life EV BatteriesLtd*.[Online].Available:https://www.secondlife-evbatteries.com/collections/ev-battery/products/tesla-6-2kwh-module-p100d. [Accessed: 27-Oct-2022].

[138] Homer pro 3.15," How HOMER Calculates the Maximum Battery Charge Power, https://homerenergy.com/products/pro/docs/3.15/how_homer_calculates_the_maximum_battery_charge_power.html (accessed Feb. 8, 2024).

Appendix A

1. Monthly load of Al Marj town in 2018 assessed with Homer pro software.

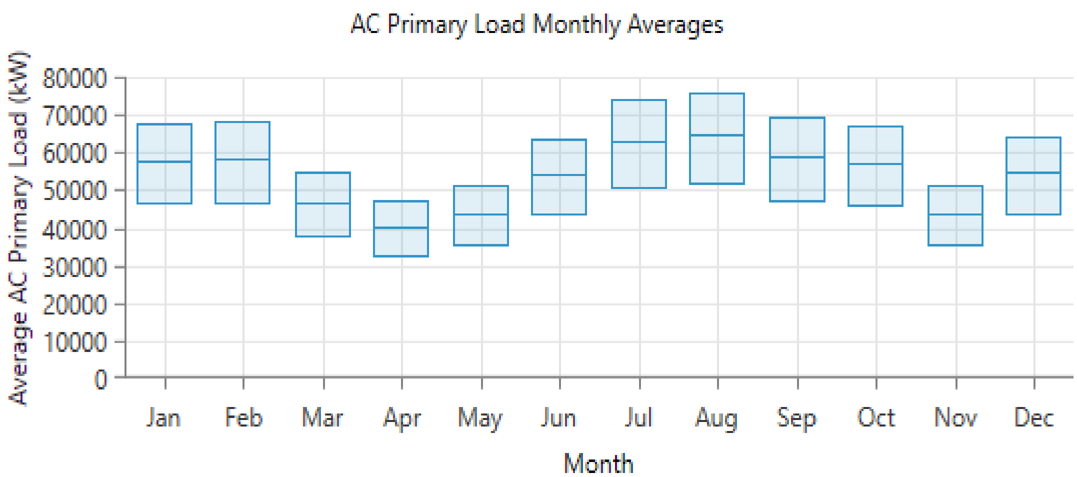

Figure 1 Al Marj city HRES Monthly load profile

2. Everyday load in 2018 aimed at Al Marj Town computed with Homer pro software.

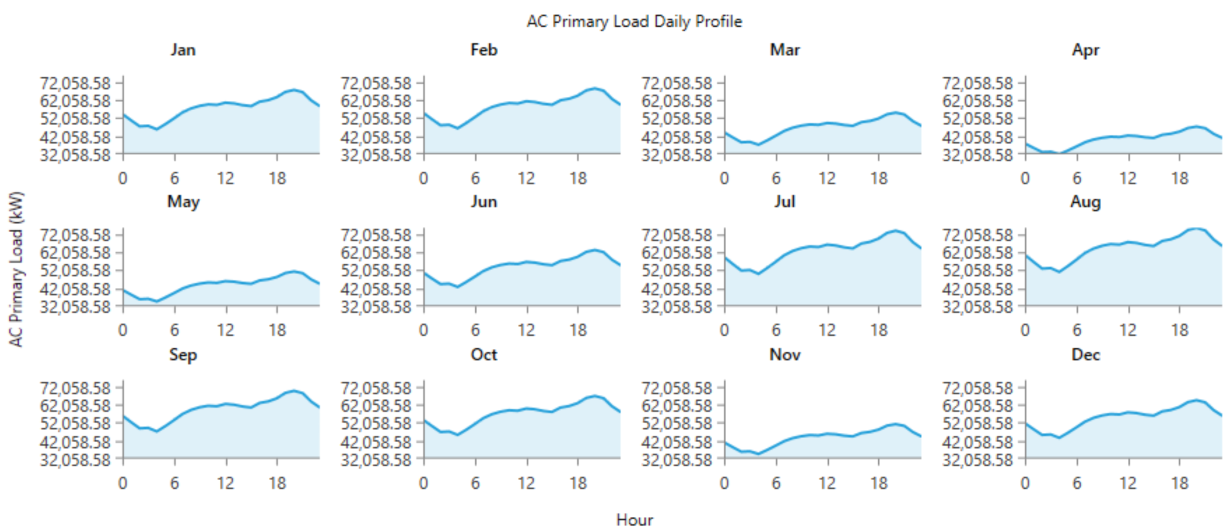

Figure 2 Everyday load profile in every month for Al Marj Town HRES computed with Homer Pro.

3. Values used to design the Al Marj town HRES based on the PV system.

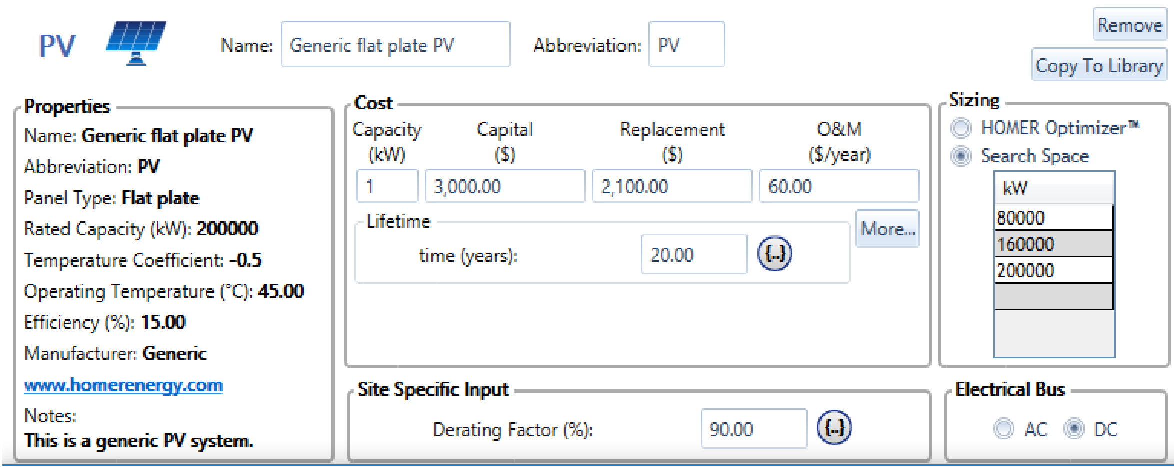

Figure 3 input values of PV system used for designing the Al Marj town HRES.

Table 1. Summary of PV system Input values plus parameters theory details

Parameters	**Values**	**Assumption references/ discussion**
Capital expenditure	3000 $ per kW	The price presumed in average price of projected installed price for efficacy -scale PV system, which it is presumed based upon the analysis carried on the global market hypothesis in 2015 for utility-scale PV system [5].
Replacement **cost**	2100 $ per kW	The replacement price in the analysis assumed as decline of 30 percent of capital price for PV system, that is considered fall in cost by 30 percent.
O&M cost	60 $/kW per year.	The price expected based upon the O&M price estimate in the desert for example in Al-Marj town HRES setting [6].

Lifespan	20 years	The maximum of the companies offers the lifespan of PV panel like 25 years. In the report expected in 20 years since it can impact through area environment where project positioned in the desert region.
Derating factor	90 percent	This value is presumed to consider the impact of temperature by PV range, normally around 90 percent [7]
Ground reflection	40 percent	This is a usual value for desert region for example in Al-Marj town region, projected as 20 percent in grass-covered regions & differed between 0.07-0.10 in marine regions.
Tracking system	Horizontal axis every day adjusted	In the study this type of tracking system has been presumed to get the sun as maximum as possible in daytime, also to evade the buildup of dust that may take place in case where permanent tracking systems is used.
Temperature coefficient of power	-0.5 percent/C	On type of PV model this value depends; it usually differs from -0.20 till -0.60 (%/C) & the assumption is based upon that range [8]
Supposed operation cell	45 degrees	Such values differ from 45°C till 48°C normally, as stated depend on technical info of PV module, hence the assumption
Temperature (NOCT)		Was into this range [8].
Efficacy at Std. test condition	15 percent	Besides, the efficacy is different depend on the type of panel & its technical info; it varies from 11-17 percent in present PV module types. Hence, the theory was average value thin film of CdTe PV panel component (in 2015) which has been stated for usage in design as Demonstrated above.
Size to take into consideration	80000 160000 200000	by this program It is adjusted automatically

4. The values used to design the Al Marj town HRES based on the wind turbine system.

Table 2. Details of wind turbine expenditure plus parameters assumption

Parameters	**Wind turbine E-82**
Rated power	2000 kW, AC
Capital cost	1,642,500 USD
Replacement cost	1,511,100 USD
O&M cost	31207.5 USD
Hub height	138 m
Lifespan	20 years
Size to consider	50, 75, 100 quantity

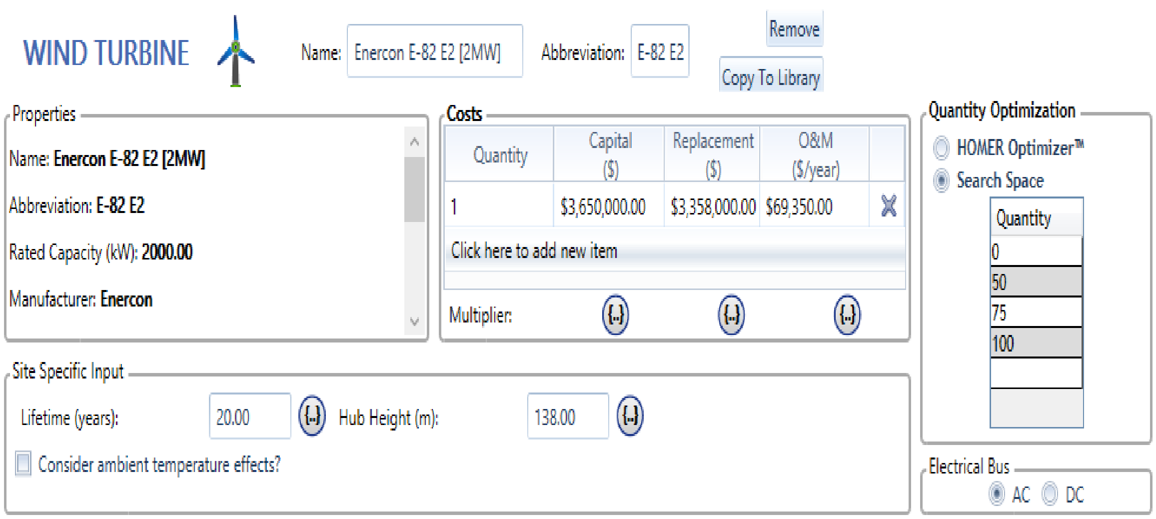

Figure 4 Input values wind turbine E-82 sourced in the designing of Al Marj Town HRES

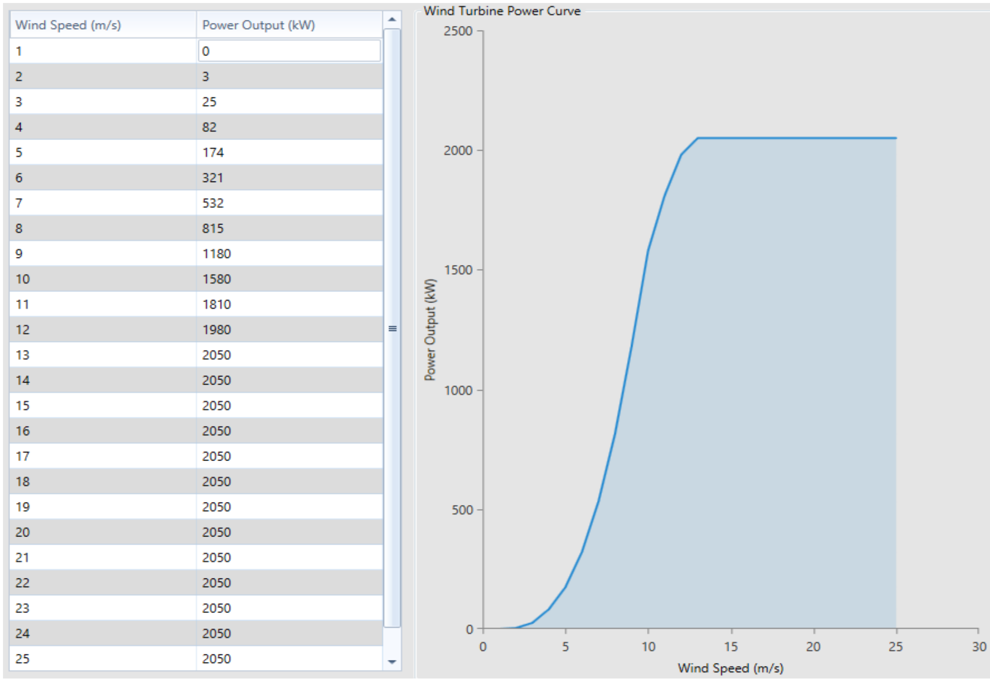

Figure 5 Wind turbine power carve used in designing of Al Marj Town HRES.

Table 3. Sensitivity report on hub height wind turbine versus COE.

Wind turbine E-82	
Hub height (m)	Hub height (m)
0.163	87
0.162	85
0.161	98
0.161	108
0.159	138

5. Generator input values used into the designing of Al Marj town HRES.

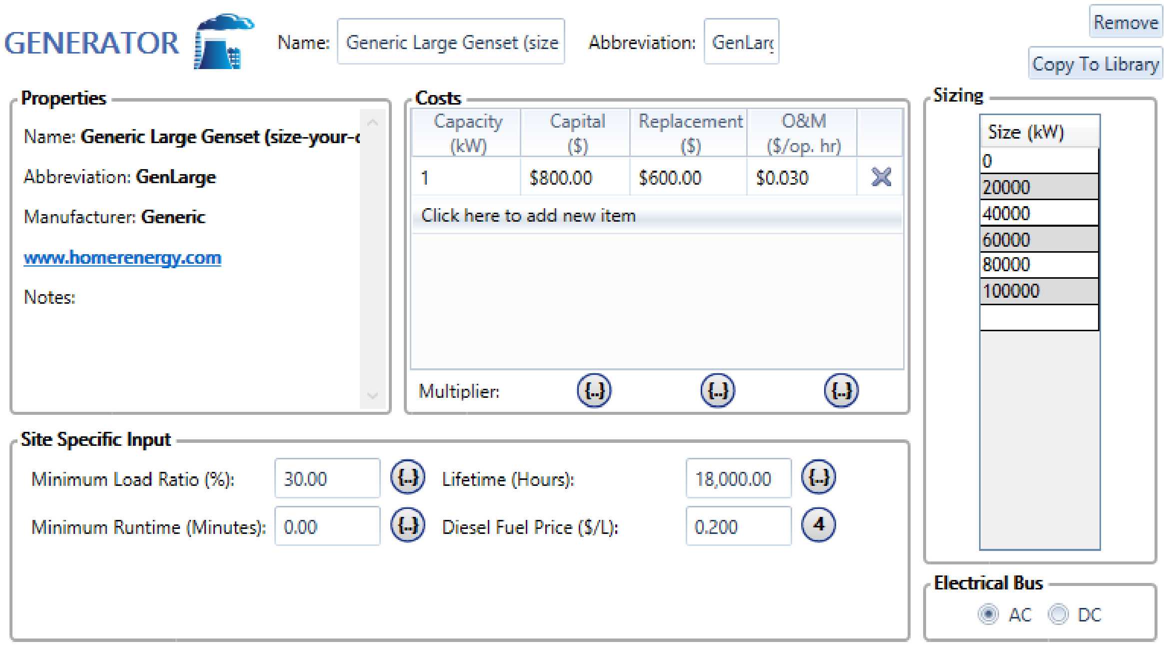

Figure 6 Generator specific values used into the designing of Al Marj town HRES.

6. The converter input values used in designing the Al Marj Town HRES

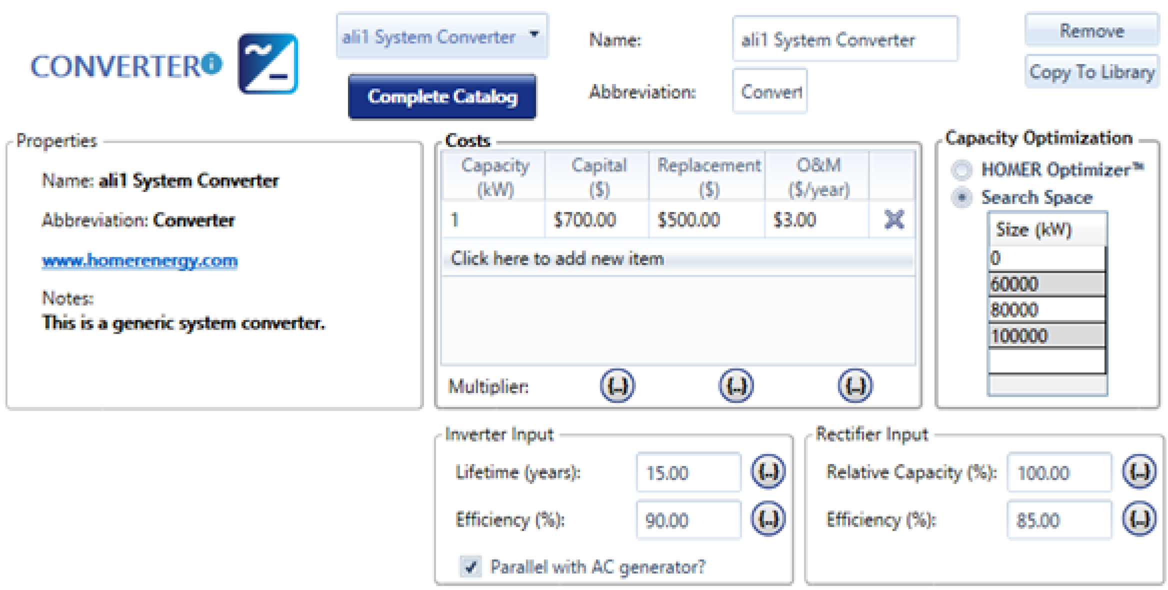

Figure 7 Converter input values sourced in the designing of Al Marj Town HRES

7. The battery input values used for the design of the HRES in Al Marj Town

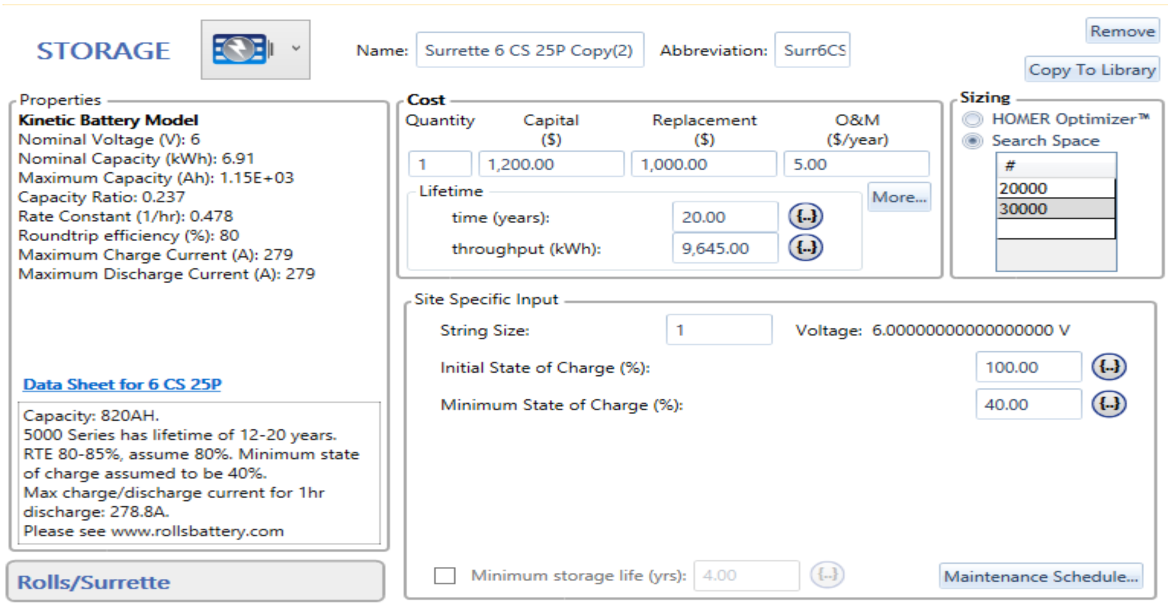

Figure 8 Battery input values used for the designing of Al Marj Town HRES.

8. Solar source in project area

Table 4. Characteristics and details of site

Description	**Item**
Place of project open land near to city	Place of project Al Marj City
Measurement date	Measurement date
05.011.2018	05.011.2018
Coordinates of the place	Coordinates of the place
Latitude 32°28.4' North, Longitude 20°50.1' East.	Latitude 32°28.4' North, Longitude 20°50.1' East.
Landform	Landform

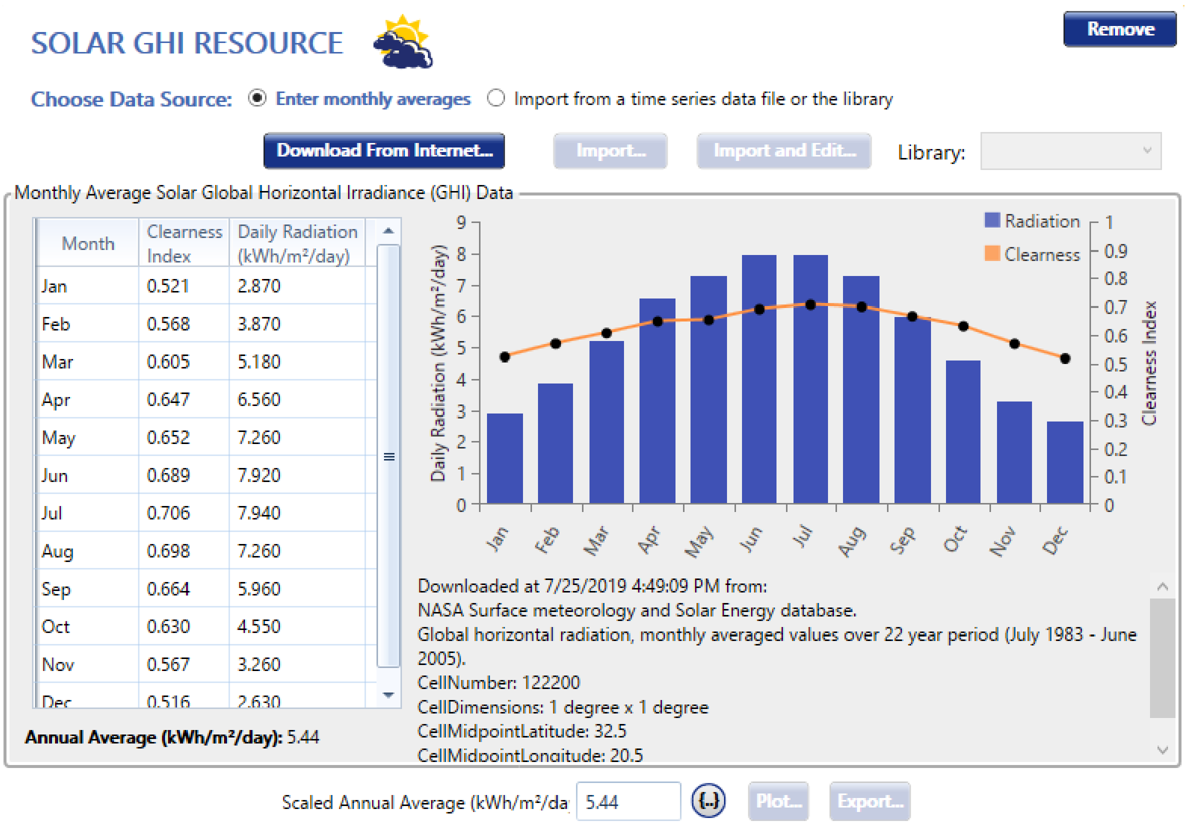

Figure 9 Monthly average solar irradiance at site of project..

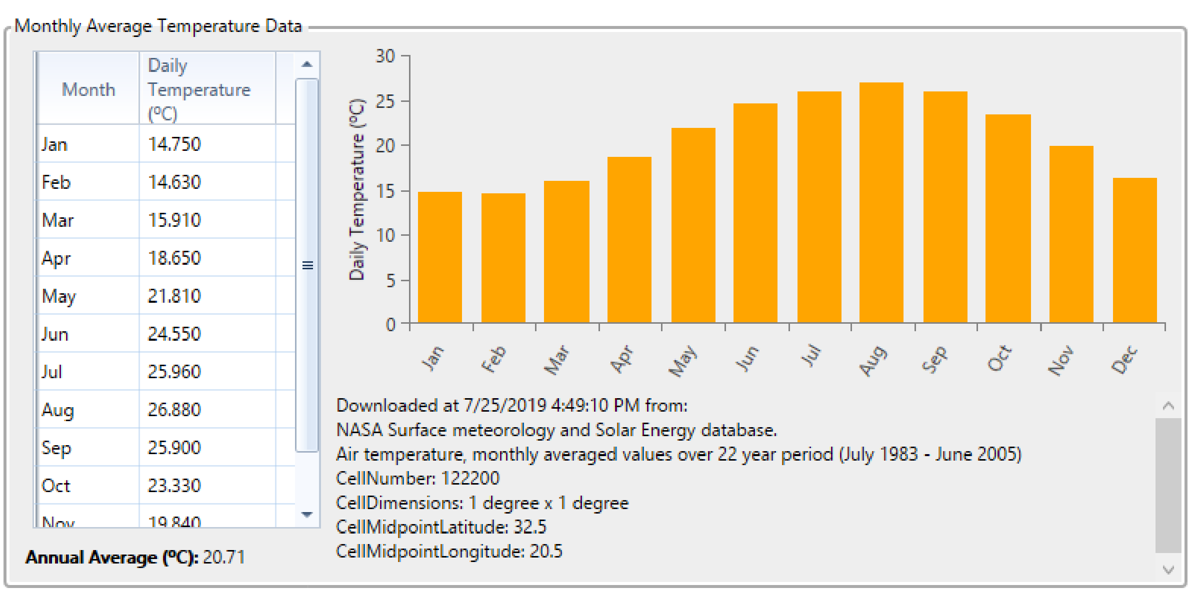

Figure 10 Temperature input values used into designing of Al Marj Town HRES

Appendix B

1. Block diagram of microgrid system in island mode by MATLAB software

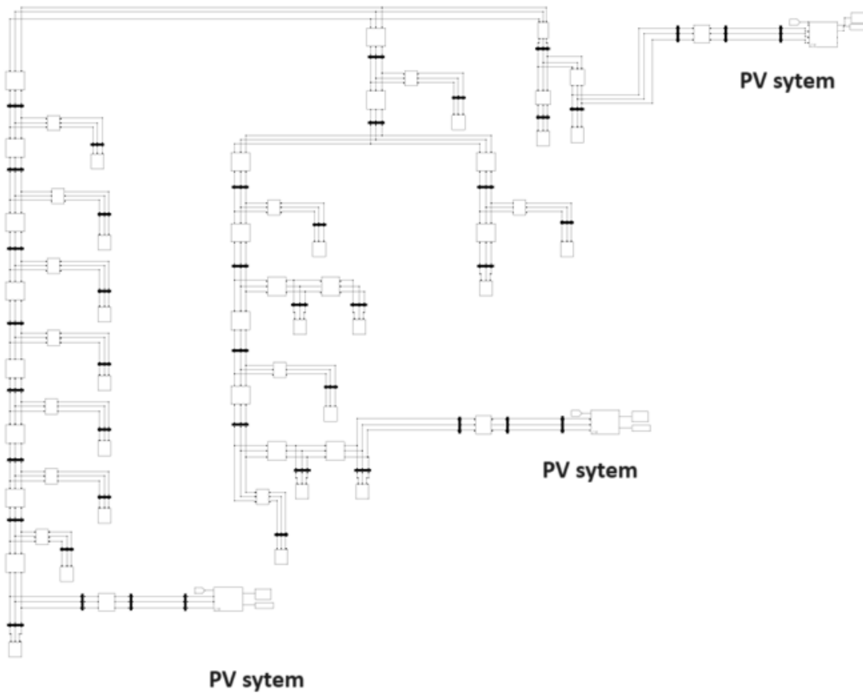

2. PV system in island mode.

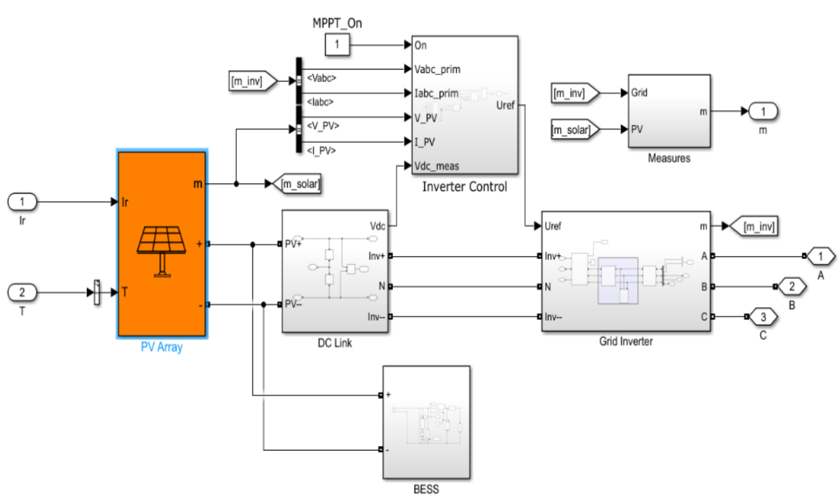

3. PV array

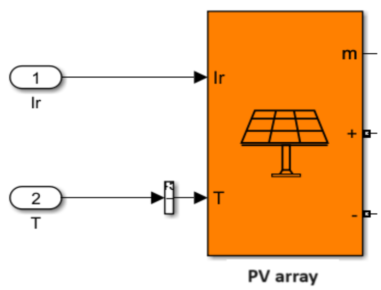

4. DC link

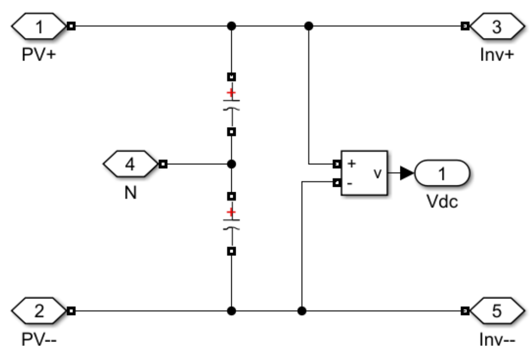

5. Inverter control

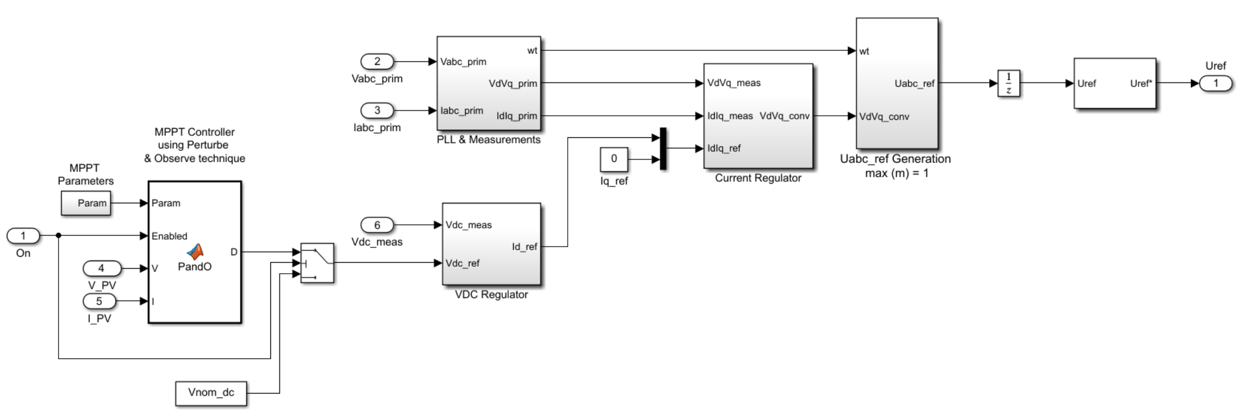

5.1 PLL measurements

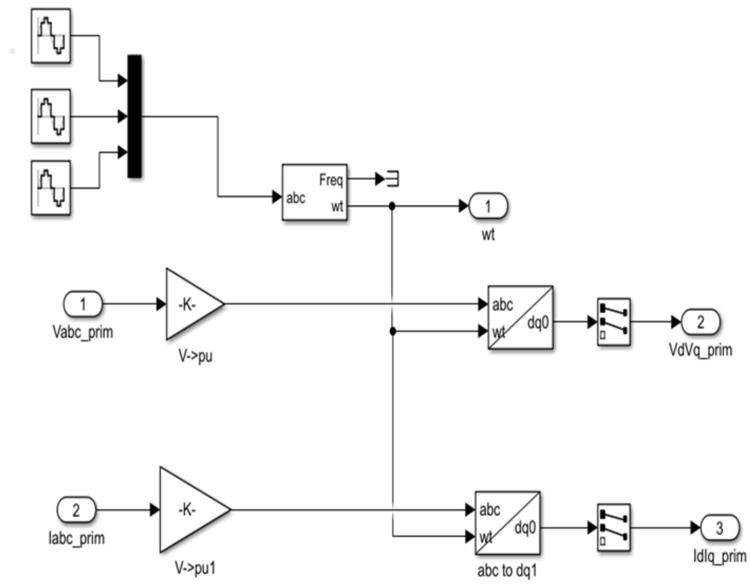

5.2 VDC Regulator

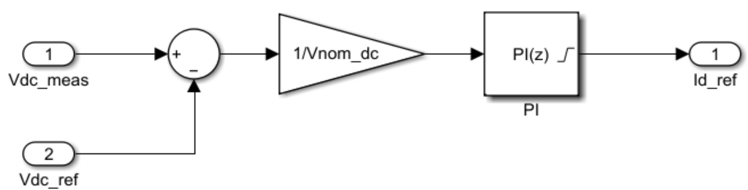

5.3 Current regulator

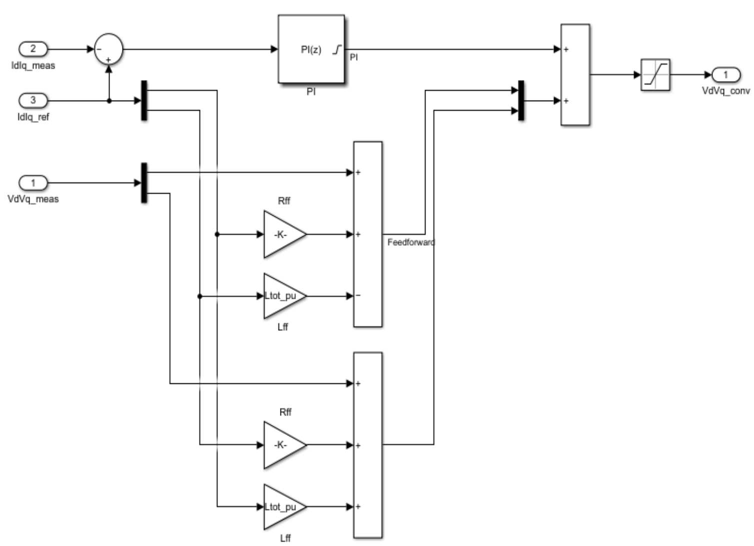

5.4 Voltage reference generation

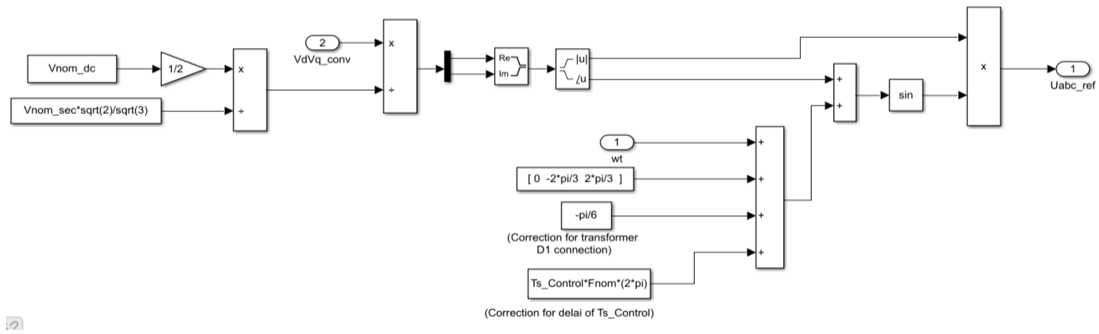

6. Grid iverter

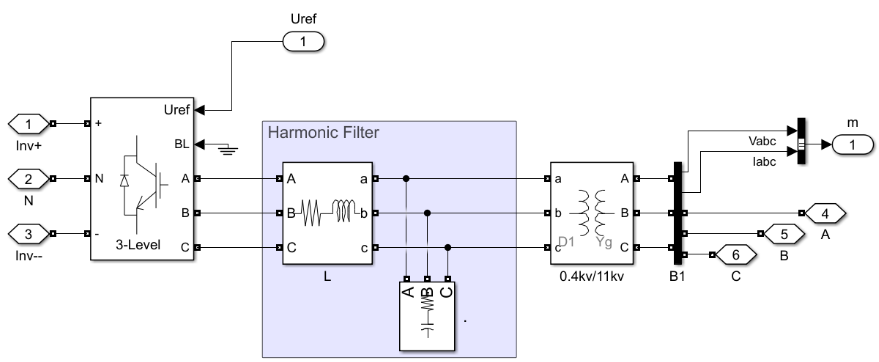

7. Measures

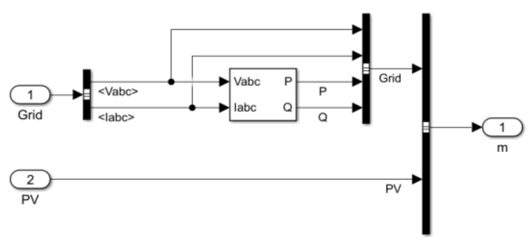

8. Battery energy storage system (BESS)

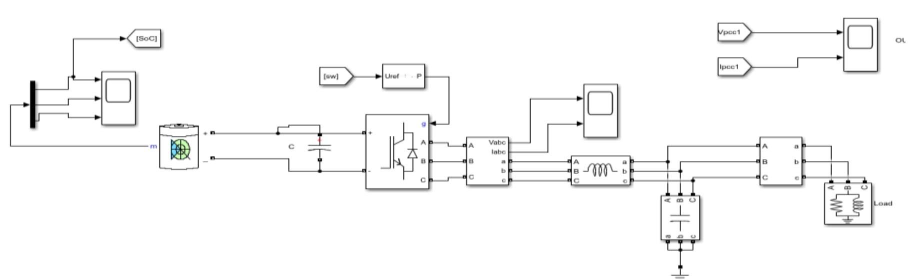

Appendix C

Forecasting Data using LSTM Network

```
%% Forecasting Data using LSTM Network

% Clear data and figures
clc
clear
close all

% Import Data
Data=importdata("ALMAR  DATA SINSE 1990-2020.xlsx");
% Extract Data
Data=Data.data;
rng(1234)

%% Predict Consumption Capita / Capita

% Response and Target Data
X=Data(:,1);
Y=Data(:,4);
% Compute Mean and std of response
muX = mean(X);
sigmaX = std(X);
% Compute Mean and std of target
muT = mean(Y);
sigmaT = std(Y);
% Compute Training Data
for n = 1:numel(X)
   XTrain(n) = (X(n) - muX) ./ sigmaX;
   TTrain(n) = (Y(n) - muT) ./ sigmaT;
end

% Create Neural Network layers with LSTM
numChannels=1;
layers = [
```

```
    sequenceInputLayer(numChannels)
    lstmLayer(256)
    fullyConnectedLayer(numChannels)
    regressionLayer];

% Training Option
options = trainingOptions("adam",MaxEpochs=2000,Plots="training-progress");
% Train NN Model
net = trainNetwork(XTrain,TTrain,layers,options);

% Predict Year
PredYear=2030;
% Predicting Data
XPred=X(1):PredYear;
% Preprocess data
for n = 1:numel(XPred)
    XTrainPred(n) = (XPred(n) - muX) ./ sigmaX;
end
% Predict Data
YPred = predict(net,XTrainPred)*sigmaT+muT;
% Compute R-Square
SSE=sum((Y'-YPred(1:numel(Y))).^2);
SS=sum((Y-mean(Y)).^2);
Rsq=1-SSE/SS;
fprintf('R-Square: %0.5f\n\n',Rsq)

% Plot Dataset and Predicted Data
figure
plot(X,Y,'-b')
hold on
plot(XPred,YPred,'--r')
grid on
xlabel('Year')
ylabel('Consumption (kWh) / Capita')


%% Predict Primary Energy Consumption
```

```
% Response and Target Data
X=Data(:,1);
Y=Data(:,3);
% Compute Mean and std of response
muX = mean(X);
sigmaX = std(X);
% Compute Mean and std of target
muT = mean(Y);
sigmaT = std(Y);
% Compute Training Data
for n = 1:numel(X)
   XTrain(n) = (X(n) - muX) ./ sigmaX;
   TTrain(n) = (Y(n) - muT) ./ sigmaT;
end
% Create Neural Network layers with LSTM
numChannels=1;
layers = [
   sequenceInputLayer(numChannels)
   lstmLayer(256)
   fullyConnectedLayer(numChannels)
   regressionLayer];

% Training Option
options = trainingOptions("adam",MaxEpochs=2000,Plots="training-progress");
% Train NN Model
net = trainNetwork(XTrain,TTrain,layers,options);

% Predict Year
PredYear=2030;
% Predicting Data
XPred=X(1):PredYear;
% Preprocess data
for n = 1:numel(XPred)
   XTrainPred(n) = (XPred(n) - muX) ./ sigmaX;
end
% Predict Data
```

```
YPred = predict(net,XTrainPred)*sigmaT+muT;
% Compute R-Square
SSE=sum((Y'-YPred(1:numel(Y))).^2);
SS=sum((Y-mean(Y)).^2);
Rsq=1-SSE/SS;
fprintf('R-Square: %0.5f\n\n',Rsq)

% Plot Dataset and Predicted Data
figure
plot(X,Y,'-b')
hold on
plot(XPred,YPred,'--r')
grid on
xlabel('Year')
ylabel('Primary Energy Consumption (GWh)')

%% Predict Population

% Response and Target Data
X=Data(:,1);
Y=Data(:,2);
% Compute Mean and std of response
muX = mean(X);
sigmaX = std(X);
% Compute Mean and std of target
muT = mean(Y);
sigmaT = std(Y);
% Compute Training Data
for n = 1:numel(X)
    XTrain(n) = (X(n) - muX) ./ sigmaX;
    TTrain(n) = (Y(n) - muT) ./ sigmaT;
end
% Create Neural Network layers with LSTM
numChannels=1;
layers = [
    sequenceInputLayer(numChannels)
    lstmLayer(256)
```

```
    fullyConnectedLayer(numChannels)
    regressionLayer];

% Training Option
options = trainingOptions("adam",MaxEpochs=2000,Plots="training-progress");
% Train NN Model
net = trainNetwork(XTrain,TTrain,layers,options);

% Predict Year
PredYear=2030;
% Predicting Data
XPred=X(1):PredYear;
% Preprocess data
for n = 1:numel(XPred)
    XTrainPred(n) = (XPred(n) - muX) ./ sigmaX;
end
% Predict Data
YPred = predict(net,XTrainPred)*sigmaT+muT;
% Compute R-Square
SSE=sum((Y'-YPred(1:numel(Y))).^2);
SS=sum((Y-mean(Y)).^2);
Rsq=1-SSE/SS;
fprintf('R-Square: %0.5f\n\n',Rsq)

% Plot Dataset and Predicted Data
figure
plot(X,Y,'-b')
hold on
plot(XPred,YPred,'--r')
grid on
xlabel('Year')
ylabel('Population')
```

Appendix D

1. Sensitivity analysis

```
%% Grid connected mode without DG

close all
clear all
data25
basemva = 100;  accuracy = 0.001; maxiter = 100;
lfybus                          % form the bus admittance matrix
tic
decouple1                          % Load flow solution by fast decoupled method
toc
busout
Vm1=Vm;
%% Grid connected mode with DG
data
basemva = 100;  accuracy = 0.001; maxiter = 100;
lfybus                          % form the bus admittance matrix
tic
decouple1                          % Load flow solution by fast decoupled method
toc
busout
bar([Vm1;Vm]')
ylim([0.85 1.05])
xlim([0 23])
xlabel('Bus Number')
ylabel('Voltage Magnitude (pu)')
legend('Grid Without DG', 'Grid With DG at 14-2-22')
grid on
%% Senstivity
for i=1:length(Vm)
dv1(i)=abs(min(Vm)-Vm(i));
SS(i)=(dv1(i)/Vm(1))/Pdt*100;
end
figure(2)
bar(SS)
xlim([0 15])
```

```
xlabel('Bus Number')
%% Isladed mode with DG at 14
data25DG14island
basemva = 100;  accuracy = 0.001; maxiter = 100;
lfybus                      % form the bus admittance matrix
tic
decouple1                     % Load flow solution by fast decoupled method
toc
busout
plot(Vm,'-*','Linewidth',2)
ylim([0.85 1.05])
xlim([0 22])
xlabel('Bus Number')
ylabel('Voltage Magnitude (pu)')
grid on
%% Isladed mode with DG at 14-2-22
data25DG14222island
basemva = 100;  accuracy = 0.001; maxiter = 100;
lfybus                      % form the bus admittance matrix
tic
decouple1                     % Load flow solution by fast decoupled method
toc
busout
plot(Vm,'-*','Linewidth',2)
ylim([0.85 1.1])
xlim([0 22])
xlabel('Bus Number')
ylabel('Voltage Magnitude (pu)')
grid on

%% Senstivity
for i=1:length(Vm)
dv1(i)=abs(min(Vm)-Vm(i));
SS(i)=(dv1(i)/Vm(1))/Pdt*100;
end
figure(2)
bar(SS)
```

```
xlim([0 15])
xlabel('Bus Number')
```

2. Particle Swarm Optimization (PSO).

```
 %x=randi([1 22],10,1);
N_DGS=input('Please enter the number of DGs to place: ');
%% Problem Definition
CostFunction=@(x) Newton_Raphson(x);
nVar=N_DGS;
VarSize=[1 nVar];
VarMin=1;
VarMax= 22;
%% PSO Parameters
MaxIt=4;      % Maximum Number of Iterations
nPop=100;
% PSO Parameters
w=1;       close all
% Inertia Weight
wdamp=0.99;
c1=1.5;
c2=2.0;
% Constriction Coefficients
phi1=2.05;
phi2=2.05;
phi=phi1+phi2;
chi=2/(phi-2+sqrt(phi^2-4*phi));
w=chi;
wdamp=1;
c1=chi*phi1;
c2=chi*phi2;
% Velocity Limits
VelMax=0.1*(VarMax-VarMin);
VelMin=-VelMax;
%% Initialization
empty_particle.Position=[];
empty_particle.Cost=[];
```

```
empty_particle.Velocity=[];
empty_particle.Best.Position=[];
empty_particle.Best.Cost=[];
particle=repmat(empty_particle,nPop,1);
GlobalBest.Cost=inf;
for i=1:nPop

% Initialize Position
particle(i).Position=randi([VarMin,VarMax],1,nVar);
% Initialize Velocity
particle(i).Velocity=zeros(VarSize);
% Evaluation
particle(i).Cost=CostFunction(particle(i).Position);
% Update Personal Best
particle(i).Best.Position=particle(i).Position;
particle(i).Best.Cost=particle(i).Cost;
% Update Global Best
if particle(i).Best.Cost<GlobalBest.Cost
GlobalBest=particle(i).Best;
end
end
BestCost=zeros(MaxIt,1);
%% PSO Main Loop
for it=1:MaxIt
for i=1:nPop
% Update Velocity
particle(i).Velocity = w*particle(i).Velocity ...
+c1*rand(VarSize).*(particle(i).Best.Position-particle(i).Position) ...
+c2*rand(VarSize).*(GlobalBest.Position-particle(i).Position);
% Apply Velocity Limits
particle(i).Velocity = max(particle(i).Velocity,VelMin);
particle(i).Velocity = min(particle(i).Velocity,VelMax);
% Update Position
particle(i).Position = floor(particle(i).Position + particle(i).Velocity);
% Velocity Mirror Effect
IsOutside=(particle(i).Position<VarMin | particle(i).Position>VarMax);
particle(i).Velocity(IsOutside)=-particle(i).Velocity(IsOutside);
```

```
% Apply Position Limits
particle(i).Position = max(particle(i).Position,VarMin);
particle(i).Position = min(particle(i).Position,VarMax);
% Evaluation
particle(i).Cost = CostFunction(particle(i).Position);
% Update Personal Best
if particle(i).Cost<particle(i).Best.Cost
particle(i).Best.Position=particle(i).Position;
particle(i).Best.Cost=particle(i).Cost;
% Update Global Best
if particle(i).Best.Cost<GlobalBest.Cost
GlobalBest=particle(i).Best;
end
end
end
BestCost(it)=GlobalBest.Cost;
BestCost(it)=BestCost(it)-rand(1).*1e-4;
disp(['Iteration ' num2str(it) ': Best Cost = ' num2str(BestCost(it))]);
w=w*wdamp;
end
BestSol = GlobalBest;
BestSol.Position=unique(BestSol.Position);
BestSol.Position=setdiff(BestSol.Position,[1,3,15]);
ms=setdiff(1:22,BestSol.Position);
for i=1:length(ms)
if length(BestSol.Position)<N_DGS
BestSol.Position=[BestSol.Position ms(i)];
end
end
%%
figure;
BestCost=BestCost-rand(length(BestCost),1).*1e-4;
plot(sort(BestCost,'descend'),'LineWidth',2);
grid on;
xlabel('iterations');
ylabel('Objective funstion value');
toc;
```

```
disp('----------------------------------------------------');
disp('The optimal location of DGs to place is');
disp(BestSol);
disp('----------------------------------------------------');
figure
bar(BestSol.Position,'m','LineWidth',1.5)
grid on
xlabel('Number of DGs placed')
ylabel('Bus numbers where DGs placed')
text(1:length(BestSol.Position),BestSol.Position,num2str(BestSol.Position'),'vert','bottom','horiz','center');
box off
```